ST. ANTHONY FALLS HYDRAULIC LABORATORY
UNIVERSITY OF MINNESOTA

Project Report No. 36

SECONDARY FLOWS IN GUIDE VANE BENDS WITH SOME NOTES ON THE PRIMARY TWO-DIMENSIONAL FLOW

Submitted by
LORENZ G. STRAUB
Director

Prepared by
EDWARD SILBERMAN

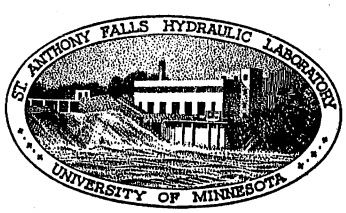

January, 1953

Prepared for
OFFICE OF NAVAL RESEARCH
Department of the Navy
Washington, D.C.

Under Office of Naval Research Contract N8onr-66204

P R E F A C E

This is the final report on the flow diversion research sponsored by the Office of Naval Research at the St. Anthony Falls Hydraulic Laboratory of the University of Minnesota. The work was performed under contract N8onr-66204, Research and Development Board No. NR-062-081.

The flow diversion research was originally undertaken about seven years ago when it became evident that the design criteria for guide vane bends and other flow diversion structures were poorly formulated in the literature. It appeared that a comprehensive study of the basic mechanics of flow diversion was needed. This study was undertaken and carried on for about four years prior to sponsorship by ONR. The work included a study of the literature, a study of ordinary radius bends, and general experimental studies of flow in guide vane bends. This earlier work led to the general conclusion that flow diversion problems could be handled by studying a basic or primary, nearly potential flow (frequently two-dimensional) with superimposed secondary flow. Since potential and two-dimensional flows through blade rows and in other types of bends had received much attention, the immediate need on completion of the earlier work was for a detailed study of secondary flows.

The research sponsored by ONR has dealt mainly with secondary flows of incompressible fluid in guide vane bends. The work also involved determination of a method of correlating the two-dimensional guide vane data used as the primary flow. This research is described fully in the technical report which follows and is summarized on p. v. The papers stimulated by the ONR research, together with the earlier papers, are listed together for ready reference at the end of this preface (p. iv).

The conclusions of the present report are applicable, at least qualitatively, to all types of flow diversion problems--turbomachine blading, ordinary bends, intake scoops, manifolds, and a number of other boundary shapes. Some or all of these problems are being worked on now by other investigators, and it is believed the present report will prove useful to them.

The present work was supervised and the report written by Edward Silberman. Many members of the Laboratory staff assisted in preparing the experimental apparatus, collecting and reducing data, preparing the manuscript and figures, checking the work, and publishing the report; and thanks are due to all of them. Major assistance was rendered by E. Roy Tinney in assembling the data and reading the final manuscript.

The flow diversion program has been under the general direction of Dr. Lorenz G. Straub, Director of the Laboratory.

FLOW DIVERSION REPORTS OF THE ST. ANTHONY FALLS HYDRAULIC LABORATORY

TECHNICAL REPORT FOR ONR

(a) Silberman, E. Secondary Flows in Guide Vane Bends with Some Notes on the Primary Two-Dimensional Flow. University of Minnesota, St. Anthony Falls Hydraulic Laboratory Project Report No. 36, January, 1953.

OTHER PAPERS

Based on Research Sponsored by ONR

(b) Silberman, E. "Application of Flow Analysis to Vaned Elbows." Unpublished paper delivered before the convention of the American Society of Civil Engineers at Denver, Colorado, June, 1952.

(c) Silberman, E. Importance of Secondary Flow in Guide Vane Bends. University of Minnesota, St. Anthony Falls Hydraulic Laboratory Technical Paper No. 14, Series B, January, 1953. (Preprint of paper offered for presentation to the Third Midwestern Conference on Fluid Mechanics.)

Based on Earlier Research

(d) Anderson, A. G. Fluid Flow Diversion. University of Minnesota, St. Anthony Falls Hydraulic Laboratory Project Report No. 1, August, 1947.

(e) Silberman, E. The Nature of Flow in an Elbow. University of Minnesota, St. Anthony Falls Hydraulic Laboratory Project Report No. 5, December, 1947.

(f) Holdhusen, J. S. and Lamb, O. P. Model Experiments for the Design of a Sixty-Inch Water Tunnel, Part V, Vaned Elbow Studies. University of Minnesota, St. Anthony Falls Hydraulic Laboratory Project Report No. 14, September, 1948.

(g) Silberman, E. Fluid Flow Diversion by Guide Vanes in Miter Bends. University of Minnesota, St. Anthony Falls Hydraulic Laboratory Project Report No. 8, April, 1949.

(h) Anderson, A. G. Hydraulics of Conduit Bends. University of Minnesota, St. Anthony Falls Hydraulic Laboratory Bulletin No. 1, December, 1948.

ABSTRACT

Incompressible flow in a guide vane bend may be considered as composed of a primary two-dimensional, nearly potential flow upon which is superimposed a secondary flow. The two-dimensional flow lies in the plane of the bend and is determined by the flow boundaries alone. If the flow entering a bend were everywhere irrotational, the two-dimensional flow pattern would be the three-dimensional pattern (nearly). Because the real flow entering a bend has a nonuniform velocity profile in planes normal to the plane of the bend, the streamlines in the nonuniform region are determined not alone by the flow boundaries but also by the entrance profile or vorticity.

To study the real flow in a guide vane bend, it is necessary to begin with the two-dimensional flow. Two-dimensional flows in cascades have been studied thoroughly by others, but no suitable means of correlating the data, both theoretical and experimental, was available. A method of correlation is presented in the report; correlation is accomplished by use of Figs. 5 and 5a.

The main purpose of this research was the study of the influence of secondary flows on the basic two-dimensional flow. It is shown in the report from experimental data that the secondary flows have a negligible influence on the average deflection of the flow by the guide vanes, but they have a major influence on the energy loss. The two-dimensional loss coefficient is increased 100 per cent and more by the secondary flows. The loss attributable to secondary flows may be divided into two parts. The smaller of the two parts occurs at the vanes and the larger part occurs in a region downstream of the vanes extending over three or four duct hydraulic diameters. This larger part of the loss is attributed mainly to increased wall shear downstream of the vanes. The increased wall shear occurs because the secondary flow brings high-energy, high-velocity fluid to the duct wall from the interior.

The loss attributable to secondary flows depends on the intensity of the secondary current. This in turn depends on such factors as the lift coefficient of the vanes in two-dimensional flow divided by the spacing-chord ratio (which takes into account both deflection angle and expansion or contraction of the two-dimensional flow), the shape of the two-dimensional passage between the vanes, and the entrance velocity profile. There may be others, but the program was discontinued before even the known factors could be investigated thoroughly.

The experimental work indicated that with plate vanes, the loss attributable to secondary flows decreased with decreasing number of vanes in the bend but that with thick vanes having constant gap width between the vanes, there was little variation in loss with variation in number of vanes. This fact can be applied practically to obtain guide vane bends of plate vanes having only slightly greater loss than bends of thick vanes. Such guide vane systems are constructed by choosing cascades having a small two-dimensional loss coefficient and by manufacturing the vanes with large chord length. The chord length is limited only by the requirement of having a certain minimum number of vanes in the bend. This minimum is determined either by the need for preventing excessive loss in the spaces between the lateral walls and adjacent vanes, or by structural limitations. In the experimental work, a minimum of five or six vanes was required by the former condition.

C O N T E N T S

LIST OF ILLUSTRATIONS

SECONDARY FLOWS IN GUIDE VANE BENDS WITH SOME NOTES ON THE PRIMARY TWO-DIMENSIONAL FLOW

I. INTRODUCTION

The designer of guide vane bends such as those occurring in water and wind tunnels often feels that there is a wide gap between performance of the guide vanes installed in a bend and the idealized two-dimensional guide vane systems which have so frequently been studied in the literature. He also wonders whether there is a scale effect in adapting the guide vanes of one bend to another, such as in going from model to prototype. Similar questions arise in connection with the design of blade systems in turbomachinery. The cause of this doubt is the existence of a disturbed-flow region near the span ends of the vanes as well as the existence of duct walls parallel to the vanes.

The questions raised are examined in this report by considering the flow through a guide vane system composed of a basic or primary two-dimensional flow with superimposed secondary flow. The main purpose of the study is the investigation of the influence of the secondary flow on the basic two-dimensional flow. As will be shown, the secondary flow is responsible for an important part of the energy loss in the bend but has little influence on the deflection of the flow. Squire and Winter [1],* among others, have studied the flow in blading systems in a similar manner; their paper shows the relation of the secondary flow to the primary two-dimensional flow but does not describe the complete role of the secondary flow.

It should be noted that this paper is not intended to give design data for guide vane systems, although the specific systems used herein should prove satisfactory for many applications. Rather, the paper examines the basic mechanics of flow in such systems with a view toward a better understanding of the problems involved. Sources of design information may be found in a bibliographical report of this Laboratory [2], and some further information regarding guide vane systems for 90° miter bends is given in another report of the Laboratory [3]. The research leading to the two references just mentioned, together with a study of flow in radius bends [4], provided background for the present work.

---

*Numbers in brackets refer to the Bibliography on p. 38.

Physically, most guide vane structures are either two-dimensional or possess axial symmetry. Only two-dimensional guide vane structures are considered specifically herein. Figure 1 is a sketch showing a typical guide vane installation in use at the St. Anthony Falls Hydraulic Laboratory and is representative of the type of structure with which this report is concerned.

The behavior of a set of guide vanes depends to a certain extent on the velocity profile of the flow approaching the vanes. In many applications, the flow approaching the vanes is uniform, or nearly so, except in a region close to the boundaries. This is the case in the bend preceding the contraction of a water tunnel, for example, and is even roughly true in fully developed turbulent flow in a pipe. The present study is based on the somewhat idealized case of a uniform, incompressible flow with boundary layers in the duct approaching the bend. Figure 2a shows the total head distribution which is representative of the entrance conditions in the present experimental work.

Figure 2b, also taken from the present work, shows the results of a total head survey made closely downstream of a guide vane bend having the entrance distribution shown in Fig. 2a. (Figure 2d is a sketch of the bend and shows where the total head surveys were taken.) It is seen that the flow distribution closely downstream of the vanes is still nearly two-dimensional over a large central part of the duct but that there is an enlarged disturbed region near the vane ends. Not only is the flow distribution nearly two-dimensional over a large part of the duct, but it is also nearly potential; in the two-dimensional region, head loss occurs only in the vane wakes. Figure 3 shows head loss data plotted in the (two-dimensional) plane of the bend and serves to illustrate further the nearly potential nature of the flow in the vicinity of the guide vanes. Figure 2c shows the total head distribution still farther downstream. The distribution resembles that which existed upstream of the vanes.

Because of the experimental results typified by Figs. 2 and 3, it is convenient to divide the study of flow in guide vane bends into two distinct parts: (1) a purely two-dimensional, potential study with boundary layer effects in the plane of the bend (and all parallel planes), and (2) a three-dimensional study in a limited region near the vane ends, with the secondary currents produced in this region considered as superimposed on the two-dimensional flow. The two-dimensional results may be looked upon as a first

approximation to the performance of an actual guide vane system installed in a bend. As already stated, the main purpose of the present study is the determination of the adequacy of this first approximation.

The nomenclature used in this report is defined in Appendix A; it is chosen to agree generally with that previously used at this Laboratory and established in reference [3] and does not always agree with that used by others. The two-dimensional vane system is called a cascade in this report. Nomenclature in the two-dimensional region is further defined in Fig. 4.

II. TWO-DIMENSIONAL FLOW

In this section, the basic two-dimensional flow will be reviewed briefly and a method for correlating two-dimensional data will be developed. The secondary flow will be discussed in succeeding sections.

The two-dimensional flow may be determined by mathematical methods, either exact or approximate. A number of these methods have been reviewed by Tyler [5]. Electric or mechanical analogy may also be used to determine the theoretical flow. Generally, theoretical methods are not entirely adequate because they fail to account for the nonpotential or boundary layer part of the two-dimensional flow. Recently, however, Schlicting and Scholz [6] introduced boundary layer theory in connection with one of the theoretical methods. Experimental methods of determining the two-dimensional flow are widely used, and a number of papers dealing with these determinations have been published by the National Advisory Committee for Aeronautics and the British Aeronautical Research Council. An experimental determination of two-dimensional cascade flow is described in reference [3] and later in this report.

The primary purpose of a cascade is the turning of the flow through an angle Δ, the deflection angle, while providing a specified ratio between the exit and entrance velocities V_2/V_1 (see Fig. 4). (In many applications $V_2/V_1 = 1$, but it is not limited to this value.) The turning and acceleration or deceleration are produced by changing the momentum of the flow as it passes through the cascade. The change in momentum is caused by the reaction (lift and drag) of the vanes of the cascade; in the absence of drag, the reaction force must act normal to the vector mean velocity through the bend. (Alternatively, the velocity vector V_1 is converted to the vector V_2 by the circulation Γ about each vane--this concept is used in Appendix C.)

As an initial step, the relation between the velocity vectors (V_1 and V_2) and the reaction of the vanes is established. This step is facilitated by expressing the magnitude of the reaction in coefficient form; that is,

$$R = C_R \, c \, \frac{\rho V_1^2}{2} \tag{1}$$

where
- R is the reaction per unit length of vane,
- C_R is the coefficient of reaction,
- c is the vane chord,
- ρ is the fluid density, and
- V_1 is the entrance velocity.

(The velocity V_2 or the vector mean between V_1 and V_2 could have been used in place of V_1. The proper choice of reference velocity facilitates the analysis of plotted experimental data. See, for example, Zweifel [7] where this matter is discussed.) It is customary to divide the reaction into lift and drag components with the definitions

$$L = C_L \, c \, \frac{\rho V_1^2}{2} \tag{2}$$

$$D = C_D \, c \, \frac{\rho V_1^2}{2} \tag{3}$$

where
- L is the lift per unit length of vane normal to the vector mean between V_1 and V_2,
- C_L is the lift coefficient,
- D is the drag per unit length of vane normal to L, and
- C_D is the drag coefficient.

The relationships between $V_2/V_1, \Delta$, C_L, and C_D are discussed in reference [3], as well as in several other papers, and are established in Appendix B. The following formulas apply:

$$\frac{V_2}{V_1} = \frac{\sin\beta_1}{\sin\beta_2} \tag{4}$$

$$\Delta = \beta_2 - \beta_1 \tag{5}$$

$$\tan \gamma = \left(\frac{V_1}{V_2} - \frac{V_2}{V_1} \right) \frac{1}{2 \sin \Delta} = \frac{1}{2} (\cot \beta_2 + \cot \beta_1) \tag{6}$$

$$\frac{C_L}{s/c} = 2 \frac{V_2}{V_1} \frac{\sin \Delta}{\cos \gamma} - \frac{C_D}{s/c} \tan \gamma \tag{7}$$

where γ is the angle (measured positive in the clockwise sense) between the cascade axis and the lift direction. The coefficient of drag is related to the pressure drop or head loss coefficient ζ by

$$C_D = \zeta \frac{s}{c} \cos \gamma \tag{8}$$

Where

$$\zeta = \frac{p'}{\rho V_1^2/2} , \tag{9}$$

$$p_1 + \frac{\rho V_1^2}{2} = p_2 + \frac{\rho V_2^2}{2} + p' \tag{10}$$

and p' is the pressure loss in the bend.

Equations (4) through (7) are represented in Fig. 5 with $\zeta = 0$. The required lift coefficient is either increased or decreased by the drag of the vanes, depending on the ratio V_2/V_1; but for guide vanes with $V_2/V_1 = 1$, the required lift coefficient is not affected. To produce a given deflection with given velocity ratio, it is essential to provide a cascade with the correct value of $C_L/(s/c)$. If this parameter is too large, the flow will be overturned and/or the velocity ratio will be too large and vice versa. For a guide vane bend in a duct where the duct walls determine both the deflection and velocity ratios, the duct will act more or less like a radius elbow depending on how closely the cascade $C_L/(s/c)$ matches the required $C_L/(s/c)$.

In an actual guide vane installation, different cascade arrangements--that is, variations in profile shape, stagger angle θ, spacing-chord ratio s/c, and entrance angle β_1--produce different values for the parameter

$C_L/(s/c)$ as well as for the drag coefficient. It is shown in Appendix C that the action of a cascade with given characteristics (fixed s/c, θ, and profile shape) will be represented approximately on Fig. 5 by the straight line

$$\cot \beta_2 = A \cot \beta_1 - B \tag{11}$$

where A and B are constants given by

$$A = 1 + \frac{2 \kappa \sin \beta_o}{2s/c - \kappa \sin \beta_o} \qquad B = \frac{2 \kappa \cos \beta_o}{2s/c - \kappa \sin \beta_o} \tag{12}$$

and where κ is a proportionality factor dependent on s/c, θ, and vane shape, and β_o is the entrance angle for which $\Delta = 0$ ($\beta_1 = \beta_2 = \beta_o$) and is given by

$$\beta_o = \theta - \alpha_o \tag{13}$$

where α_o is the angle of attack for zero lift of the profile measured from the velocity vector. The straight lines of Eq. (11) are an integral part of Fig. 5. Equation (11) is valid as an approximation only as long as stalling does not occur.

Typical representations of Eq. (11) are shown in Fig. 5a, which is an overlay to Fig. 5. Each line given by Eq. (11), when plotted on Fig. 5, may be called a cascade line. There are an infinite number of such lines through each point of Fig. 5, and each line may represent more than one combination of s/c, θ, and vane shape. (The cascade lines drawn on Fig. 5a have been chosen to represent experimental data obtained from two sources--Davis [8], and Harris and Fairthorne [9]. Davis expressed surprise that his data caused all cascade lines with identical stagger to intersect in a point; this is explained, of course, by Eq. (13). Harris and Fairthorne determined the angle of attack for zero lift for their profile acting as a single airfoil; this was found to be -11.5°, and the cascade lines have been drawn in Fig. 5a to intersect the β_o axis at $\beta_o = \theta + 11.5$.)

Over the unstalled length of a cascade line, C_D will vary from a maximum at each stalled end of the line to a minimum near its center. (This was indicated by Davis for his data and is apparent in the data of Harris and Fairthorne.) In selecting a cascade for a fixed bend, it is desirable to

choose the cascade so that ζ [not necessarily C_D--see Eq. (8)] will be a minimum. In a variable bend, such as might occur in a turbomachine, it is essential to select a cascade which will give an unstalled cascade line long enough to cover the anticipated range of operation, minimum loss being a secondary although important consideration. For flow straighteners, a horizontal cascade line in the diagram (β_2 = constant) is required, and again a fairly long unstalled length is desirable.

Given sufficient cascade lines to cover the entire diagram of Fig. 5, together with the variation of drag coefficient along those lines, it would be possible to select efficient cascades for any operating condition. Data to cover Fig. 5 are still very fragmentary, however. As already indicated, there have been a great many solutions, both theoretical and experimental, for two-dimensional cascades, but most of these have been confined to one point on the diagram of Fig. 5. Work has been devoted to finding the best cascade for some given condition of deflection and velocity ratio, and no effort has been made to find the range of conditions for which the cascades investigated would be suitable. The present experimental work falls in the former category. Useful experimental data from two sources have already been cited, and perhaps mention should also be made of a mathematical solution by Resnick and Green [10] wherein the parameters in a simplified form of Eq. (11) were determined and were found to agree reasonably well with experimental data. It would be useful if two-dimensional cascade data obtained in the future were correlated on the basis of Fig. 5 and Eq. (11).

A question arises as to the effects of changes in Reynolds number, surface roughness, and scale of turbulence on the curves in Fig. 5a. It seems reasonable to believe that these parameters should have a primary effect in determining the unstalled length of the cascade line and the drag, but that within the unstalled region of each line there should be no effect on the deflection or velocity ratio.

III. EXPERIMENTAL TWO-DIMENSIONAL AND THREE-DIMENSIONAL HEAD LOSS MEASUREMENTS IN A 90° BEND

A. Scope of the Experimental Work

The main purpose of the present study, as already indicated, was the determination of the influence of secondary currents on the primary two-dimensional flow through guide vane cascades. For this reason, no extensive experimental program was undertaken to fill in the diagram in Fig. 5a. Rather, the experimental work was confined to one point of the diagram in order to keep the number of factors influencing the flow to a minimum. This point is $V_2/V_1 = 1.0$, $\Delta = 90^\circ$ (the 90° miter bend). Several cascades satisfying this condition have been investigated experimentally, both in the two-dimensional region and in the region affected by secondary currents. The present section describes this experimental work in detail.

The experimental program is a continuation of the work reported in reference [3]. Some of the material and diagrams from reference [3] are repeated here for completeness. In particular, the cascades which satisfied the condition $V_2/V_1 = 1.0$, $\Delta = 90^\circ$ have been taken from that reference.

It might be noted that the cascade line for one of the Harris and Fairthorne cascades plotted in Fig. 5a passes through the point $V_2/V_1 = 1.0$, $\Delta = 90^\circ$. This cascade has such small camber, however, that it would stall before reaching such a large value of Δ. The cascades of the present program had larger camber so that they were able to operate efficiently at the required conditions.

B. Experimental Equipment

Only three of the vane shapes studied in reference [3] were adopted for the present program. Two of these were plate vanes (0.050-in. sheet brass) of the NACA four-digit series with the first "digit" consisting of two numbers, and the third was a thick vane (extruded aluminum) made up of circular arc sections. Profiles of the vanes are shown in Fig. 6. The plate vanes were designated (30)400 and (21)300, and the thick vanes Type I. The Type I vanes were shaped to provide gaps of uniform width between the surfaces of two adjacent vanes. The Type I vanes were available in one chord length only, while the (21)300 were available in two chord lengths and the (30)400 in three chord lengths. The vane surfaces were given no special finish. The trunnions

of the vanes were located so that the leading edges of the vanes would be approximately 1/3 chord length upstream of the miter line when the vanes were installed in the test bends. The (21)300 vanes of 2.83-in. chord length were provided with an alternate set of trunnions which could be used to place the vanes approximately 1/10 chord length further downstream. Not shown in Fig. 6 are pressure taps provided in the walls of several of the thick vanes.

The present data were taken in a small, non-recirculating wind tunnel, one form of which is shown in Fig. 7. The duct cross section was 6 by 9 in.; either dimension could be oriented in the plane of the bend. The tunnel was made up of duct sections of various lengths which could be assembled to obtain a range of tunnel lengths both before and after the test section. The arrangement shown in Fig. 7 is the one usually used, and its dimensions are given in Fig. 8. The duct sections were made of 16-gage galvanized steel and were stiffened at intervals with steel frames. At intervals the duct walls were perforated with piezometer taps and with holes for inserting pitot cylinders. These measuring sections permitted total head and flow direction surveys to be made across the duct. They are designated for future reference by the letters E-E, J-J, L-L, M-M, etc., as shown in Fig. 8.

Test sections were interchangeable. Three were actually provided. Two of these were 90° bends, one 9 in. high and the other 6 in. high. The bend walls parallel to the vanes were made of 0.050-in. sheet brass bent on circular arcs. The walls perpendicular to the vanes were of 1/2-in. Lucite plate and were interchangeable between the two 90° bends. The brass walls were fitted with piezometer taps and in the 6-in. high bend with holes for inserting a pitot cylinder at various short distances and heights behind the vanes. The Lucite walls were provided with trunnion holes for the vanes, piezometer holes, and slots at various distances downstream from the trunnion holes for traversing a pitot cylinder behind the vanes. The 90° test bends are sketched in Fig. 9, and Fig. 10 is a close-up photograph of the 9-in. high bend in place in the tunnel.

The trunnion holes in the Lucite plates were relocated from time to time as the vane spacing of the individual experiments required. The vanes were located in the bends by their trunnions, whose positions are indicated in Fig. 6, and by setting the stagger angle of each vane individually from a protractor laid on the top Lucite plate. It was later discovered that some of the data were influenced by what appeared to be a slight angular misalignment among the vanes of the cascade.

The third test section was a straight section of the same length as the center-line length of the bend sections. It was constructed of the same materials as the 90° bends and was provided with piezometer taps and traversing slots at corresponding positions. The straight test section is sketched in Fig. 11. Test sections of any deflection other than 90° may be added to the apparatus in the future.

A suction type tunnel was chosen to permit study of the secondary-current effects downstream of the vanes while keeping turbulence and entrance problems to a minimum. On an earlier part of the program, a pressure type, non-recirculating, combined water and air tunnel was used for experimental work. This apparatus has been described in reference [3]. It was of 6- by 6-in. cross section and had many of the features of the present tunnel, except that the bend and duct walls between the contraction and diffuser were entirely of Lucite.

Pitot cylinders were used for obtaining total head and direction measurements. A 1/8-in. cantilevered cylinder was used in the traversing slots and a 1/4-in. long cylinder elsewhere. The 1/8-in. cylinder and its traversing carriage are shown in Fig. 12; the same cylinder with traversing head removed is shown in place of the 90° bend in Fig. 10. The 1/4-in. cylinder and other instruments used are described in reference [3]. Where it was not convenient to insert pitot cylinders, flow direction was estimated by holding short threads in the flow. These were carried to the desired point through small hypodermic needles inserted through piezometer taps or, in some instances, were cemented to the vane or wall surfaces. Surface coatings were also used to obtain flow directions at the boundaries, particularly in the earlier work; these are described in reference [3]. The piezometer taps already mentioned were used for determining static head on the walls. Internal static head was obtained using a static tube oriented in the flow direction.

Manometer lines from the pitot cylinders and static orifices were led to one side of the inclined manometer, which is identified in Fig. 7. The other side of the manometer was connected to four manifolded piezometer taps, one located on the center line of each duct wall just downstream of the bell-mouthed entrance. Thus, all heads were measured relative to the head at this reference section. Alcohol and water were used in the manometer at different times. Experimental readings on the manometer were reproduceable within

0.01 to 0.02 in. of water in a dynamic head of about 3.00 in. of water, except in the vane wakes. The four manifolded taps were also connected to another manometer which was open to the atmosphere. This manometer was calibrated and was used for establishing the flow rate in the tunnel. Lines for the pitot cylinders were also led to a V-shaped manometer which was used in balancing heads to obtain flow direction. The "V" manometer is also identified in Fig. 7. Directions could be determined and reproduced within 1° except in fluctuating regions of the flow.

C. Experimental Data

Experimental measurements consisted of surveys for total head and flow direction in various cross sections behind the vanes, and at the corresponding cross sections with the straight test section in place. Static head surveys on the tunnel walls were also made for each experimental run, and internal static head surveys were made for one run of the present experiments and for several of the earlier experiments. On the remaining runs, internal static head variations were ignored and the wall static head was used throughout the cross section. Figure 13 shows a static head survey at 0.5 chord behind the vanes and indicates a maximum variation of 2 per cent of the dynamic head. Further downstream the variation was less.

Complete surveys for total head and flow direction were made at station M-M for most cascades, and at some of the other measuring stations and at the slots 0.5 chord length behind the vanes for some of the cascades. Many of the surveys at the measuring stations were obtained in the 6- by 6-in. duct; the remainder and those taken from the slots were obtained in the 6- by 9-in. tunnel with either 6-in. or 9-in. high test section. Partial surveys at the slot 0.5 chord length behind the vanes were made for most of the cascades. These covered half the span and one or two of the central vane spaces in the 6- by 9-in. tunnel using both 6-in. and 9-in. high bends. Surveys were also made for all the cascades in the two-dimensional region of the 9-in. high tunnel, principally at 0.5 chord length behind the vanes, but also at 0.0, 0.1, 1.0, and 2.0 chord lengths behind the vanes. Since the surveys were symmetrical about the central plane of the bend, many of the data in the present experiments (other than two-dimensional) were taken on one side or the other of the central plane of the bend.

All of the data were obtained at the single Reynolds number based on vane chord $Re_c = 1.5 \times 10^5$; the maximum approach velocity V_1 was used as reference velocity. It had been determined earlier in the 6- by 6-in. tunnel that the performance of a cascade was the same in air and water if the Reynolds number based on chord length was constant, and that only the head loss varied (and that slightly) when the Reynolds number was varied over a range from about 0.5 to 4.0×10^5 [3]. The duct Reynolds number Re_d varied, of course, as vanes with different chord lengths were used. The duct Reynolds number was based on the hydraulic diameter of the test section (7.2 inches in the 6- by 9-in. section) and the average approach velocity. It ranged from about 2.0 to 5.5×10^5, and V_1 (in air) ranged from about 50 to 140 fps. Local velocities, of course, exceeded 140 fps, but no compressibility effects were anticipated.

Typical results of total head and flow direction surveys are shown in Figs. 2, 3, and 14 to 24, inclusive. In the figures, the total heads have been made dimensionless, for plotting purposes only, by dividing by the static head measured at the reference manifold; this was approximately equal to the dynamic head of the mean flow and eliminated variations due to minor changes in tunnel speed. Flow directions were measured in the plane of the bend at all points where total head was read. These points are indicated on Figs. 15 to 23, inclusive, by secondary-flow arrows or by dots where the flow was parallel to the downstream tangent. In the planes normal to the plane of the bend, directions were obtained for only some of the runs as indicated on the figures. In preparing these figures, all data were plotted in the upper half of the duct only; where data were available from both upper and lower halves, average values were plotted.

Figure 2a was obtained with the straight test section in place, using the tunnel arrangement otherwise shown in Fig. 7; it corresponds to a section closely behind the vanes in the bend. Figures 14a and 14b were obtained with the same tunnel arrangement at sections corresponding to the miter line and to station M-M, respectively. Although Re_d is different for each of these three total head diagrams, the Reynolds number effect is small enough that the diagrams may be compared. The tunnel arrangement of Fig. 7 was used to obtain most of the data, and Fig. 14a may be considered as typical of the entrance conditions at the vanes in this tunnel. Figures 2b, 2c, 3, and 15 to 21, inclusive, represent data obtained using this tunnel arrangement. Pertinent information is given on the figures.

Some data were also obtained with a 7-3/4 ft added length of duct between the bell-mouthed entrance and test section of the 6- by 9-in. duct. Figure 22a shows the total head distribution in the straight duct, and Fig. 22b shows a partial survey behind the vanes for that tunnel arrangement. Another entrance condition was established by installing a splitter plate whose leading edge was just upstream of the vane leading edges in the tunnel arrangement of Fig. 7. The arrangement of the plate and the resulting survey just behind the plate are shown for the straight duct in Fig. 23a and for the bend in Fig. 23b.

The total head distribution in the 6- by 6-in. tunnel at 15 in. upstream of the miter line is shown in Fig. 24a and at station M-M with one of the cascades in place in Fig. 24b. The reference station is located differently in this tunnel than in the 6- by 9-in. tunnel, consequently the total heads read on the differential manometer have a different zero. For plotting purposes, however, these data have been reduced to the same zero as the previous data.

Figures 25 and 26 are typical of the flow direction data obtained visually and photographically. Except for Fig. 25b, these photographs were obtained in the 6- by 6-in. tunnel.

With the object of obtaining energy loss per unit volume or head loss per unit weight, the total head data obtained from each survey were reduced to an average total head by the formula

$$\overline{h_t} = \frac{\Sigma\, h_t \sqrt{h_t - h_s}\, \cos\alpha\, dA}{\Sigma \sqrt{h_t - h_s}\, \cos\alpha\, dA} \qquad (14)$$

where $\overline{h_t}$ is the average total head,

h_t is the total head at each point,

h_s is the static head at the point where h_t is taken and is obtained by interpolation from static head measured at the wall,

$\cos\alpha$ is the cosine of the angle formed between the local velocity vector and the downstream duct direction, and

dA is the increment of area to which h_t applies and is determined by the spacing of the h_t readings.

It should be noted that the measured total head in the plane of the bend does not always yield the correct value for h_t. Where the flow makes an appreciable angle with the plane of the bend, $h_t - h_s$ is the measured difference in head divided by the cosine squared of that angle [11], and h_t is the latter value plus h_s.

It was a difficult matter to determine h_s accurately on the walls closely behind the vanes because of the varying proximity of the vanes to the piezometer taps. However, at the measuring points in a cross section where the dynamic head was large, errors in h_s had a negligible influence on h_t. At the few measuring points where the dynamic head was small and of the same order as the error in h_s, the error in h_t was large, but the relatively inaccurate small values of h_t contributed very little to $\overline{h_t}$. It is believed that the values of $\overline{h_t}$ are correct within 2 per cent or less of the average dynamic head.

The head loss attributable to the guide vanes was taken as the difference in average total heads at corresponding distances from the entrance in the straight duct and in the duct containing the bend. A head loss coefficient ζ was then defined by Eqs. (9) and (10) in the form

$$\zeta = \frac{\overline{h_t}' - \overline{h_t}}{V_1^2/2g} \tag{15}$$

where $\overline{h_t}'$ is the average total head in the straight duct,

$\overline{h_t}$ is the average total head [defined in Eq. (14)] behind the vanes, and

V_1 is the approach velocity in the two-dimensional region, as before.

The head loss coefficient was computed for several different conditions. These are

ζ_2--based on surveys in the two-dimensional region only. The coefficient ζ_2 was determined from measurements in the 6- by 9-in. tunnel using the 9-in. height.

ζ_3--based on surveys covering the vane span and one or two vane spaces at 0.5 chord length behind the vanes. The coefficient ζ_3 was determined in the 6- by 9-in. tunnel with the test sections both 6 in. and 9 in. high.

ζ_b--based on surveys covering the cross section at 0.5 chord length behind the vanes in the 6- by 9-in. tunnel.

ζ_m--based on surveys covering the cross section at Station M-M. Both the 6- by 6-in. and 6- by 9-in. tunnels were used to obtain ζ_m.

Similar subscripts were applied to values of $\overline{h_t}$ and $\overline{h_t}'$. These definitions are illustrated in Fig. 27.

In the form shown, Eq. (15) is not suitable for accurate determination of the coefficient ζ from the measured data. The values of $\overline{h_t'}$ and $\overline{h_t}$ are determined quite accurately, as already noted, but the value of V_1 to be used is difficult to determine. First, there is the problem of jet contraction which causes V_1 to increase as the flow passes down the duct because of boundary layer growth. For these studies, V_1 was arbitrarily defined as that maximum velocity which would exist at the miter line of the bend if there were no bend. Thus, V_1 could be measured readily in the straight test section but could only be inferred in the bend test section from measurements either farther upstream or in the straight test section. The latter method of determining V_1 in the bend was adopted because of the second difficulty--the difficulty of determining h_s accurately near the guide vanes. Thus, Eq. (15) was given the form

$$\zeta = \frac{h_t'}{V_1^2/2g}\left(\frac{\overline{h_t'}}{h_t'} - \frac{\overline{h_t}}{h_t'}\right) \tag{15a}$$

where h_t' is the total head of the central stream filament upstream of the test section. The value of h_t' was measured at frequent intervals during each survey. The ratio $h_t'/(V_1^2/sg)$ is characteristic of the tunnel for each duct Reynolds number and was obtained in the straight duct.

The coefficient ζ_2 was reduced to a drag coefficient C_{D_2} by means of Eq. (8) wherein for the present conditions

$$C_{D_2} = \zeta_2 \frac{s}{c} \tag{16}$$

The flow direction data did not lend itself to reduction in as direct a manner as the total head data. The principal value of the direction measurements lay in establishing the secondary-current pattern downstream of the cascades. No attempt is made at this point to evaluate this secondary current numerically in terms of vorticity or circulation. It is to be observed that at the station M-M, the flow direction in the interior is parallel to the downstream tangent, except for random variations. At the duct walls normal to the vane spans, however, there is still some evidence of the secondary flow even this far downstream.

The flow direction data alone are not useful in determining whether or not the cascades are making the proper turn (see p. 5). This was determined principally by inference from static head distribution measurements across the duct upstream of the vanes and by comparing pressure distributions on the thick vanes. Flow direction measurements upstream and downstream, static head measurements around the bend, and some other measurements were used as secondary checks. Methods of determining proper stagger angle for a given three-dimensional duct deflection are discussed at some length in reference [3] and, incidentally, are corroborated by Salter [12]. It is believed that errors in stagger angle of as little as 1° for the 90° average deflection produced in the present experiments could be detected by the methods used.

D. Experimental Results

1. Stagger Angle

The cascades which satisfied the condition $\Delta = 90^\circ$, $V_2/V_1 = 1.0$ are shown in Fig. 28. This figure, except for some experimental points which have been added from the present program, is reproduced from reference [3]. The figure is discussed in that reference.

It should be noted that these data were actually obtained in three-dimensional bends. However, by variation of chord length, vane spacing, and duct height, a range of chord aspect ratios from about 1 to 4.5 and of space aspect ratios from about 2 to 9 were represented in the figure. Within the limits of the experimental errors, these variables appear to have no influence on the straight lines of Fig. 28. The same variables do influence the head loss coefficient, as will be shown presently. It has therefore been concluded that the stagger angles shown in Fig. 28 would also apply to two-dimensional cascades.

2. Two-Dimensional Head Loss Coefficients

The two-dimensional head loss coefficient ζ_2 is plotted against spacing-chord ratio s/c for each cascade in Fig. 29a. Smooth curves have been drawn through the plotted points for each vane shape. Where only one point is plotted for a given cascade and s/c, that point represents data obtained at 0.5 chord length behind the trailing edges of the vanes and in the central or one of the two central spaces of the cascade. Where more points

are plotted, the additional points are usually from additional spaces or sometimes from other distances behind the vanes. The scatter is well within the limits of experimental error, but it is believed that some of the scatter is attributable to small errors in angular setting. Two curves have been drawn for the (21)300 vanes. It is to be noted that ζ_2 is independent of chord length. The curves of ζ_2 have been converted to curves of C_{D_2} by Eq. (16) and the latter curves are plotted in Fig. 29b.

The trends exhibited by the ζ_2 and C_{D_2} curves are best explained in terms of C_{D_2}. The C_{D_2} curves for each shape show a minimum at a particular value of s/c (and θ). As s/c and θ increase, stalling is approached and C_D increases. As s/c is decreased, θ also decreases at first, and again stalling approaches. However, below a certain value of s/c, as may be seen from Fig. 28, θ becomes constant and the tendency toward stalling is arrested. Slight increases in C_D thereafter may be attributed to local velocity increases caused by vane thickness.

The split curve of the (21)300 vane shape may be explainable as a transition phenomenon. The lower curve may represent data from boundary layers in which transition occurs without separation, while the upper curves may represent data from boundary layers exhibiting laminar separation followed by reattachment. The two curves rejoin where the boundary layer is entirely turbulent. Shifting the cascade position in the bend apparently influences the type of boundary layer. The boundary layer on this vane shape was not studied, but in connection with the work of reference [3], some boundary layer studies on a thick vane built on the same mean line did show a tendency at some spacing-chord ratios toward laminar separation followed by turbulent reattachment. A similar phenomenon occurred for the Type I vane cascade shown in Fig. 26a.

It is to be noted that the minimum values of ζ_2 occur at slightly higher values of s/c than the minimum for C_{D_2}. Also, the minimum ζ_2 is less for the (30)400 vane than for the thick vane, even though the minimum C_{D_2} of the former is greater than the latter. Of course, neither the thick nor thin vane cascades necessarily represent the optimum in low head loss coefficients.

3. Three-Dimensional Head Loss Coefficients

The head loss coefficients ζ_3, ζ_b, and ζ_m are plotted against spacing-chord ratio s/c in Figs. 30a, 30b, and 30c for the three vane shapes. The tunnel used for each data point is indicated in the figures; data shown in this figure for the 6- by 9-in. tunnel were obtained using the entrance condition of Fig. 14a, only. It is to be remembered that ζ_3 and ζ_b were determined at 0.5 chord behind the trailing edges of the vanes and that ζ_m was determined at 30 in. downstream from the miter line (4+ duct hydraulic diameters, 6.25 chord lengths behind the long chord vanes, or 14 chord lengths behind the short chord vanes).

For comparative purposes, values of ζ_2 integrated over the 9-in. span and one vane space and integrated over the duct cross section are also plotted in Fig. 30. The integration was accomplished by the formula

$$\zeta_2 \text{ (integrated)} = \zeta_2 \int \left(\frac{V}{V_1}\right)^3 dA \Big/ \int \left(\frac{V}{V_1}\right) dA \qquad (17)$$

where V is the local approach velocity, and the integrals are taken over the vane span or over the entire cross section as the case may be. In the integration, it has been assumed that ζ_2 may be taken as constant over the cross section. Actually, ζ_2 varies with Reynolds number Re_c; however, for the entrance conditions used in these experiments there is little change in Re_c except close to the walls, and this region contributes so little to the integral that the assumption is unimportant.

The substantial differences between the various three-dimensional and integrated two-dimensional head loss coefficients are immediately apparent. There are also substantial differences within the data for ζ_m, but of these differences only those attributable to variation in chord length appear to follow a definite pattern. There is a definite decrease in ζ_m at any given s/c as the chord is lengthened. Salter [12] reports a similar influence of chord length. Chord length has apparently no influence on ζ_3.

The experimental errors in ζ_3, ζ_b, and ζ_m are greater than in ζ_2 since the former involve differences in average total heads, each of which is itself subject to an error of as much as 2 per cent of the dynamic head. Aside from experimental error, variations in ζ_m can be attributed to the different tunnel configurations which were used, and those in ζ_3 to small misalignments in angular setting of the vanes.

Smooth curves have been drawn through the data for ζ_3 and for ζ_m for each chord length as an aid to the eye in surveying the data. The data tend to follow the two-dimensional head loss curves surprisingly well. The ζ_b points fall somewhat above the ζ_3 curves but far below the ζ_m curves. Evidently the differences between ζ_b and ζ_3 indicate the effects of the lateral walls and their boundary layers. Comparison of the ζ_b points with the ζ_m curves indicates that a large part of the loss attributable to the guide vanes occurs downstream from the vanes.

The differences between ζ_3 and the corresponding integrated value of ζ_2 (designated ζ_i) have been plotted in Figs. 31a, 31b, and 31c, while the differences between ζ_m and ζ_2 integrated over the cross section (designated ζ_t) have been plotted in Figs. 32a, 32b, and 32c. The integrations of ζ_2 for these figures have been performed over the appropriate area in each case. In Fig. 31, data obtained from the altered velocity profile produced by the added entrance length are included with that from Fig. 30 and are distinguished by separate symbols. The points plotted in these figures are the small differences of two already small quantities and they scatter badly. Based on a possible 2 per cent error in the original average total heads, ζ_i and ζ_t may have errors as large as 6 per cent of the dynamic head --that is, absolute errors of 0.06 in ζ_i or ζ_t.

Considering these large possible errors, it is impossible to establish a trend in the ζ_i plots. If there is any trend, it is for ζ_i to remain constant with both spacing-chord and aspect ratio; it may vary slightly with vane shape. In any event, ζ_i is considerably smaller than ζ_t.

The values of ζ_t shown in Fig. 32 do not show too definite a trend either. Lines have been drawn indicating a decrease of ζ_t with increasing spacing-chord ratio for the thin vanes, but lines with the opposite trend could have been drawn through some of the data. Values of ζ_t do remain relatively constant for the thick vanes. The available data for the thin vanes are somewhat better correlated in Fig. 33 where an apparent decrease in ζ_t with decreasing number of vanes in the bend is shown. Of course, when the number of vanes is too few, separation effects at the lateral walls cause ζ_t to rise sharply again; such separation was actually observed at the outside bend wall in some of the cascades containing only four vanes. The decrease of ζ_t with decreasing number of vanes is consistent with the observation that at a given spacing-chord ratio, the loss is less if longer chord vanes

are used. For the Type I vanes (which were designed with constant gap between the vanes), there was little variation of ζ_t with number of vanes, and this may indicate that there would be little variation with chord length; experimental proof is not at hand. The thin-vane data are even better correlated if for abscissas in Fig. 33 the number of vane spaces divided by duct cross-sectional area is used. This has been done in Fig. 34 where the abscissa is now the reciprocal of the passage area.

The variation of the difference in three-dimensional and two-dimensional head loss coefficients with distance of the measuring station downstream from the vanes is shown in Fig. 35. The loss coefficient increases at a decreasing rate and should reach a constant value at or before the station where ζ_t is measured. The same effect is shown in another manner in Fig. 36 where average total heads have been plotted against distance. (In this figure only, average total heads have been made dimensionless based on dynamic head of the mean flow where the mean flow was obtained by integration over the cross section.) It is to be noted that beyond station M-M in Fig. 36, the rates of loss have approached those in the straight duct; the decision to use ζ_m as a measure of the total loss in the three-dimensional bend was based on this fact. Had station P-P or some other station beyond M-M been used for this purpose, the values of ζ_t would have been altered only slightly.

4. Velocity Profiles

Experimental data have been reduced to typical velocity profiles in Figs. 37, 38, and 39. (In these figures, the velocity u is the magnitude of the velocity vector at each point while V_1 is the maximum approach velocity.) In Fig. 37a, the approach profiles normal to the duct walls are seen to follow the logarithmic law. Downstream of the vanes the velocities are higher near the wall than they are upstream and gradually approach the upstream values as the distance beyond the vanes increases. The diamond-shaped points represent data at station M-M; the velocity here is seen to have returned closely to its upstream value. Profiles parallel to the duct wall, taken over one vane space, are shown in Fig. 37b. At both 1/16 in. and 1/8 in. from the wall, the profiles are quite similar (for this cascade) at 0.5 and 1.0 chord behind the vanes, but at 2.0 chord behind the vanes, the profile at 1/16 in. from the wall shows the influence of boundary layer growth very strongly. This boundary layer growth is associated with a higher rate of energy loss than in the fully developed flow in a straight duct and must be related to the head loss curves of Figs. 35 and 36.

Figures 38a, 38b, 38c, and 38d also show velocity profiles in the boundary layer similar to those in Fig. 37b. These profiles are presented in an attempt to correlate the velocity profiles with the trends in ζ_t shown in Figs. 32 and 33. In Fig. 38a, profiles for two other cascades of (30)400 vanes with longer chord lengths are compared with the profiles of Fig. 37b; one of the cascades has approximately the same spacing-chord ratio while the other has the same spacing or number of vanes. In Fig. 38b, three (21)300 cascades, one of one chord length and the other two of another chord length, are compared with each other; these were selected so that there are two cascades having the same spacing-chord ratio and two having the same spacing. In Fig. 38c, three cascades of Type I vanes, all of the same chord length but with three different spacing-chord ratios and spacings, are compared with each other. In Fig. 38d, velocity profiles obtained from cascades of 6-in. span are compared with those obtained from cascades of 9-in. span for the three vane shapes.

The comparisons are not too conclusive, but it is believed the following points may be drawn:

a. In Fig. 38c, the profiles closest to the vanes in terms of spacing have the higher velocities. This is also true in Fig. 37b. If the Type I vane profiles in Fig. 38c had been compared at the same distance behind the vanes in terms of spacing, they would have been more nearly identical--possibly exactly so.

b. On the other hand, if the profiles for the (21)300 vane cascades of Fig. 38b were adjusted in accordance with point (a) above to the same relative distance behind the vanes in terms of spacing, the cascade with the smaller spacing would have the higher boundary layer velocities. The opposite would be true for the (30)400 vane cascade profiles of Fig. 38a.

c. The preceding points appear to be associated with the values of ζ_t plotted in Figs. 32 and 33. The Type I vanes show approximately constant ζ_t and also nearly constant boundary layer velocity at the same relative distance in terms of spacing downstream of the vanes. The plate vanes generally show a decrease in ζ_t with decreasing number of vanes (or increasing spacing); the (21)300 vane data show a decreasing boundary layer velocity with increasing

spacing. At the spacing of 2.075 in., the (30)400 vanes showed an increase in ζ_t in Fig. 33 (because of separation at the wall), and an increase in boundary layer velocity in Fig. 38a.

d. Figure 38d shows a general tendency for the 6-in. span cascades to produce a higher velocity near the boundary than the 9-in. span cascades. To some extent Fig. 33 indicates that for the same spacing (not the same number of vanes) ζ_t is larger for the 6-in. than for the 9-in. span cascades.

e. Considering all the above points, the thesis is made that ζ_t is directly related to the boundary layer velocity profiles measured immediately downstream of the vanes. These profiles, in turn, are determined principally by the vane shape, vane spacing, and probably also by the deflection and velocity ratio of the cascade $\left[C_L/(s/c)\right]$ in Fig. 5 and entrance velocity profile. It may also be true that for vanes having constant gap width, vane shape is no longer a factor; if this is true, the effect of vane shape is measured by the relative change in gap in passing through a vane space.

Figure 39 again presents profiles taken parallel to the duct wall and across one vane space, but these profiles represent data in the interior of the flow passing through the "hole" in the total head pattern. The distance from the wall of 0.7 space (the normal distance between vane wakes) best represents the location of the center of the "hole" for most of the data. The profiles are grouped by vane spacing in the figure, but this grouping should not be interpreted as indicating that the dimensionless profiles depend on the spacing. Since most of the data were taken at 0.5 chord behind the vane trailing edges, the three parts of Fig. 39 actually represent data for three different distances behind the vane trailing edges in terms of spacing. For the 2.83-in. chord vanes, for example, the profiles in Figs. 39a, 39b, and 39c were taken at approximately $1/2\sqrt{2}$, 1, and $\sqrt{2}$ spaces, respectively, behind the vanes. The closest profiles show the steepest gradient, as would be expected. In Fig. 39c, data taken for a 2.02-in. chord vane at about $\sqrt{2}$ spaces behind the vanes but with a spacing of 1.414 in. is seen to group reasonably well with other data taken at the same relative distance behind the vanes but at the lesser spacing of 1.04 inch.

Examination of the velocity profiles indicates that the three-dimensional surveys would better have been taken at, say, 1 space behind the vanes instead of 0.5 chord. This was not apparent before the experimental work was begun and would have been difficult to provide for in the experimental apparatus. It is believed that the interior velocity profiles would be closely similar if compared at a distance behind the vanes fixed in terms of vane spacing, but that the boundary layer profiles would probably vary with spacing, the larger spacings exhibiting the smaller velocities except when separation interferes.

E. Extension to Other Bends

Finally, it must be noted again that these experimental data pertain to a bend of rectangular cross section with $\Delta = 90^{\circ}$, $V_2/V_1 = 1.0$. In a recent visual study of secondary currents by Hansen, Costello, and Herzig [13], it is brought out that the intensity of the secondary current varies with certain cascade characteristics; these characteristics can be related to the deflection angle Δ and the velocity ratio V_2/V_1, and thus to $C_L/(s/c)$ through Fig. 5. From the cited reference, it is inferred that the secondary-current intensity is directly related to $C_L/(s/c)$. It is seen, then, from Fig. 5 that secondary currents in compressor cascades would be less intense than in the present experiments, but that turbine cascades would have secondary currents of about the same (somewhat more or less) intensity. The relation of secondary-current strength to the ratio $C_L/(s/c)$ forms the basis for the statement in Section 4 of Part D (p. 22) that boundary velocity profiles downstream of the vanes probably depend on $C_L/(s/c)$.

The influence of a circular or other shaped cross section on the results obtained is not known, but it is supposed that the principal effect would be on the minimum number of vanes for small head loss in a plot like that shown in Fig. 33.

IV. SECONDARY FLOW

A. Origin of the Secondary Flow

As already indicated in Parts I and II, the primary or two-dimensional flow in a guide vane bend is determined by the flow boundaries alone. It was shown in Part III from experimental results, that for practical purposes the general flow pattern far downstream of the vanes is not influenced by the three-dimensional nature of the flow and that, therefore, the two-dimensional deflection could be taken as the three-dimensional deflection. On the other hand, the two-dimensional head loss is only a nominal part of the total head loss in a three-dimensional bend. The difference between the three-dimensional and two-dimensional head loss coefficients in a bend must be attributable to the secondary flow which is superimposed on the two-dimensional flow. It is therefore desirable to examine this secondary flow and to determine its relation to the head loss.

An exact determination of the secondary flow would involve solution of the Navier-Stokes equations, together with an accounting for the effects of turbulence in the duct approaching the vanes and in the vanes. Such a solution would be exceedingly complicated if not impossible. Mager and Hansen [14] have discussed this matter and have obtained an approximate solution in laminar flow for certain assumed conditions. Approximate solutions can be obtained in another form by neglecting viscosity and turbulence in the bend and solving the nonviscous equations of motion. In this form of solution, the experimental or computed boundary layer velocity profile at the beginning of the bend represents the effects of viscosity and turbulence upstream of that point. The flow downstream of the entrance is then determined both by the boundary conditions and by the entrance velocity profile. This type of solution has been obtained by Hawthorne [15] for a single bend and by Squire and Winter [1] for a guide vane bend. A short form of solution is presented here for convenience in further discussion.

For steady incompressible flow, the equations of motion in Helmholtz' form are

$$\vec{q} \cdot \nabla \vec{\Omega} = \vec{\Omega} \cdot \nabla \vec{q} \qquad (18)$$

where $\vec{q}$ is the vector velocity and $\vec{\Omega} = \nabla \times \vec{q}$ is the vector vorticity [16]. If an orthogonal curvilinear coordinate system is so chosen that one axis

lies along a streamline of the basic two-dimensional flow and another along the instantaneous radius of curvature $\vec{r}$ of that streamline, unit vectors i_1, i_2, and i_3 are defined by

$$i_1 = \frac{\vec{q}}{q}, \quad i_2 = -\frac{\vec{r}}{r}, \quad i_3 = i_1 \times i_2$$

The sides of an elementary rectangular parallelepiped in this coordinate system are designated $i_1 ds = i_1 r d\theta$, $i_2 dn$, and $i_3 dz$. Since the flow in the bend is not, in general, two-dimensional, $\vec{q} = i_1 u + i_2 v + i_3 w$, but at the beginning of curvature, $\vec{q} = i_1 u\,(n, z)$. The vorticity is

$$\vec{\Omega} = i_1 \xi + i_2 \eta + i_3 \zeta = i_1 \left(\frac{\delta w}{\delta n} - \frac{\delta v}{\delta z}\right) + i_2 \left(\frac{\delta u}{\delta z} - \frac{\delta w}{\delta s}\right) + i_3 \left(\frac{u}{r} - \frac{\delta u}{\delta n} + \frac{\delta v}{\delta s}\right) \qquad (19)$$

where ξ is the component along a streamline of the two-dimensional flow. At the beginning of curvature, $\xi = 0$, $\eta = (\delta u/\delta z)$, and $\zeta = (u/r - \delta u/\delta n)$. Writing the component of Eq. (18) in the i_1 direction, there results

$$\frac{1}{r}\frac{\delta}{\delta\theta}\left(\frac{\xi}{u}\right) = \frac{\delta}{\delta s}\left(\frac{\xi}{u}\right) = \frac{2\eta}{ur} = \frac{2}{ur}\frac{\delta u}{\delta z} \qquad (20)$$

at the beginning of curvature.

Where the streamlines are straight and parallel, as in the approach to a guide vane bend, ξ is zero and remains so even though η and/or ζ are unequal to zero. Even when the streamlines curve, Eq. (20) shows that there is no increment in ξ (the vortex lines remain normal to the streamlines determined by the boundaries) unless there is a velocity gradient normal to the plane of curvature. This is the case in the two-dimensional region of a cascade where the flow is uniquely determined by the boundaries alone. However, when the streamlines are forced to curve by the boundaries and there is a velocity gradient normal to the plane of curvature, the downstream flow pattern is determined not only by the boundaries but also by the existing velocity gradient. The ξ component of the vorticity which develops is associated with the development of flow components v and w producing the secondary flow. The vorticity vector is still normal to the actual streamlines but there is a vorticity component parallel to the streamlines which would have been determined by the boundaries only.

Squire and Winter [1] have integrated Eq. (20), making the further assumptions that (1) the two-dimensional streamlines in the bend are concentric circular arcs parallel to the plane of the bend, (2) the secondary-flow components v/u and w/u, which develop in the boundary layer, are so small that they do not influence the primary potential flow pattern in the bend, and (3) $\eta = \partial u/\partial z$ is independent of θ. Under these assumptions r, the product ur, and therefore u, are constant along a streamline, as is η, and the integral becomes

$$\xi = 2\eta_o \epsilon \tag{21}$$

where η_o is the constant value of η, and ϵ is the angle through which the streamline has turned. By making a further assumption that (4) $\partial^2 u/\partial z^2 = 0$, Squire and Winter go on to compute the secondary flow between the vanes associated with the value of ξ given by Eq. (21) and suggest that there is an energy loss of about half the kinetic energy of the secondary flow.

Equation (21) is adequately descriptive of the formation of secondary currents in a guide vane bend. Quantitative deductions from that equation must be made with caution, however, because of the assumptions involved. More detailed examination of the secondary-flow effects is necessary to obtain reliable results.

B. Detailed Description of the Secondary Flow

Two typical curves of velocity distribution in the boundary layer upstream of the vanes are shown in Fig. 37a. Values of $\eta = \partial u/\partial z$ upstream of the vanes taken from that figure are plotted in Fig. 40. Of course, η does not continue asymptotic to the axes in Fig. 40 but is zero at the edge of the boundary layer and approaches a limiting value in the laminar sublayer at the wall.

If ϵ in Eq. (21) is considered as an incremental turn of the potential streamlines in the boundary layer parallel to the plane of the bend, ξ will be the resulting vorticity along those streamlines. It is seen from Fig. 40 that at 0.005 ft from the wall, the vorticity will be of the order of ten times its value at 0.04 ft after the first small increment of turning. Since η is constant along planes parallel to the plane of the bend upstream of the vanes, ξ will be constant in such planes at first if r is assumed constant. The resulting vorticity components in the potential flow direction

after a small amount of turning in the bend may be visualized as in the adjoining sketch (a). The relative size of each vortex figure is intended to represent schematically the relative strength of vorticity concentrated along each short vortex line normal to the paper. (There are also vorticity components in the plane of the paper.)

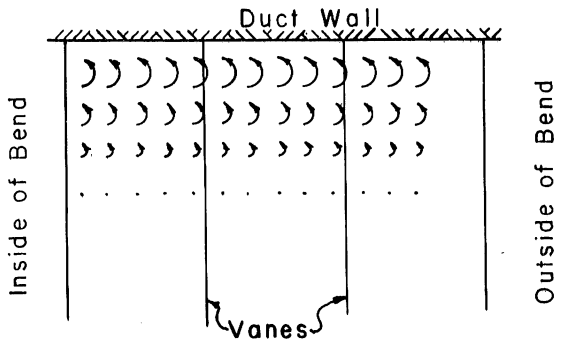

(a) Schematic Vortex Distribution

The flow pattern associated with this vortex distribution is approximately that shown in sketch (b) adjoining. It depends on the vortex system and its image in the duct wall and vane surfaces. The secondary currents along the duct wall can become very large compared to the through-flow velocity near the wall, while a short distance away from the wall it is still true that the two-dimensional potential flow predominates.

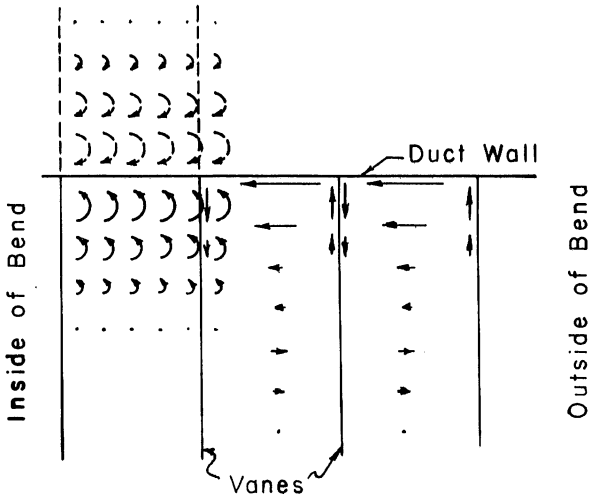

(b) Schematic Secondary-Flow Pattern

The important result of the preceding discussion is not that a secondary flow develops. Rather, it is that the secondary flow is such that the low-energy fluid along the duct wall is swept from the wall, down the suction surfaces of the vanes, and into the interior of the fluid. It is replaced, in turn, by fluid from the interior which is, of necessity, of higher energy content and higher velocity.

Even though the assumptions (1) and (2) of Squire and Winter remain roughly true between the vanes, assumptions (3) regarding the constancy of $\partial u/\partial z$ along a streamline and (4) regarding the constancy of $\partial u/\partial z$ across the boundary layer are considerably at variance with the above reasoning. Nevertheless, additional increments in ξ are still given by Eq. (21) for additional increments in ϵ, and although the magnitude of the increment continually changes (and may even become negative as for some of the profiles in

Fig. 37), sketches (a) and (b) should continue to represent the actual case schematically to the end of the curvature. Beyond that point, no additional vorticity ξ can be generated. Fluid of higher and higher energy and velocity is thus brought to the duct wall between the vanes. (There will be variations near the vane surfaces because r here lies out of the plane of the bend and is far from constant, but these regions are a small part of the total and are ignored.)

Beyond the trailing edges of the vanes, the two vertical currents of the secondary flow near each vane surface meet and are annihilated in a vortex sheet. This vortex sheet is identical with the one which would be deduced from the decrease in circulation along the vane span in the duct boundary layer. The horizontal current near the duct wall continues downstream until it is partially damped by viscosity and some of its kinetic energy is converted to pressure energy by stagnation.

The schematic pattern of sketch (b) was recognizable in all of the experimental data. In Figs. 2b, 15, and 17 to 23, inclusive, the transport of the low-energy fluid from the boundary layer to the interior of the fluid is clearly shown, as is its replacement by high-energy fluid. In Fig. 19a, this motion has been indicated by a large arrow and the location of the vortex sheet has also been indicated. In Figs. 22b and 23b, the effects produced by altered entrance values of η are shown. In the former figure, the entrance boundary layer was thickened from the usual case, but the value of η near the wall was hardly changed, as may be seen in Figs. 37a and 40, so that the resulting flow pattern was unaltered. In the latter, the entrance boundary layer was practically eliminated by the splitter plate, and a marked reduction in secondary-flow effect is observable.

Figures 25 and 26 show even more graphically the close resemblance of the actual secondary flow to that represented in sketch (b). In both Figs. 25a and 26a, for example, threads show the annihilation of the secondary-current component parallel to the span at the trailing edge. In Fig. 25b, the relatively large secondary flow at the duct wall compared with that 1/4 in. away from the wall is obvious. Other photographs in reference [2] show similar effects for a single curved passage. Some excellent photographs showing secondary flows have just been published by the National Advisory Committee for Aeronautics [13 and 17].

The flow in a guide vane bend is summarized schematically in Fig. 41. The two-dimensional potential streamlines in the interior are designated A-A. Two-dimensional boundary layer effects and separation on the vane surface are represented at B. The streamlines which lie along the duct wall upstream and which finally emerge in the vane wakes at some distance from the wall are designated C-C, while C'-C' are streamlines from the interior which form the new boundary layer downstream of the vanes. At D are shown the trailing vortices which are assumed to form from a rolling-up of the trailing vortex sheet.

A short distance downstream of the guide vane bend, the results of the secondary flow are manifest as (1) an unusual distribution of total head, as seen in Figs. 2b, 15, and 17 to 23, inclusive, and (2) a strong current along the duct walls toward the inside of the bend and along the inside wall toward its center, as seen in Fig. 26b. The current along the duct walls can still be detected long after the total head pattern has been rectified.

C. Head Loss Associated with the Secondary Flow

It is now possible to discuss the energy loss or head loss in the flow through the guide vanes. Since the equations of motion for frictionless fluid were used in developing Eqs. (20) and (21), the loss must be inferred from the flow pattern.

First, there is the two-dimensional loss associated with boundary layer development and separation on the vane surfaces. This was discussed in Part II and measured in Part III. In Part III, it was assumed that, ignoring Reynolds number effects, the two-dimensional loss coefficient would be constant over the span. It may be necessary to modify this assumption, however, because of the secondary-flow effect on the separation. Figure 26a shows the effect referred to strikingly, but should not be taken too literally. Actually, the boundary layer reattaches as a turbulent layer in the two-dimensional region after separation and is not too different from that near the span ends. In the case of a radius elbow of aspect ratio unity [4], there was a pronounced effect of the secondary flow on the two-dimensional separation loss and it is probable that there is some effect in the present case, although the aspect ratios of the passages are higher. It would be expected that for a situation like that shown in Fig. 26a, the two-dimensional loss would be less near the span ends than in the interior. This reduction in loss, if it exists, is included in the measured coefficients ζ_i of Fig. 31 and ζ_t of Figs. 32 to 34, inclusive.

Next, there is the direct loss of energy attributable to the dissipation of the secondary flow. A part of the secondary-flow energy goes into the generation of the trailing vortex sheets. The energy of these vortices represents an immediate loss at the trailing edges of the vanes since it is not measurable in a total head survey downstream from the trailing edges and will be dissipated entirely. Carter and Cohen [18] have computed a coefficient of "induced drag" C_{D_i} due to these vortices, obtaining the strength of the vortices from the decrease in circulation about each vane between the two-dimensional region and the wall. Their result may be put in the form

$$C_{D_i} = \frac{1}{2} \frac{s}{c} \left(\frac{C_L'}{s/c} \right)^2 \frac{h}{\ell} \tag{22}$$

where C_L' is the coefficient of lift based on the magnitude of the vector mean velocity in the two-dimensional region,

h is the distance from the duct wall to the center of each rolled-up vortex, and

ℓ is the span of the vanes.

The loss due to C_{D_i} is included in ζ_i of Fig. 31 and ζ_t of Figs. 32 to 34, inclusive.

The remaining energy of the secondary flow is partly dissipated and partly recovered as pressure energy. These parts are not directly estimable, but the dissipated part may be included with the loss discussed in the next paragraph.

There is still another source of energy loss. Loss results from the increased wall shear (and also new vortex sheets in the interior) created by the redistributed total head pattern behind the vanes. The secondary flow downstream of the vanes contributes to this increased wall shear through its contribution to the velocity magnitude at the wall. The loss due to this cause must be very large immediately behind the vanes and decrease with distance until at some point downstream the total head distribution resembles approximately that existing at the entrance to the vanes. Beyond this point, the loss due to wall shear is that attributable to the straight duct only. Figures 35 and 36 indicate the rate of head loss with distance downstream of the vanes. The greater part of the measured loss due to added wall shear is included only in ζ_t (Figs. 32 to 34) and not in ζ_i (Fig. 31) since the new boundary layer development is barely apparent at the slot 0.5 chord downstream of the vanes as shown in Fig. 37b.

The coefficient ζ_i of Fig. 31 (measured 0.5 chord downstream of the vanes) is now seen to include the effect of the secondary flow on the two-dimensional loss coefficient (negative) and the induced drag of Carter and Cohen (positive), together with some small part of the additional wall drag. If Eq. (22) of Carter and Cohen is applied to the present experiments, $C_L' = 2C_L$ and $C_L/(s/c) = 2.0$ (from Fig. 5) so that

$$C_{D_i} = 8 \frac{s}{c} \frac{h}{\ell} \tag{22a}$$

and since Eq. (8) (p. 4) applies approximately,

$$\zeta_i \approx 8 \frac{h}{\ell} \tag{22b}$$

Disregarding other effects, Fig. 31 would indicate that h/ℓ is of the order 0.0025 to 0.005 and is roughly constant for each vane shape. The apparent constancy of ζ_i might be explained by the fact that both the computed ζ_i and the effect of the secondary flow on ζ_2 are inversely proportional to ℓ, the two effects roughly canceling each other.

The coefficient ζ_i applies to a cascade with an infinite number of vanes of finite span. When there are lateral walls, there is some increased loss in the vane spaces nearest the walls so that in a finite bend ζ_i must be increased somewhat over the values given in Fig. 31. Except when there are too few vanes in the bend (less than 5 or 6 in the present experiments), this increase appears to be of the order of 0.01 or 0.02 from the ζ_b points in Figs. 30b and 30c. No attempt is made to compute this lateral wall effect. The increased coefficient is designated ζ_i'.

The coefficient ζ_t of Figs. 32 to 34, inclusive, is seen to include only the loss attributable to the additional wall shear if ζ_i' is first subtracted from it. It should therefore be possible to compute a coefficient $\zeta_{\bar{\tau}}$ based on the velocity profiles downstream of the vanes and this coefficient should be comparable to $\zeta_t - \zeta_i'$. The coefficient $\zeta_{\bar{\tau}}$ has been computed roughly in Appendix D, and the following formula was obtained:

$$\zeta_{\bar{\tau}} \approx 0.03 \, \overline{K} \, \frac{s x_2}{s \ell} \tag{23}$$

where $\bar{K}$ is a parameter depending on the entrance velocity profile,

x_2 is the distance downstream from the vanes required for the entrance boundary layer to be reestablished, and

ℓ is the vane span.

The ratio $sx_2/s\ell$ is half the ratio of surface area experiencing additional shear, to the passage area through which flow passes. As indicated in the argument on p. 20, for the thin vanes, when the vane spacing increases, the velocities in the boundary layer behind the vanes probably decrease; hence, x_2 should decrease with increasing spacing. If the product sx_2 is constant, Eq. (23) indicates that $\zeta_{\bar{\tau}}$ is inversely proportional to passage area. Since ζ_i' is roughly constant, this is the trend that is shown by the ζ_t plots of Fig. 34. On the other hand, for the thick vanes with constant gap width, it was indicated that the boundary layer velocities appeared independent of spacing. Hence, x_2 should be independent of spacing and $\zeta_{\bar{\tau}}$ (and therefore ζ_t) should remain roughly constant; this agrees with Fig. 32a.

In Appendix D, $\bar{K}$ is estimated at about 0.33 for the present experiments. Assuming that for the plate vanes at the smallest vane spacings (about 1.0 in.) the original boundary layer is not reestablished until the measuring station M-M is reached (30 in. downstream from the miter line), Eq. (23) becomes

$$\zeta_{\bar{\tau}} \approx \frac{0.3}{s\ell} \tag{23a}$$

where $s\ell$ is measured in square inches. The slope of Eq. (23a) is flatter that the slopes of the lines drawn through the experimental data in Fig. 34. Since ζ_i' is still to be added to the value of $\zeta_{\bar{\tau}}$ given by Eq. (23a) to obtain the value of ζ_t plotted in Fig. 34, the computed value is not unreasonable. It is probable that one or more factors in addition to wall shear influence the trend in $\zeta_t - \zeta_i'$ or that the method of estimating ζ_τ is not entirely adequate. Nevertheless, it has been established both experimentally and analytically that a large part of the secondary-current loss in a guide vane bend is attributable to the additional wall shear downstream of the bend and that for plate vanes, at least, this loss is inversely proportional to the passage area between the vanes.

In accordance with the previous arguments, the ratio $sx_2/s\ell$ probably depends on vane shape, entrance velocity profile, and the ratio $C_L/(s/c)$ discussed in Part III-E. No attempt is made to express the relationships formally in an equation since the data available are not entirely adequate for this purpose. Further study of the parameters in Eq. (23) is required.

No attempt has been made to assess the effect of Reynolds number on the secondary-current losses, but it is believed that this effect is minor over the usual working range compared to the assumptions which have been made.

In summary, the loss coefficient ζ to be applied to a guide vane installation in a three-dimensional bend may be written

$$\zeta = \zeta_2 + \zeta_i' + \zeta_\tau \tag{24}$$

where, strictly speaking, ζ_2 should be integrated over the approach velocity profile. The coefficient ζ_2 represents the two-dimensional loss; ζ_i' represents the secondary-current effects and lateral wall effects in the bend; and ζ_τ is the additional loss downstream of the bend which may be attributed principally to increased wall shear. The value of ζ_2 is to be obtained from experimental data or boundary layer theory; ζ_i' may be estimated by adding to ζ_i, obtained from Eqs. (22) and (8), an arbitrary wall loss coefficient of 0.01 or 0.02; and ζ_τ is to be determined from Eq. (23). The wall loss coefficient becomes extremely large when there are too few vanes in the bend (less than 5 or 6 in the present experiments) and Eq. (24) can no longer be used.

V. SUMMARY AND CONCLUSIONS

Incompressible flow in a fixed guide vane bend has been analyzed by dividing the flow into a two-dimensional part and a superimposed secondary flow. It has been shown that the two parts can be studied separately. The secondary flow has only a small influence on the two-dimensional deflection and this can be neglected. However, the two dimensional head loss is increased materially because of the secondary-flow effects.

Two-dimensional cascade data can be correlated using Figs. 5 and 5a. Data for completely filling Fig. 5a with cascade lines are not available; in their absence two-dimensional data can be obtained, as in the past, by experiment or by theoretical methods, using experimental methods or boundary layer computation methods to obtain coefficients of drag.

The secondary currents have been shown to be confined largely to the region of the flow in the duct boundary layer near the ends of the vanes. Figure 41 illustrates the effects of these currents on the two-dimensional flow. Components of the secondary current parallel to the vane spans are nearly annihilated at the trailing edges of the vanes, forming trailing vortex sheets which are identical with those attributable to the decrease in circulation near the span ends. The secondary currents are recognizable a short distance downstream of the vanes in (1) a redistributed total head pattern showing "holes" of low total head in each vane wake and high total head at the duct wall between the vanes, as seen in Fig. 2b, and (2) a flow along the duct walls directed toward the inside of the bend and on the inside wall toward its center. The anomalies in total head disappear within two or three duct hydraulic diameters, but the secondary currents are still detectable much further downstream.

The effects of the secondary flow on the head loss have been divided into two parts for convenience in discussion and computation. The first part is measurable immediately downstream of the vanes and is composed of the secondary-flow effect on the two-dimensional loss coefficient (which is generally negative), the loss in the trailing vortex sheets, and the loss in the spaces between the end vanes and adjacent walls. The second part of the loss is attributable to increased wall shear downstream of the vanes. It is generally considerably larger than the first part.

The loss due to the secondary flows may be added directly to the two-dimensional loss when both are expressed as head loss coefficients

$$\zeta = \zeta_2 + \zeta_i' + \zeta_\tau \qquad (24)$$

where ζ is the head loss coefficient, and the subscripts represent two-dimensional loss, loss measurable immediately behind the vanes, and loss attributable to increased wall shear downstream of the vanes, respectively. The coefficient ζ_2 is to be obtained experimentally or from boundary layer computations. A part of ζ_i' (that due to trailing vortex sheets) can be computed,

to a certain extent, by a formula derived by Carter and Cohen [18], but the remaining part must be estimated arbitrarily. A formula for ζ_τ was developed in this report:

$$\zeta_\tau \approx 0.03\ \overline{K}\ \frac{sx_2}{s\ell} \tag{23}$$

where $\overline{K}$ is a parameter depending on approach velocity profile only, and $sx_2/s\ell$ is half the ratio of wall area experiencing additional shear to passage area through which the flow passes. Values of ζ_τ for practical application cannot be obtained from Eq. (23) until a formula for obtaining sx_2 is developed.

The experimental part of the present work substantiated the general description above and provided numerical values for ζ_2, ζ_i', and ζ_τ. The coefficient ζ_2 was found to be independent of scale but to vary with spacing-chord ratio, showing a minimum at some particular spacing-chord ratio. Values of ζ_2 of the order of 0.05 (based on maximum approach velocity head) were obtained with a plate vane at a spacing-chord ratio of 0.5 but there is no reason to believe that this is an optimum vane design. It was found that the coefficient ζ_i' may be independent of scale and may also be independent of spacing-chord ratio. It was dependent to some extent on vane shape and probably on the boundary layer profile approaching the vanes. The measured values of ζ_i' were less than the smallest value of ζ_2 for each shape in the present experiments, except when there were less than 5 or 6 vanes in the cascade. With too few vanes in the cascade, there was a large separation loss between the end vanes and walls, and ζ_i' became very large.

Measurements of $\zeta_t (\approx \zeta_i' = \zeta_\tau)$ confirmed the form and order of magnitude of results obtained from Eq. (23). It was found from the data that the wall area experiencing additional shear (sx_2) would tend to remain constant for plate vanes making ζ_t and thus ζ_τ inversely proportional to passage area $(s\ell)$. For the thick vanes which had uniform gap between the vanes, it was found that ζ_t and thus ζ_τ were roughly constant. It was therefore assumed that sx_2 depends on the variation in gap between the vanes--that is, vane shape. It was also noted that sx_2 should be a function of the ratio $C_L/(s/c)$ where C_L is the lift coefficient of a vane in a two-dimensional cascade of spacing-chord ratio s/c. The ratio $C_L/(s/c)$ is related to the deflection angle of the bend and the contraction or expansion of the flow and

is obtainable from Fig. 5. If the analysis in fixed bends can be applied to a turbomachine (and it probably can be applied to the first row of blades) the last point indicates that ζ_T would be less for compressor cascades than for turbine cascades.

The experimental work also indicated that vane spacing appears to be a better length parameter than chord length in comparing total head distribution, energy loss, and velocity profiles downstream of a guide vane bend.

More study should be given to Eq. (23) for ζ_T, particularly to the parameters which determine the surface area subject to additional shear, sx_2. Although ζ_i' is generally smaller and therefore not as important as ζ_T, it too requires some further study. In the two-dimensional field, additional experimental data contributing to the completion of Fig. 5a are required. It is believed, however, that the above summary outlines the essential elements in determining the performance of a guide vane system in a bend.

In conclusion, the following points regarding the design of guide vane systems may be drawn:

A. Guide vanes for a bend may be selected from known, two-dimensional guide vane systems. For practical purposes, the deflection produced by the guide vanes in the bend will be the same as the two-dimensional deflection, but the head loss will be increased over the two-dimensional loss as indicated by Eq. (24), above. In that equation, for a 90° bend, the additional loss at the vanes will be of the order of 0.05 of the velocity head or less, while that occurring downstream may vary from 0.05 to 0.10 of the velocity head. These losses are to be added to the two-dimensional loss near optimum spacing-chord ratio of 0.05 to 0.10 velocity head.

B. In scaling a guide vane bend up or down, the deflection will remain the same for practical purposes if the spacing-chord ratio is held constant. However, the head loss will change somewhat because the chord length will be changed. If the bend is scaled up, the loss should decrease, and if scaled down, it should increase. The amount of change should be calculable through an equation similar to Eq. (23) above, but the parameters in this equation are not well enough determined to be useful.

C. A guide vane bend with minimum loss can be constructed of plate vanes as well as of thick vanes. To do so, a two-dimensional cascade with small loss coefficient is selected and the vanes are manufactured with as large a chord as possible.

D. There is a minimum number of vanes which should be used in a bend. Below this minimum, there is excessive loss between the end vanes and adjacent walls; above the minimum the loss in this region is only a small fraction of the two-dimensional loss. The minimum for the rectangular and square ducts used in the present experiments was five or six vanes, but it may be different for a duct of circular cross section.

BIBLIOGRAPHY

[1] Squire, H. B. and Winter, K. G. "The Secondary Flow in a Cascade of Airfoils in a Nonuniform Stream." Journal of Aeronautical Science, Vol. 18, No. 4, pp. 271-277. 1951.

[2] Anderson, A. G. Fluid Flow Diversion. University of Minnesota, St. Anthony Falls Hydraulic Laboratory Project Report No. 1, August, 1947. 229 pages.

[3] Silberman, E. Fluid Flow Diversion by Guide Vanes in Miter Bends. University of Minnesota, St. Anthony Falls Hydraulic Laboratory Project Report No. 8, April, 1949. 185 pages.

[4] Silberman, E. The Nature of Flow in an Elbow. University of Minnesota, St. Anthony Falls Hydraulic Laboratory Project Report No. 5, December, 1947. 100 pages.

[5] Tyler, R. A. "The Available Theoretical Analyses of Two-Dimensional Cascade Flow." National Research Council of Canada, Aero Note, AN-4, Ottawa, 1949. 58 pages.

[6] Schlicting, H. and Scholz, N. "Theoretical Determination of Flow Losses in a Plane Cascade" (Über die Theoretische Berechnung der Strömungsverluste eines ebenen Schaufelgitter). Ingenieur-Archiv, Vol. 19, pp. 42-65. 1951.

[7] Zweifel, O. "The Spacing of Turbo-Machine Blading, Especially with Large Angular Deflection." Brown-Boveri Review, Vol. 32, pp. 436-444. 1945.

[8] Davis, H. "A Method of Correlating Axial-Flow-Compressor Cascade Data." Transactions of the ASME, Vol. 70, pp. 951-955. 1948.

[9] Harris, R. G. and Fairthorne, R. A. "Wind Tunnel Experiments with Infinite Cascades of Airfoils." British Aeronautical Research Council, Reports and Memoranda, No. 1206. 1928.

[10] Resnick, R. and Green, L. J. "Velocity Distributions and Design Data for Ideal Incompressible Flow through Cascades of Airfoils." Journal of Applied Mechanics, Vol. 18, pp. 253-259. 1951.

[11] Silberman, E. The Pitot Cylinder. University of Minnesota, St. Anthony Falls Hydraulic Laboratory Circular No. 2, 1947. 18 pages.

[12] Salter, C. "Experiments on Thin Turning Vanes." British Aeronautical Research Council, Reports and Memoranda, No. 2469. 1952 (originally prepared in 1946).

[13] Hansen, A. G., Costello, G. R., and Herzig, H. Z. "Effect of Geometry on Secondary Flows in Blade Rows." National Advisory Committee for Aeronautics, Research Memorandum, RM E 52H26, October, 1952. 38 pages.

[14] Mager, A. and Hansen, A. G. "Laminar Boundary Layer Over Flat Plate in a Flow Having Circular Streamlines." National Advisory Committee for Aeronautics, Technical Note, No. 2658, March, 1952. 28 pages.

[15] Hawthorne, W. R. "Secondary Circulation in Fluid Flow." Proceedings of the Royal Society, London, Series A, Vol. 206, pp. 374-387. 1951.

[16] Milne-Thomson, L. M. Theoretical Hydrodynamics, 2nd edition. New York: The Macmillan Company, Chapter III. 1950.

[17] Herzig, H. Z., Hansen, A. G., and Costello, G. R. "Visualization of Secondary-Flow Phenomena in Blade Row." National Advisory Committee for Aeronautics, Research Memorandum, RM E 52F19, August, 1952. 20 pages.

[18] Carter, A. D. S. and Cohen, E. "Preliminary Investigation into the Three-Dimensional Flow through a Cascade of Aerofoils." British Aeronautical Research Council, Reports and Memoranda, No. 2339. 1946.

[19] Rouse, H. Elementary Mechanics of Fluid. New York: John Wiley & Sons, Inc., p. 194. 1946.

APPENDIX A
LIST OF SYMBOLS

A, B = Constants.

AR_c = Aspect ratio ℓ/c.

AR_s = Aspect ratio ℓ/s.

b = Width of duct.

C_D = Coefficient of drag based on approach velocity head $V_1^2/2g$.

C_L = Coefficient of lift based on approach velocity head $V_1^2/2g$.

C_L' = Coefficient of lift based on head of vector mean velocity.

C_R = Coefficient of Reaction--Resultant of C_L and C_D.

c = Chord length of vane measured along straight line connecting leading and trailing edges.

D = Drag per unit span of vane.

D_H = Hydraulic diameter, $D_H = 4 \times$ Area/Wetted Perimeter.

f = Functional relationship.

g = Acceleration of gravity.

h = Distance from duct wall to trailing vortex.

h_s = Static head.

h_t = Total head.

h_t' = Total head of control stream filament upstream of test section.

i = Unit vector.

K = Proportionality parameter in duct boundary layer.

K_1 = Value of K in boundary layer approaching vanes.

$\overline{K}$ = Parameter describing effect of entrance velocity profile on boundary layer downstream of vanes.

L = Lift per unit span of vane.

ℓ = Span length of vane.

n = Curvilinear coordinate in direction of radius of curvature of streamline.

p - Pressure at a point in the fluid.

p' - Pressure loss due to drag.

$\vec{q}$ - Velocity vector.

R - Reaction per unit span of vane, components R_x and R_y in x and y coordinate directions.

Re_c - Reynolds number based on vane chord, $Re_c = V_1 c/\nu$.

Re_d - Reynolds number based on duct hydraulic diameter, $Re_d = V_1 D_H/\nu$.

$\vec{r}$ - Radius of curvature of streamline.

s - Spacing of vanes measured between corresponding points of two adjacent vanes.

s - Also curvilinear coordinate in direction of streamline.

u - Magnitude of velocity vector (velocity component along a streamline).

V_1 - Velocity in center of duct approaching guide vanes.

V_2 - Velocity in center of duct leaving guide vanes.

V - Vector mean of V_1 and V_2.

$\overline{V}$ - Average velocity in duct.

v - Velocity component parallel to radius of curvature of streamline.

w - Velocity component normal to u and v.

x, y - Cartesian coordinates normal to and along cascade axis.

x - Also coordinate along center of duct measured downstream from vanes.

y - Also coordinate normal to duct wall and parallel to vane span.

z - Curvilinear coordinate normal to n and s.

α - Angle of attack of guide vane measured from the approach velocity direction to the chord line.

α_o - Angle of attack for zero lift.

β_1 - Entrance angle measured from cascade axis to approach velocity.

β_2 - Exit angle measured from cascade axis to exit velocity.

β - Angle between cascade axis and vector mean velocity.

β_o - Entrance angle for zero lift.

Γ - Circulation about a two-dimensional vane profile.

γ - Angle between cascade axis and lift direction.

γ' - Angle between cascade axis and reaction direction.

Δ - Deflection angle of cascade.

δ - Thickness of laminar sublayer.

ϵ - Deflection angle of a streamline.

ζ - Head loss coefficient.

Subscripts used with ζ:

2 -- Two-dimensional.

3 -- Three-dimensional measured immediately behind one or two vanes.

b -- Three-dimensional measured immediately behind vanes and including entire cross section.

m -- Three-dimensional measured far downstream.

τ -- Computed from additional wall shear downstream of vanes.

i -- $\zeta_i = \zeta_3 - \zeta_2$, $\zeta_{i'} = \zeta_b - \zeta_2$.

t -- $\zeta_t = \zeta_m - \zeta_2$.

ζ, η, ξ - Vorticity components along a streamline, along the radius of curvature of the streamline, and normal to the streamline and radius of curvature, respectively.

θ - Stagger angle--angle between cascade axis and chord line of vanes.

κ - Proportionality factor.

μ - Coefficient of viscosity.

υ - Kinematic viscosity.

ρ - Density.

τ_o - Wall shear stress.

$\vec{\Omega}$ - Vorticity vector.

APPENDIX B

RELATION BETWEEN VELOCITY RATIO, DEFLECTION ANGLE, AND REACTION

From Fig. A-1, the following relationships are available:

Momentum:
$$p_1 s + \rho V_1^2 \sin^2 \beta_1 = p_2 s + \rho V_2^2 \sin^2 \beta_2 - R_x \tag{A-1}$$

$$s (\rho V_1^2 \sin \beta_1 \cos \beta_1 - \rho V_2^2 \sin \beta_2 \cos \beta_2) = R_y \tag{A-2}$$

Continuity:
$$V_1 \sin \beta_1 = V_2 \sin \beta_2 \tag{A-3}$$

Bernoulli Eq.:
$$p_1 + \frac{\rho V_1^2}{2} = p_2 + \frac{\rho V_2^2}{2} + p' \tag{A-4}$$

where p' is the average pressure loss in each passage and is due to drag of the vanes.

Combining Eqs. (A-1), (A-3), and (A-4)

$$R_x = (p_2 - p_1)s = -\frac{\rho V_1^2}{2}\left[\left(\frac{V_2}{V_1}\right)^2 - 1 + \frac{p'}{\rho V_1^2/2}\right] s = -\frac{\rho V_1^2}{2}\left[\left(\frac{\sin \beta_1}{\sin \beta_2}\right)^2 - 1 + \zeta\right] s \tag{A-5}$$

where
$$\zeta = \frac{p'}{\rho V_1^2/2}$$

$$R_y = \frac{\rho V_1^2}{2} (\sin 2\beta_1 - 2 \sin^2 \beta_1 \cot \beta_2)s = \frac{\rho V_1^2}{2} 2 \sin^2 \beta_1 (\cot \beta_1 - \cot \beta_2)s \tag{A-6}$$

$$R = \sqrt{R_x^2 + R_y^2} = \frac{\rho V_1^2}{2} s \sqrt{\left(\frac{\sin^2 \beta_1}{\sin^2 \beta_2} - 1 + \zeta\right)^2 + 4 \frac{\sin^2 \beta_1}{\sin^2 \beta_2} \sin^2 (\beta_2 - \beta_1)}$$

$$C_R = \frac{R}{c\ (\rho V_1^2)/2} = 2 \frac{s}{c} \frac{V_2}{V_1} \sin \Delta \sqrt{\left[\frac{1 - (V_2/V_1)^2 - \zeta}{2\ (V_2/V_1) \sin \Delta}\right]^2 + 1} \tag{A-7}$$

where

$$\frac{V_2}{V_1} = \frac{\sin \beta_1}{\sin \beta_2} \tag{A-3}$$

$$\Delta = \beta_2 - \beta_1 \tag{A-8}$$

$$\tan \gamma' = \frac{R_x}{R_y} = \frac{1 - (V_2/V_1)^2 - \zeta}{2\,(V_2/V_1)\sin\Delta} \quad \text{or} \quad \cos \gamma' = 2\,\frac{s}{c}\,\frac{V_2}{V_1}\,\frac{\sin\Delta}{C_R} \tag{A-9}$$

For $p' = 0 = \zeta$, $R = L$, and $\gamma' = \gamma$, so that

$$\tan \gamma = \left(\frac{V_1}{V_2} - \frac{V_2}{V_1}\right)\frac{1}{2\sin\Delta} = \frac{1}{2}\,(\cot \beta_2 + \cot \beta_1) \tag{A-10}$$

With $p' \neq 0$, let $R^2 = L^2 + D^2$ and let L act in the direction given by Eq. (A-10). Then

$$C_D = C_R \sin(\gamma - \gamma') = \frac{2\,\zeta\,(s/c)^2\,(V_2/V_1)\sin\Delta}{C_L} = \zeta\,\frac{s}{c}\cos\gamma \tag{A-11}$$

and

$$C_L = \sqrt{C_R^2 - C_D^2} = 2\,\frac{s}{c}\,\frac{V_2}{V_1}\,\frac{\sin\Delta}{\cos\gamma} - \zeta\,\frac{s}{c}\sin\gamma \tag{A-12}$$

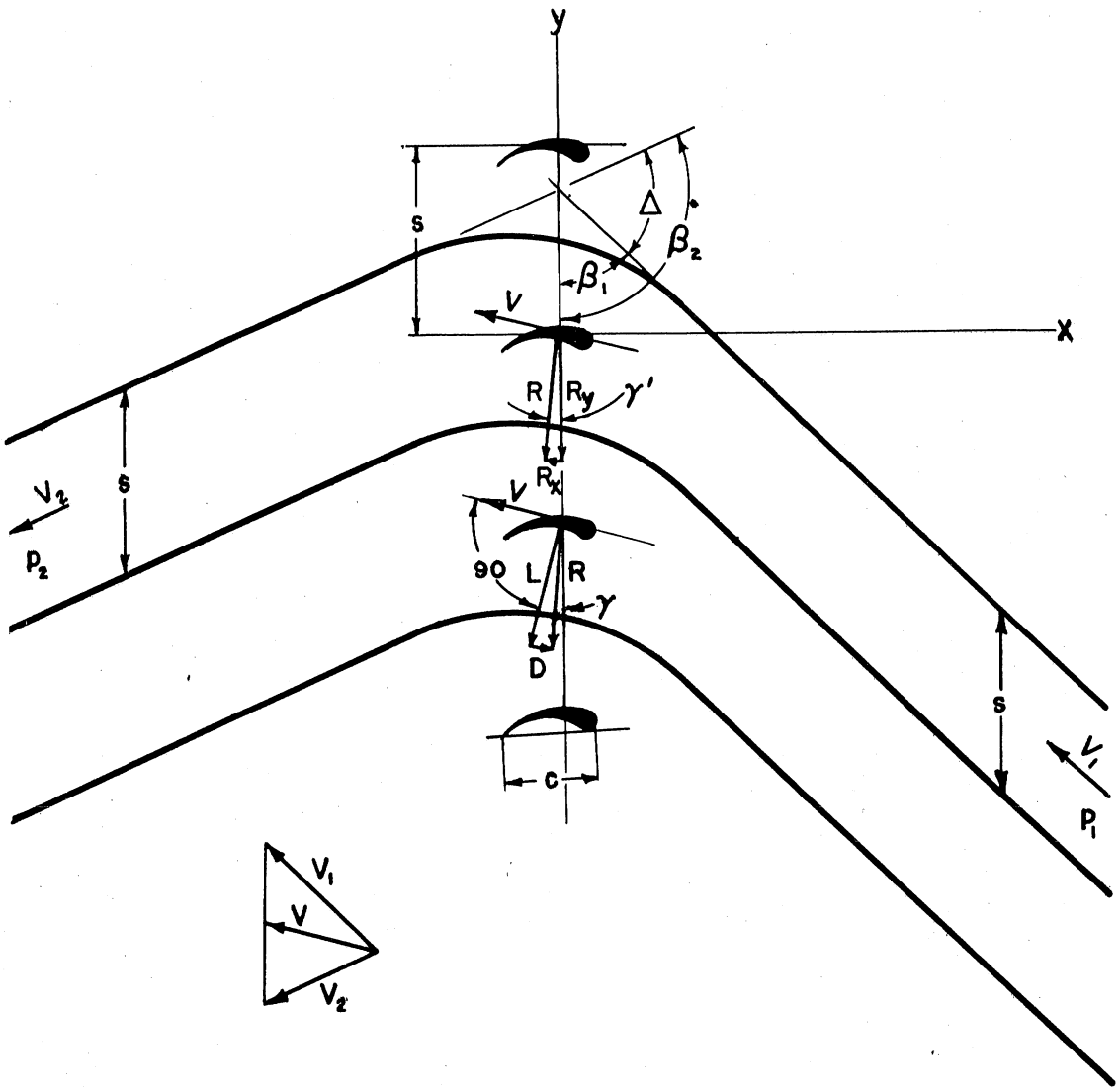

Fig. A-1 — Analysis of a Two-Dimensional Flow Strip

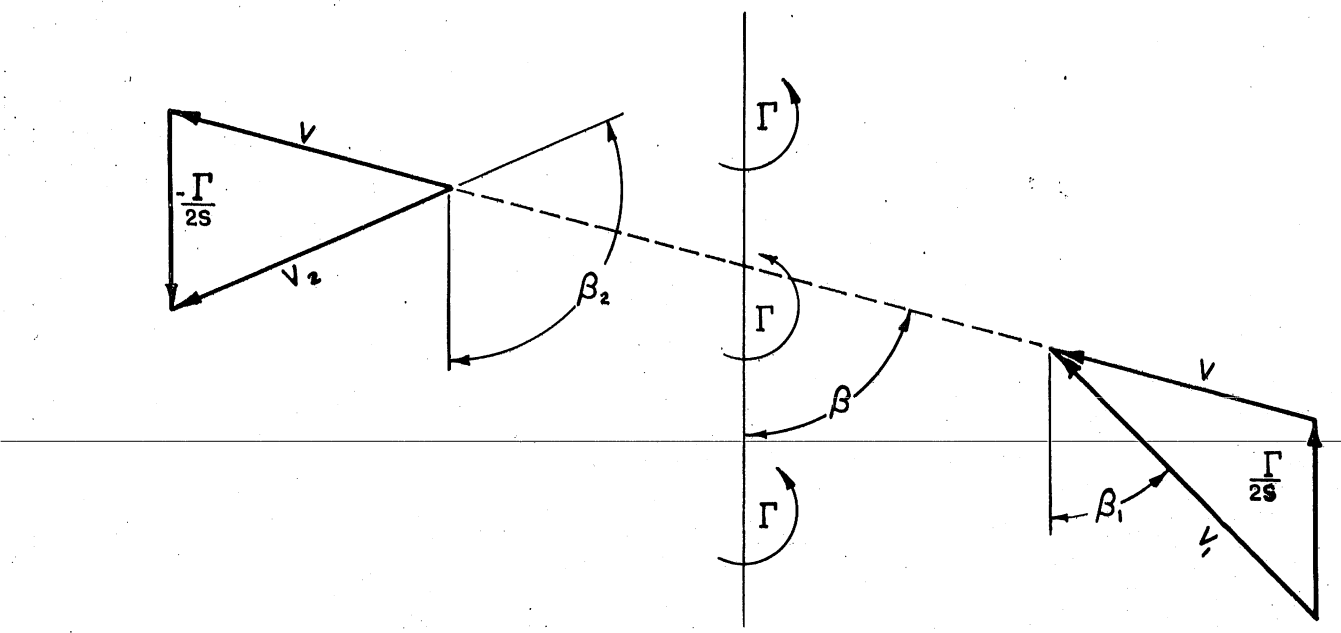

Fig. A-2 — Representation of a Cascade by an Infinite Row of Vortices

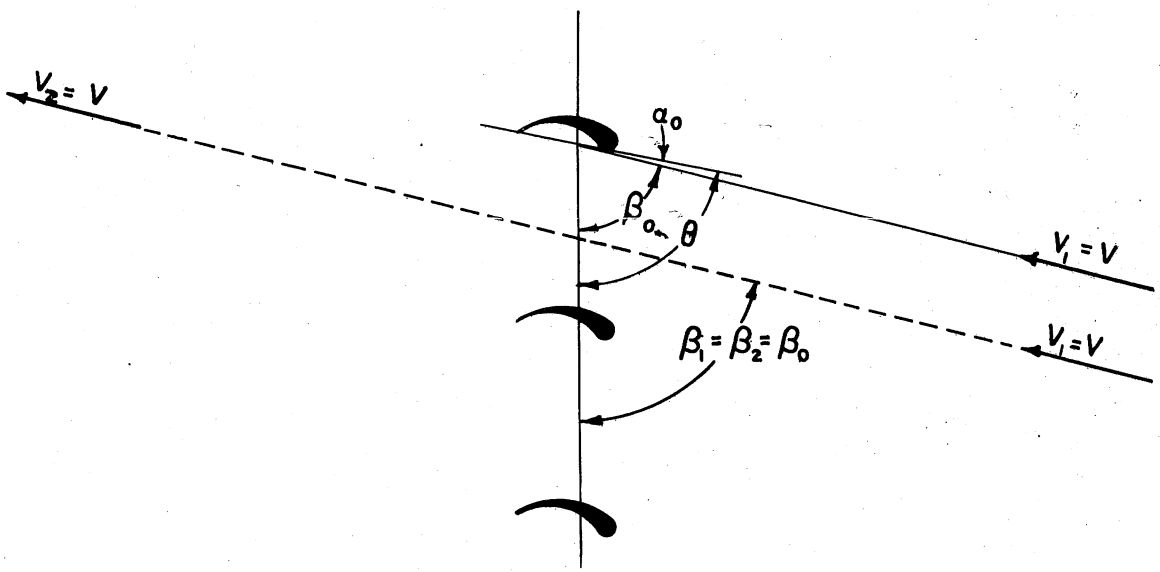

Fig. A-3 — Flow through a Cascade at Zero Lift

APPENDIX C

EFFECT OF CASCADE CHARACTERISTICS ON PERFORMANCE

In Fig. A-2 an infinite cascade is represented by replacing each vane by a vortex of strength Γ equal to the circulation about that vane. The vector mean velocity V making the angle β with the cascade axis is also defined in the figure. The infinite row of vortices produces at a great distance from the cascade the velocities $\pm \Gamma/2s$ with direction parallel to the cascade axis. From the figure, these relationships exist:

$$V_1 \cos\beta_1 - V \cos\beta = \Gamma/2s \quad \text{and} \quad V_1 \sin\beta_1 = V \sin\beta$$

or
$$\cot\beta = \cot\beta_1 - \Gamma/2sV \sin\beta \tag{A-13}$$

also
$$\cot\beta = \cot\beta_2 + \Gamma/2sV \sin\beta$$

and
$$\cot\beta = \frac{1}{2}(\cot\beta_2 + \cot\beta_1) \quad (= \tan\gamma) \tag{A-14}$$

The circulation developed by each vane in cascade depends on s/c, θ, the vane shape, V, c, and β. For each combination of s/c, θ, and vane shape, there is some mean flow direction β_o for which $\Gamma = 0$ ($C_L = 0 = \Delta$) ($\beta_1 = \beta_2 = \beta_o$). Since θ defines the orientation of the chord of the profile, it may be seen from Fig. A-3 that

$$\beta_o = \theta - \alpha_o \tag{A-15}$$

where α_o is the angle of attack for zero lift of the profile in cascade measured from the velocity vector. Profile camber is the predominant factor governing the value of α_o; other shape parameters, s/c, and θ are minor factors. In a physical cascade the guide vanes may not be able to actually operate at $\beta = \beta_o$ without stalling, but β_o exists theoretically. Now $\beta - \beta_o$ may be called the incidence angle of the cascade; and for fixed s/c, θ, and vane shape, Γ is given by the functional form

$$\Gamma = f(\beta - \beta_o, V, c) \tag{A-16}$$

By analogy with thin airfoil theory, it is now assumed that Eq. (A-16) can be written

$$\Gamma = \kappa V c \sin (\beta - \beta_o) \tag{A-17}$$

Equation (A-17) is valid as an approximation only as long as stalling does not occur. The proportionality factor κ will vary with s/c, θ, and vane shape. (Experimentally, κ increases both with s/c and with θ.)

Combining Eqs. (A-17) and (A-13), there results

$$\cot \beta = \cot \beta_1 - \frac{\kappa}{2s/c} (\cos \beta_o - \cot \beta \sin \beta_o)$$

or

$$\cot \beta = \frac{2s/c \cot \beta_1 - \kappa \cos \beta_o}{2s/c - \kappa \sin \beta_o}$$

Combining the last equation with Eq. (A-14) yields

$$\cot \beta_2 = 2 \cot \beta - \cot \beta_1 = \left(1 + \frac{2 \kappa \sin \beta_o}{2s/c - \kappa \sin \beta_o} \right) \cot \beta_1 - \frac{2 \kappa \cos \beta_o}{2s/c - \kappa \sin \beta_o}$$

or

$$\cot \beta_2 = A \cot \beta_1 - B \tag{A-18}$$

where A and B are constants for any given cascade depending only on s/c, θ, and the vane shape.

No account has been taken here of boundary layer effects which must cause A and B to vary somewhat.

APPENDIX D

ESTIMATE OF INCREASED WALL FRICTION DOWNSTREAM OF THE GUIDE VANES

Typical velocity profiles upstream and immediately downstream of the guide vanes are shown in Figs. 37 and 38. The profiles far enough downstream resemble those upstream. While the original profile is being reestablished, however, there is greater energy loss at the wall due to dissipation than would otherwise have been the case. In the laminar sublayer (not shown in Figs. 37 and 38), the important term in the energy dissipation function is $\partial u/\partial y$ if u is taken as the magnitude of the vector velocity and y is the distance measured normally from the wall. The rate of dissipation per unit volume ϕ in the laminar sublayer is then

$$\phi = \mu \left(\frac{\partial u}{\partial y}\right)^2 \tag{A-19}$$

The $\partial u/\partial y$ may be taken as constant and equal to its value at the wall.

Taking b as the normal distance between vane wakes and δ as the thickness of the sublayer, assumed uniform normal to the vanes, the rate of energy dissipation per unit length is $\mu\,(\partial u/\partial y)^2 \delta\, b$. In the flow upstream of the vanes, this rate was $\mu\,(\partial u/\partial y|_1)^2\, \delta_1 b$ where the subscripts "1" refer to the existing values measured upstream of the vanes. The discharge between each pair of vanes is $\overline{V} \ell b$ where $\overline{V}$ is the average velocity and ℓ is the span of the vanes. Considering both walls normal to the vanes, the head loss coefficient attributable to wall shear ζ_τ is

$$\zeta_\tau = \frac{2\mu}{\overline{V} \ell\, \rho V_1^2/2} \int_{x_o}^{x_2} \left[\left(\frac{\partial u}{\partial y}\right)^2 \delta - \left(\frac{\partial u}{\partial y}\Big|_1\right)^2 \delta_1\right] dx \tag{A-20}$$

The distance x is measured in the downstream direction from an origin near the vanes and $(x_2 - x_o)$ is the distance required downstream of the vanes to reestablish the upstream velocity profile at the wall.

In Eq. (A-20), δ is related to $\partial u/\partial y$ through the wall shear τ_o. As an estimate [19]

$$\delta = \frac{11.6\nu}{\sqrt{\tau_o/\rho}} \tag{A-21}$$

Since $\partial u/\partial y$ was taken constant in the sublayer, wall shear is given by

$$\tau_o = \mu \frac{\delta u}{\delta y} \tag{A-22}$$

Also, $\delta u/\delta y$ may be approximated by

$$\frac{\delta u}{\delta y} = \frac{K(x)\, V_1}{\delta} \tag{A-23}$$

where $$1 \geq K(x) \geq K_1$$

and $K_1 = 11.6\sqrt{\tau_{o_1}/\rho}/V_1$ is the value of K at $x = x_2$ and also upstream of the vanes. It is determinable by obtaining $\sqrt{\tau_{o_1}/\rho}$ from the profiles upstream of the vanes as in Fig. 37a. For purposes of computation $K(x)$ is assumed linear of the form

$$K(x) = 1 - (1 - K_1)\frac{x}{x_2} \tag{A-24}$$

but the exact assumption is not too important.

Combining Eqs. (A-20) through (A-24) and performing the indicated integration, there results

$$\zeta_\tau = 0.03 \frac{V_1}{\overline{V}} \frac{x_2}{\ell} \left\{ \frac{1 + K_1 + K_1^2 - 3K_1^3}{4} - \frac{x_o}{x_2}(1 - K_1) \left[1 + K_1 + K_1^2 - \frac{1}{2}\frac{x_o}{x_2} - \frac{x_o}{x_2}\left(1 - \frac{1}{2}(1 - K_1)\frac{x_o}{x_2}\right) \right] \right\} \tag{A-25}$$

If the reasonable assumption is made that $x_o/x_2 \ll 1$, Eq. (A-25) can be written

$$\zeta_\tau \approx 0.03\, \overline{K} \frac{s x_2}{s \ell} \tag{A-26}$$

where $$\overline{K} = \frac{1}{4}\frac{V_1}{\overline{V}}(1 + K_1 + K_1^2 - 3K_1^3)$$

and depends on the entrance velocity profile only. The product $s\ell$ represents the passage area between vanes.

In the present experiments, K_1 is of the order of 0.6 from Fig. 37a and $V_1/\overline{V} \approx 1.05$ upstream of the vanes. Therefore $\overline{K} \approx 0.33$.

A P P E N D I X E

FIGURES 1 to 41

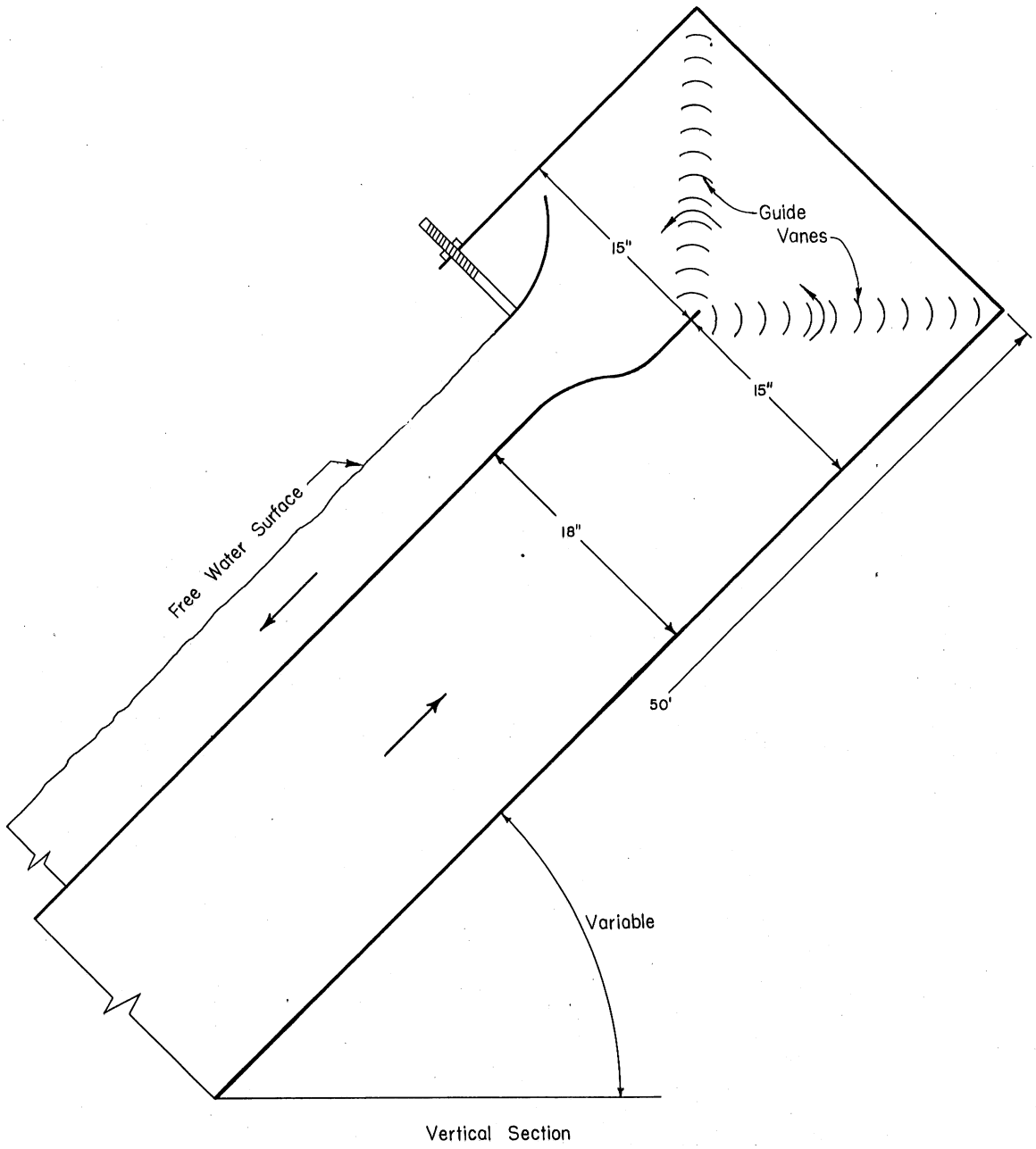

Fig. 1 – Guide Vane Installation in High-Velocity Channel

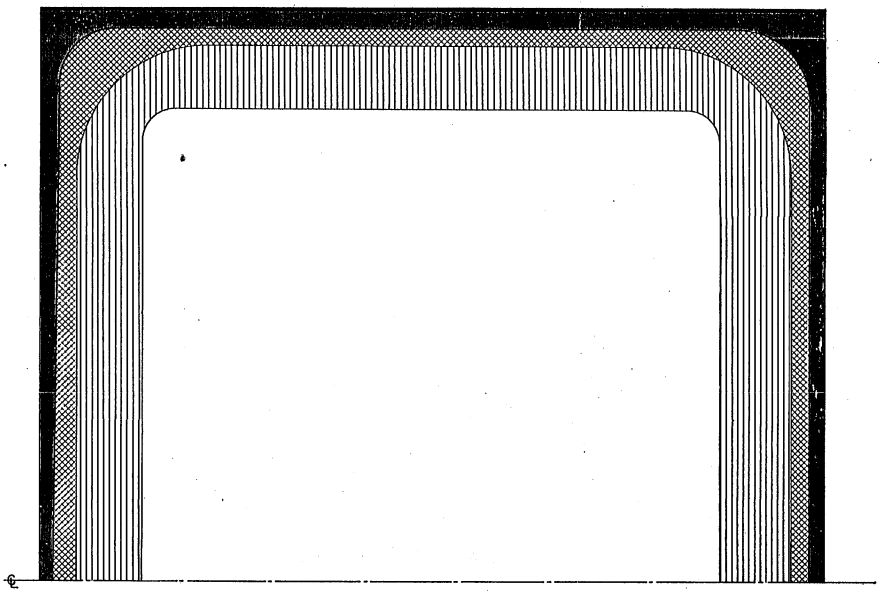

a. Straight Duct, Section A-A

Dimensionless Total Head	
	0 – 0.3
	0.3 – 0.7
	0.7 – 0.98
	0.9
	Over 0.98

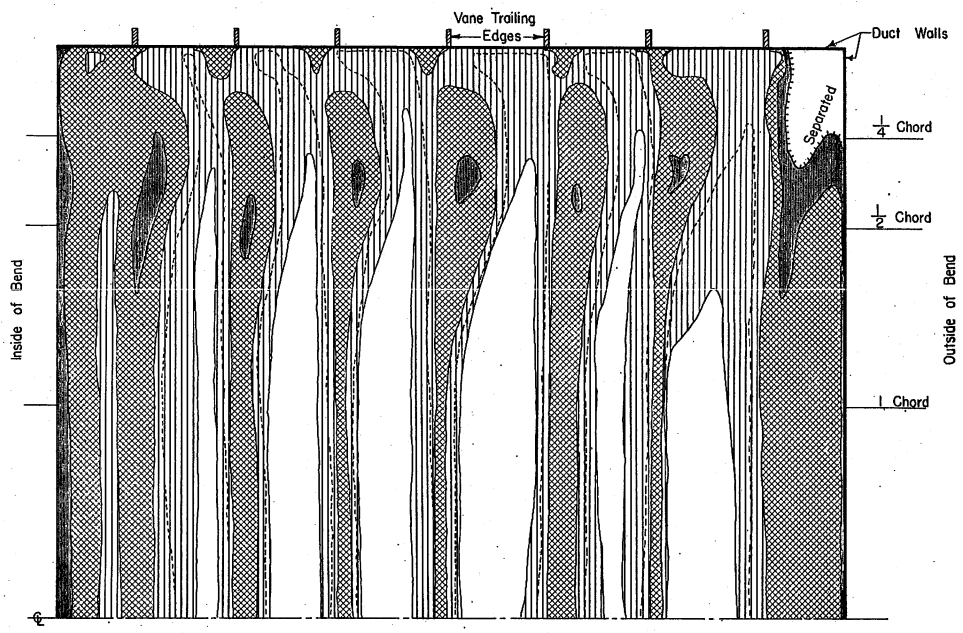

b. Immediately Downstream of Miter Elbow, Section B-B

Fig. 2 — Total Head Distribution in a Three-Dimensional Guide Vane Bend

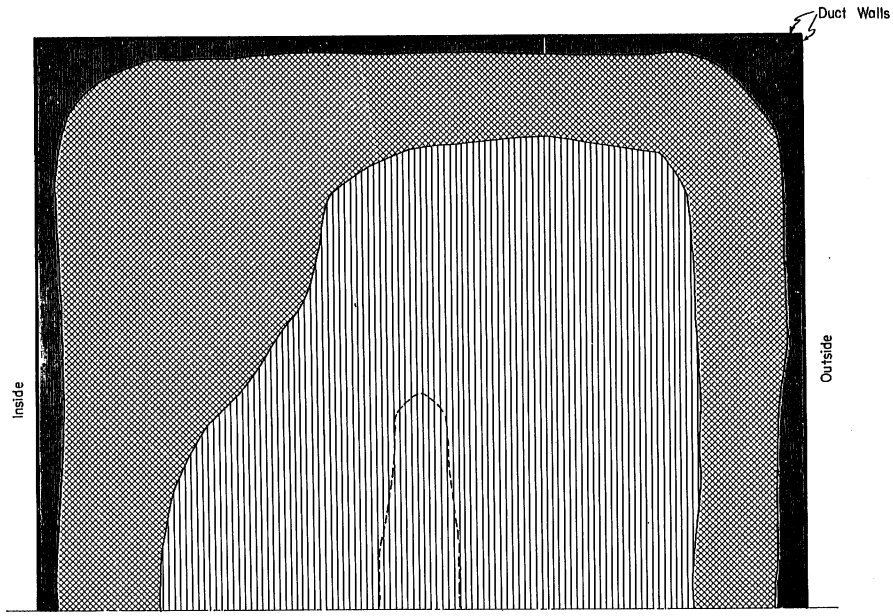

c. Downstream of Bend, Section M-M

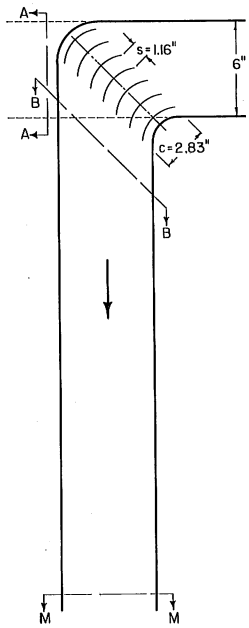

(21) 300 Vane Shape
$Re_c = 1.5 \times 10^5$
$Re_d = 3.8 \times 10^5$

d. Vane Arrangement

Dimensionless Total Head	
	0 – 0.3
	0.3 – 0.7
	0.7 – 0.98
----	0.9

Fig. 2 (Cont'd) – Total Head Distribution in a Three-Dimensional Guide Vane Bend

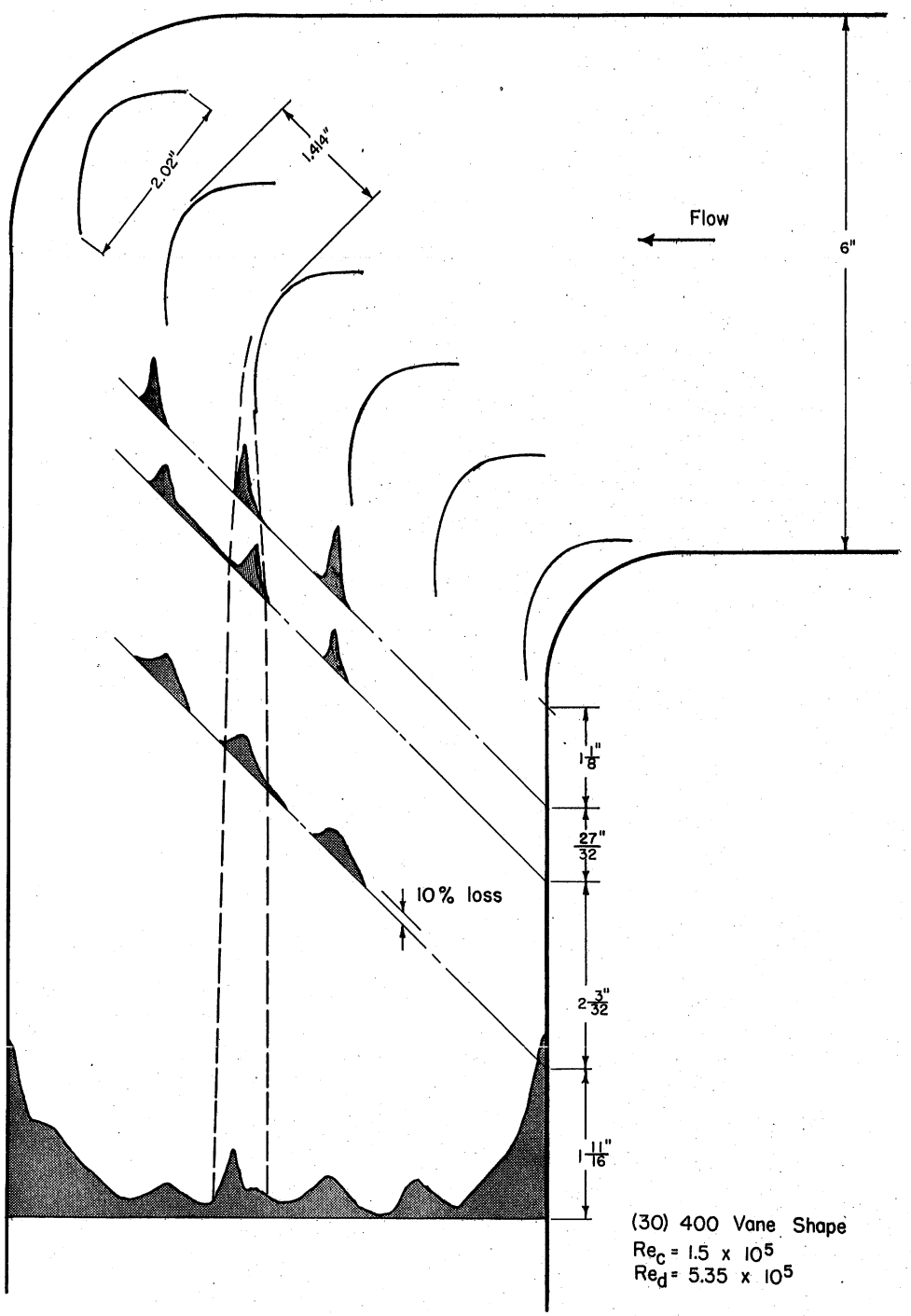

Fig. 3 - Head Loss Behind a Two-Dimensional Cascade

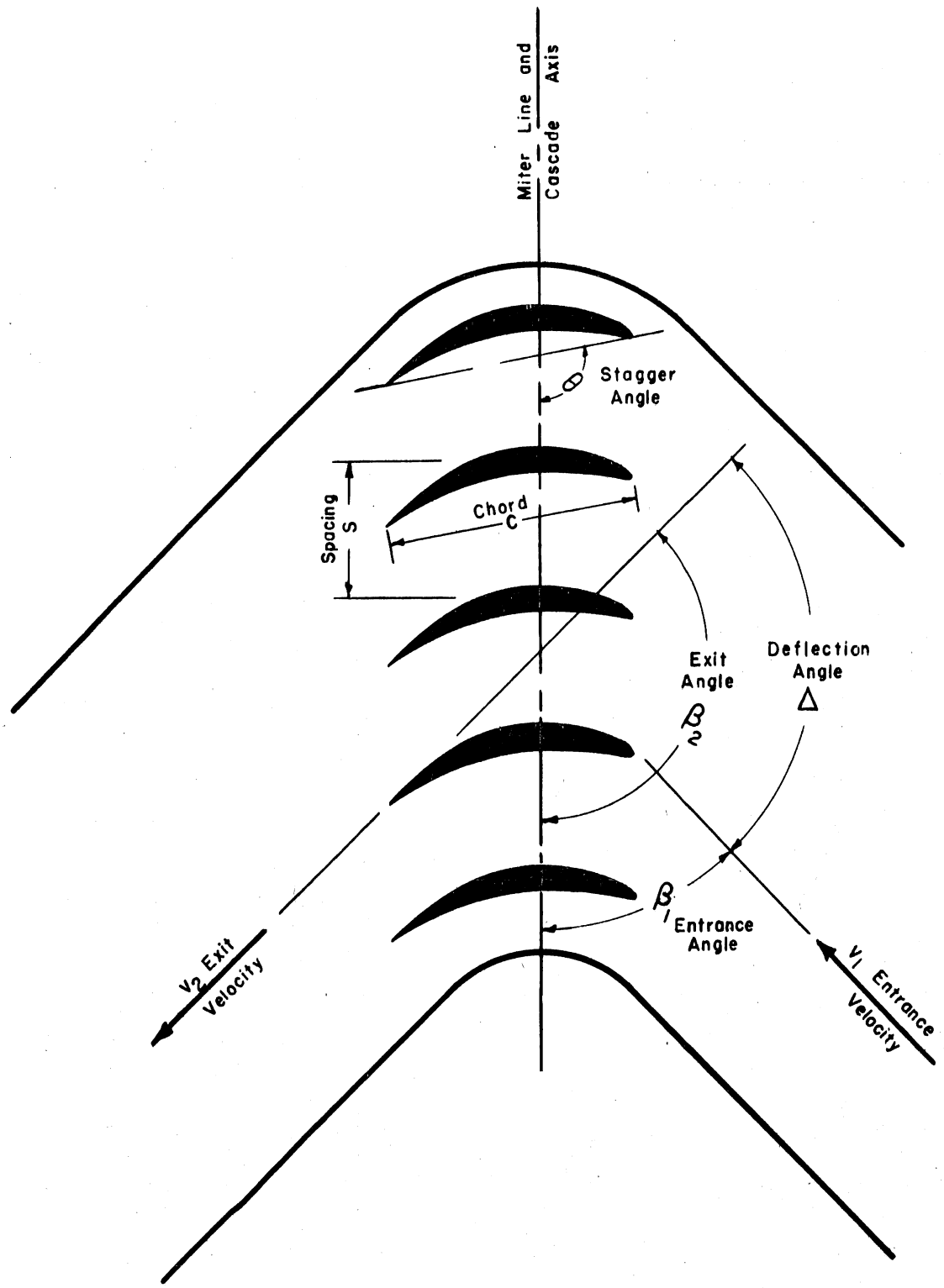

Fig. 4 — Cascade Characteristics

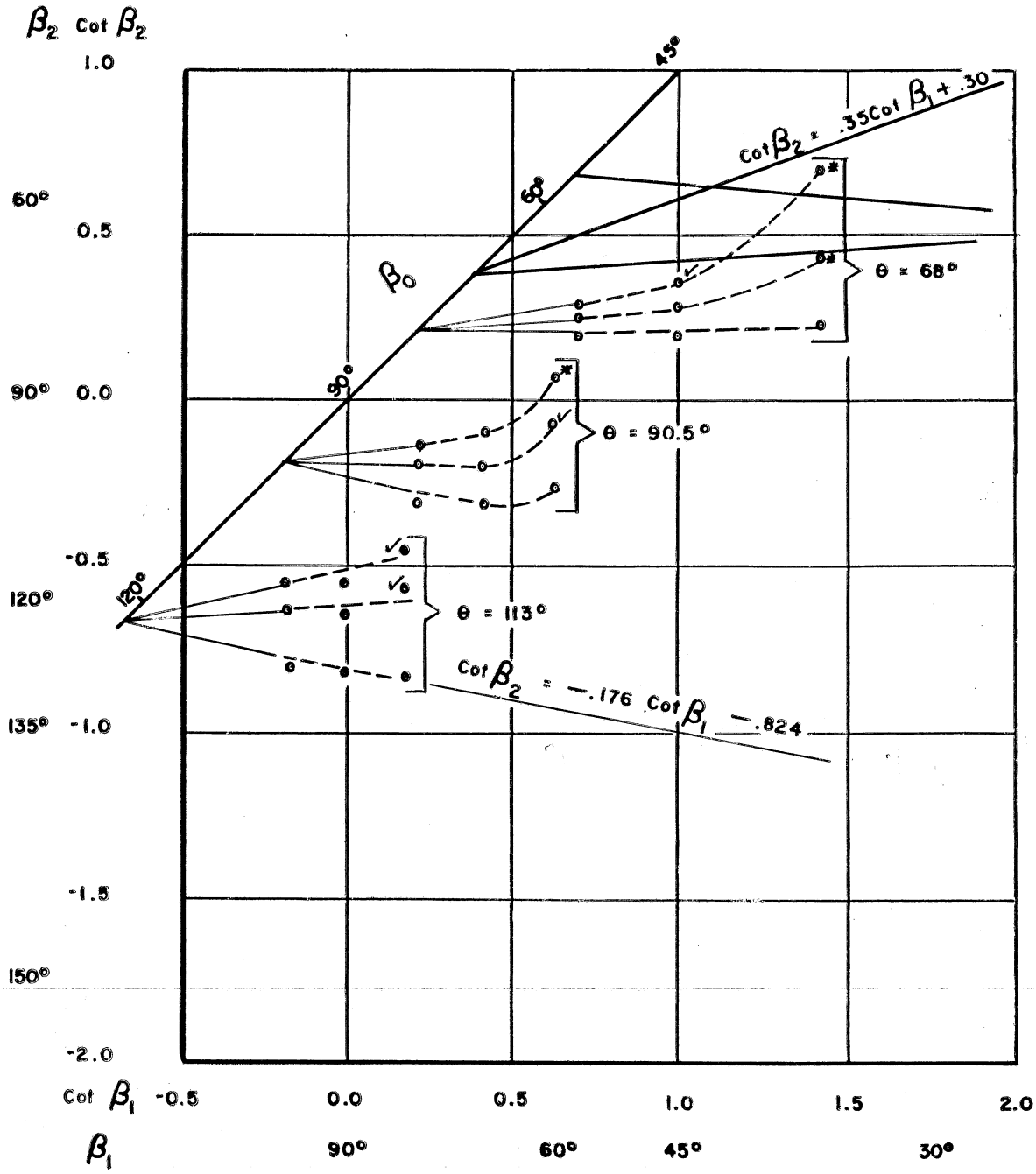

——— From Fig. 2 by Davis [8] representing experimental data
– – ● – – From Harris and Fairthorne [9]

(Starred points represent stalled cascades according to reference. Checked points represent cascades with abnormally high drag.)

Fig. 5a — Typical Cascade Lines

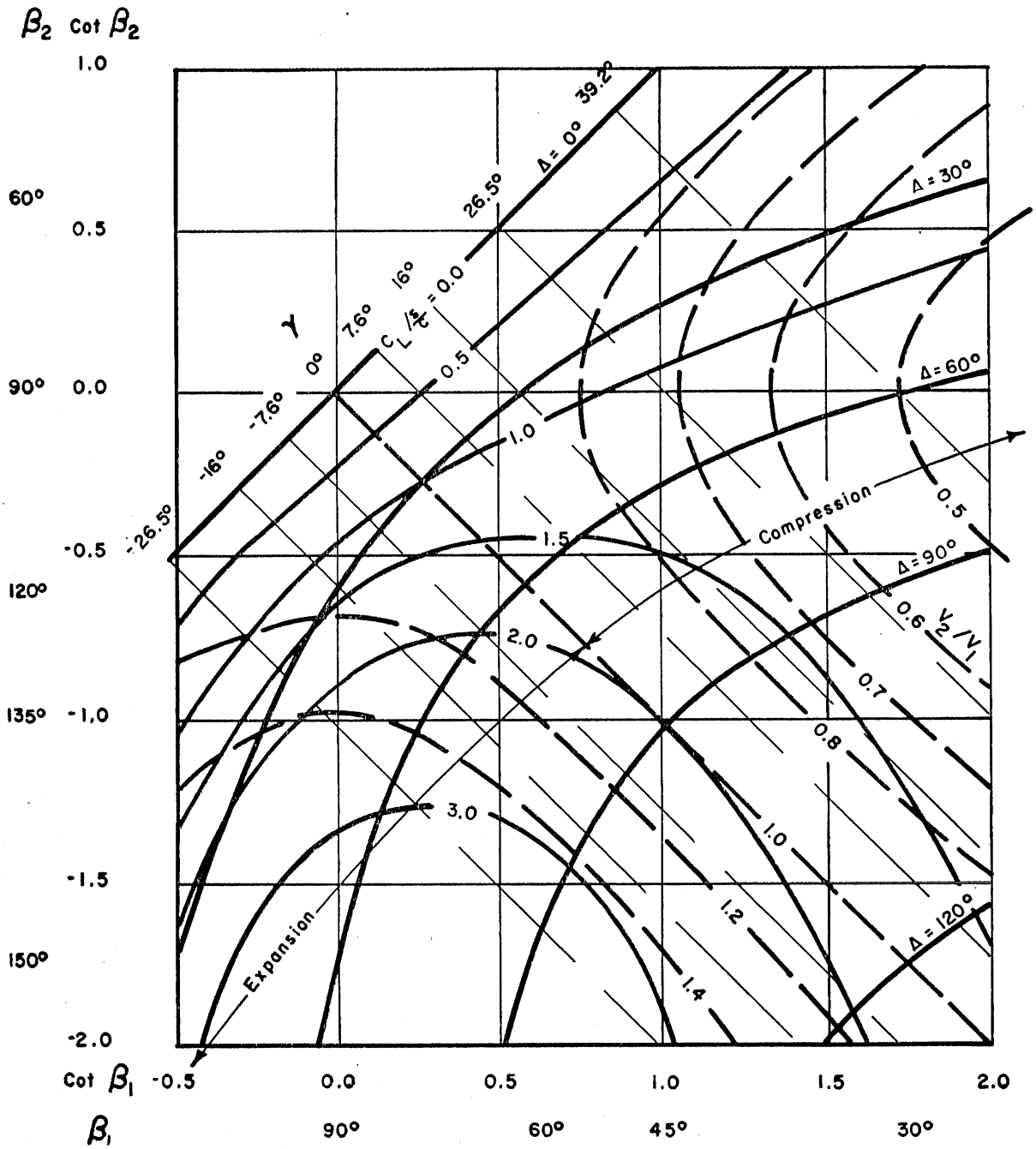

Fig. 5 — Relation Between Entrance and Exit Angles, Deflection Angle, Velocity Ratio, and Required Reaction in a Guide Vane Bend

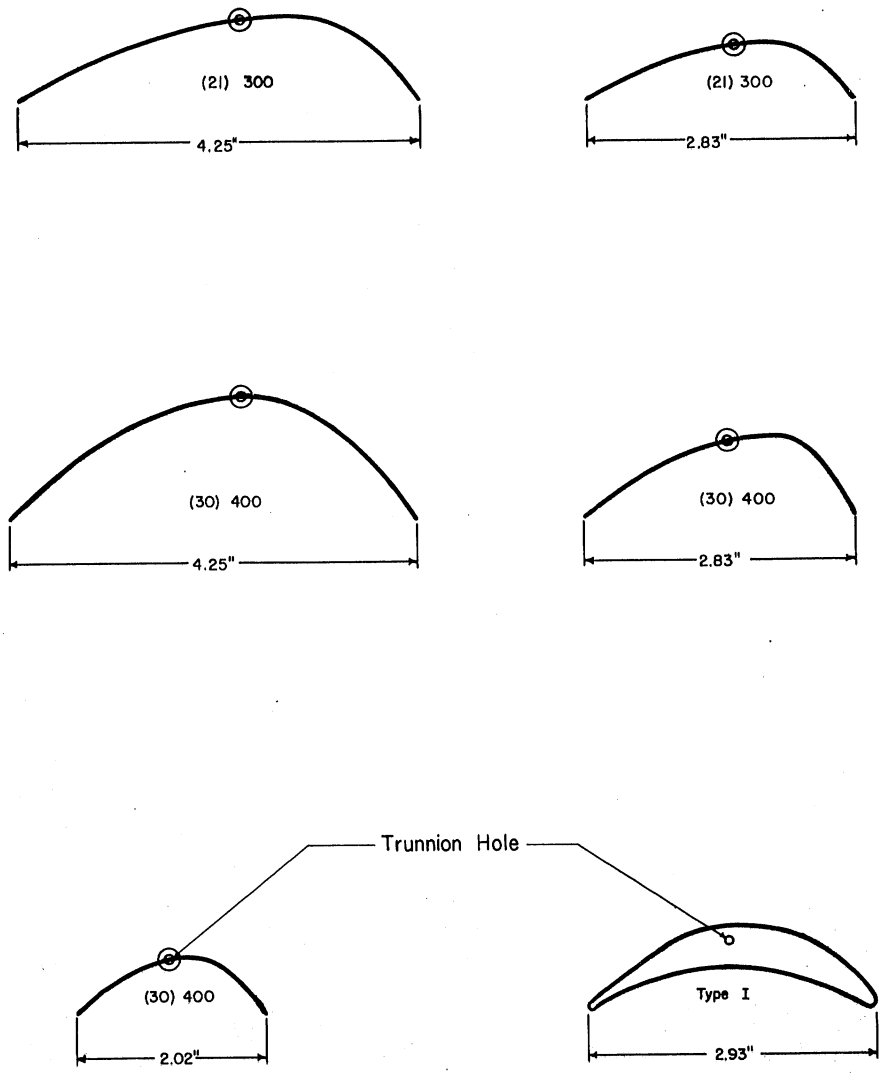

Fig. 6 - Guide Vane Profiles Used in the Experimental Work

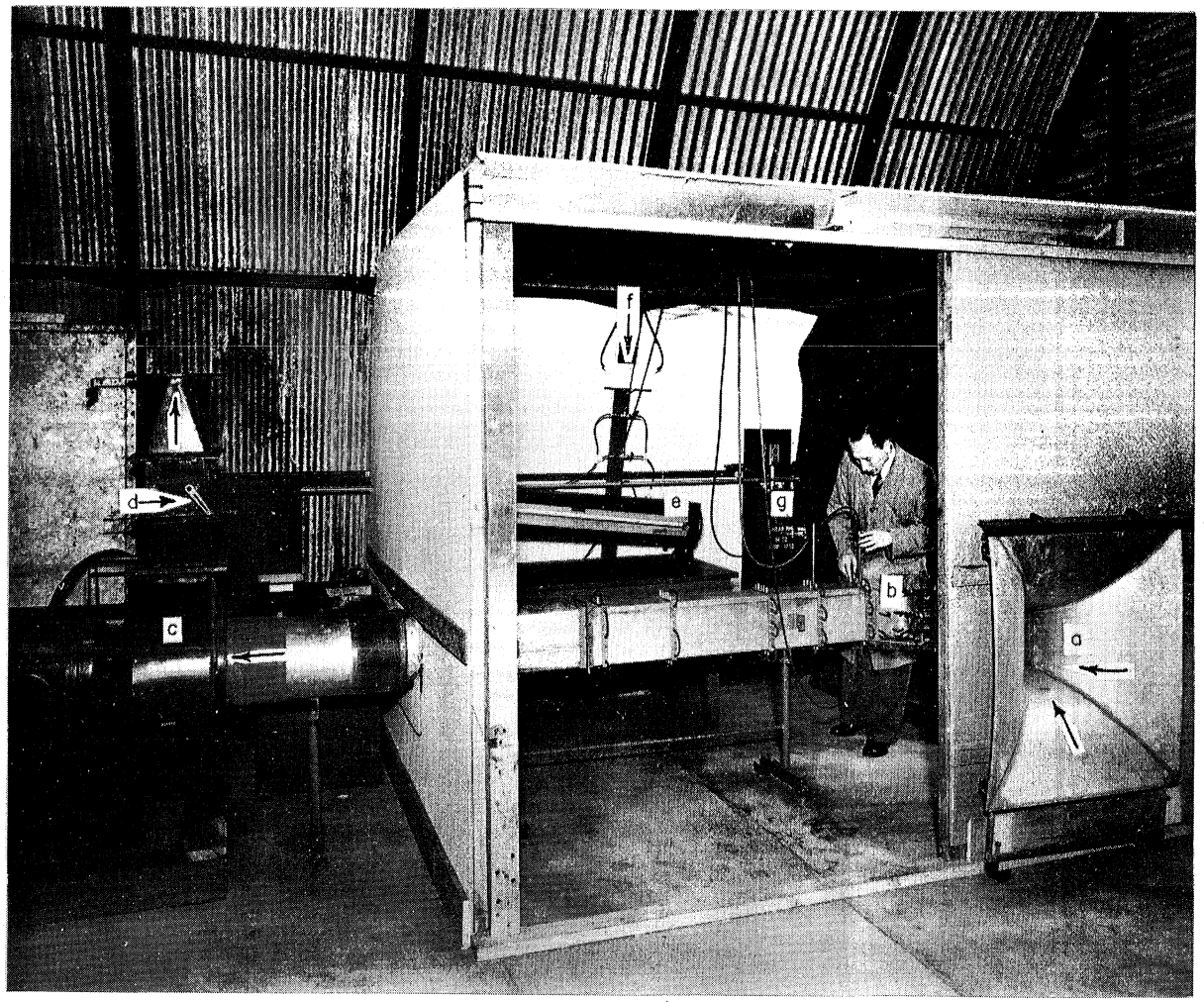

LEGEND

a - Intake
b - Test Section
c - Blower
d - Discharge Control Valve (Butterfly)
e - Inclined Manometer
f - "V" Manometer used for Direction Readings
g - Blower Controls

Fig. 7 - The 6-in. by 9-in. Tunnel

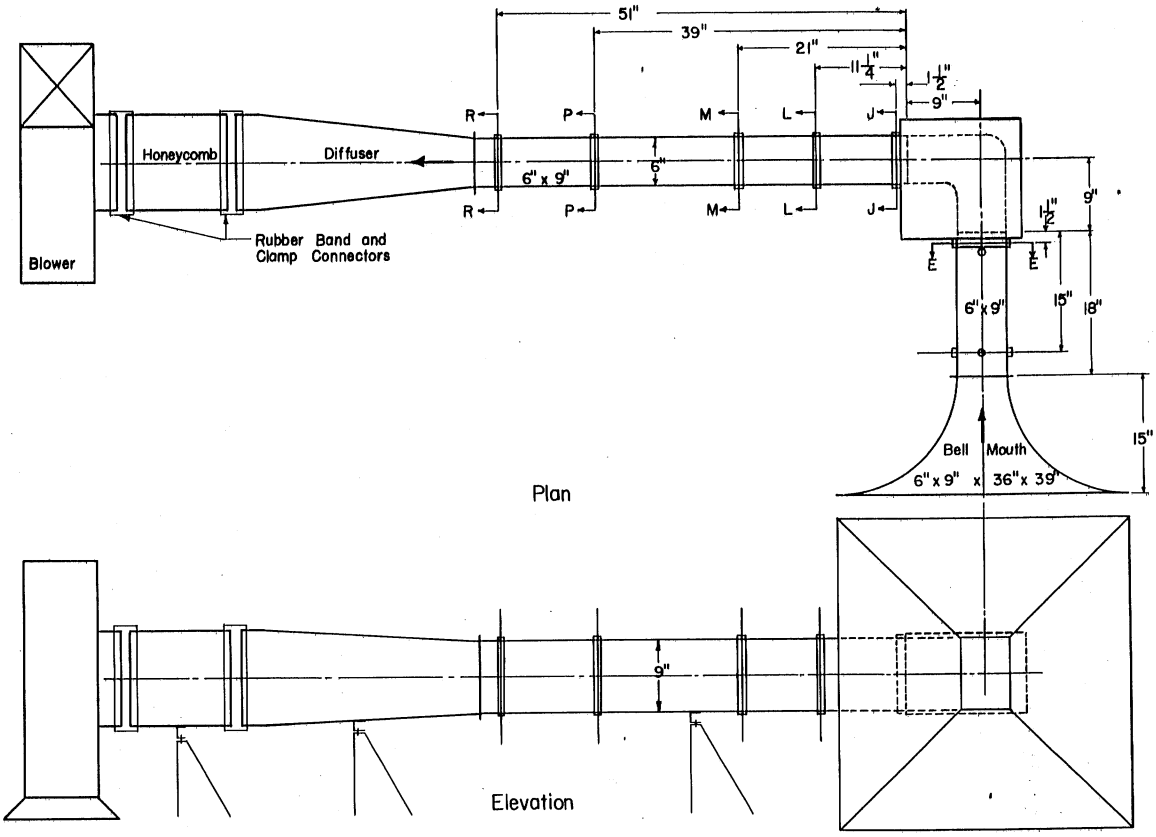

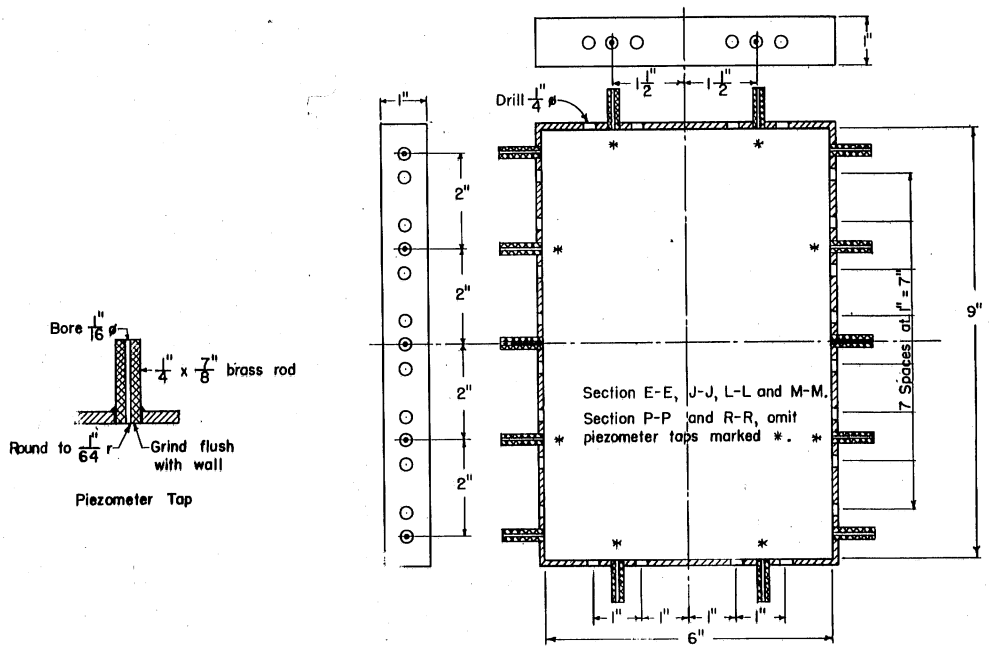

Fig. 8-Principal Dimensions of the 6-in. by 9-in. Tunnel

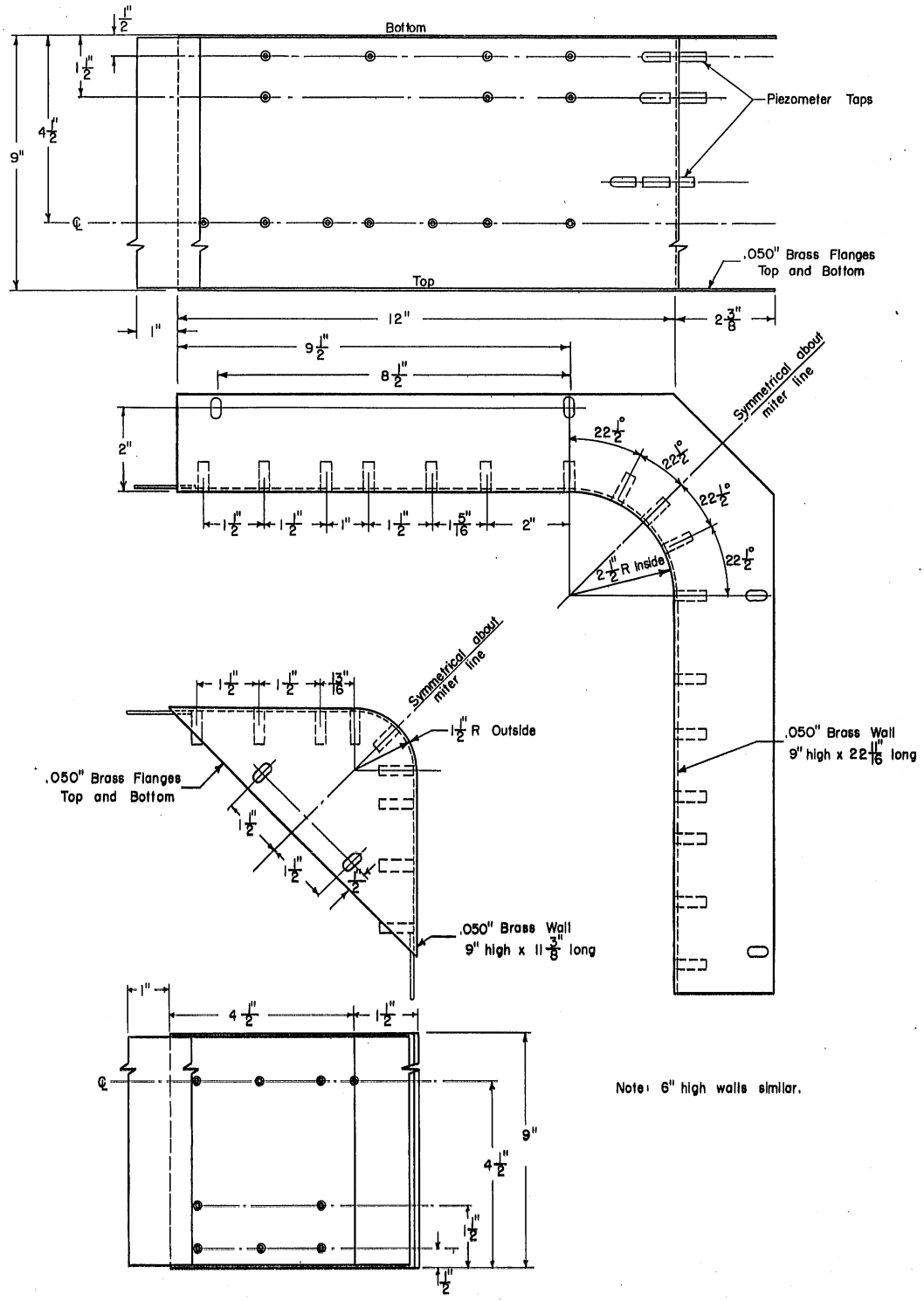

a. Inside and Outside Walls

Fig. 9 - Principal Dimensions of the Test Bends

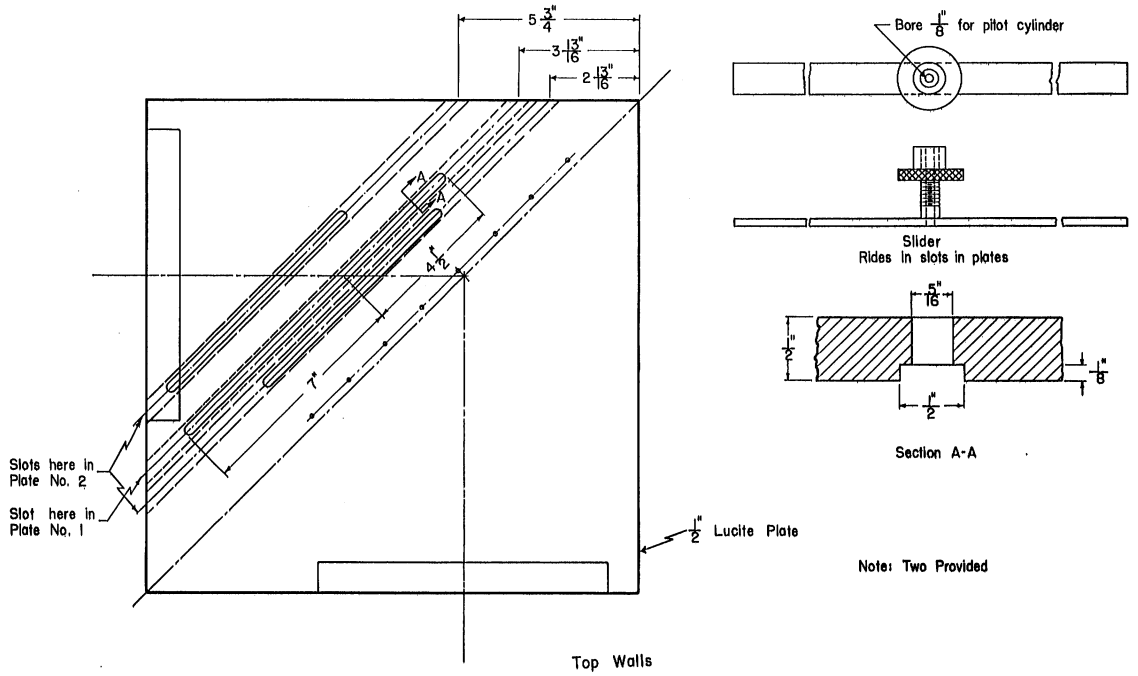

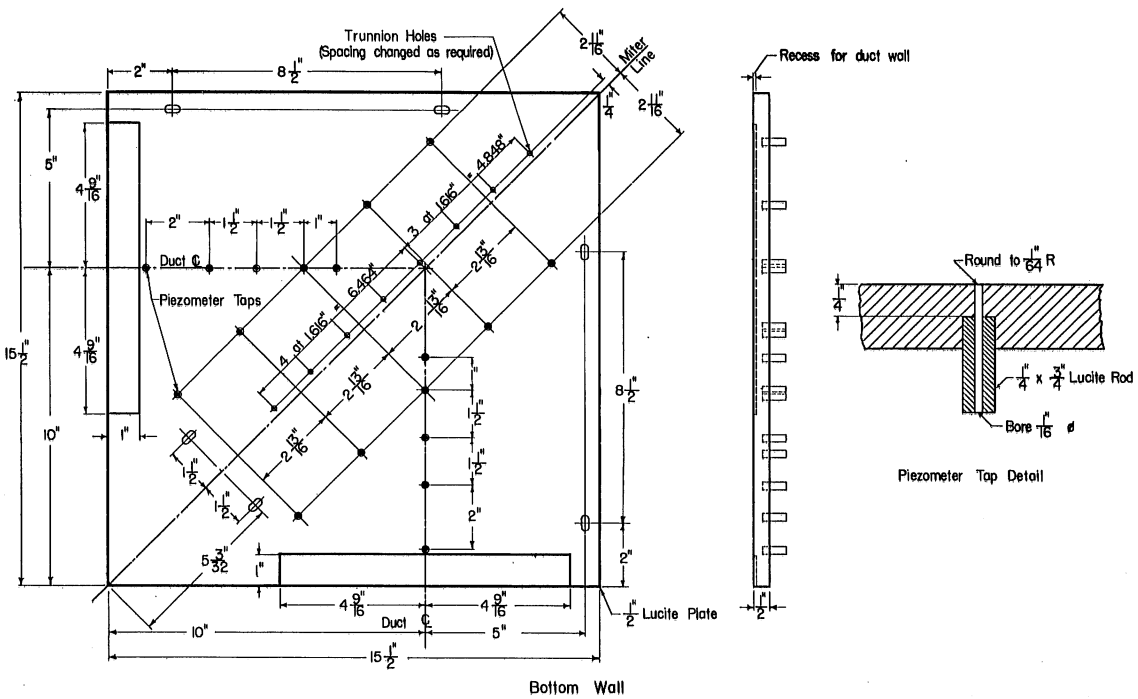

b. Top and Bottom Walls

Fig. 9 (Cont'd) — Principal Dimensions of the Test Bends

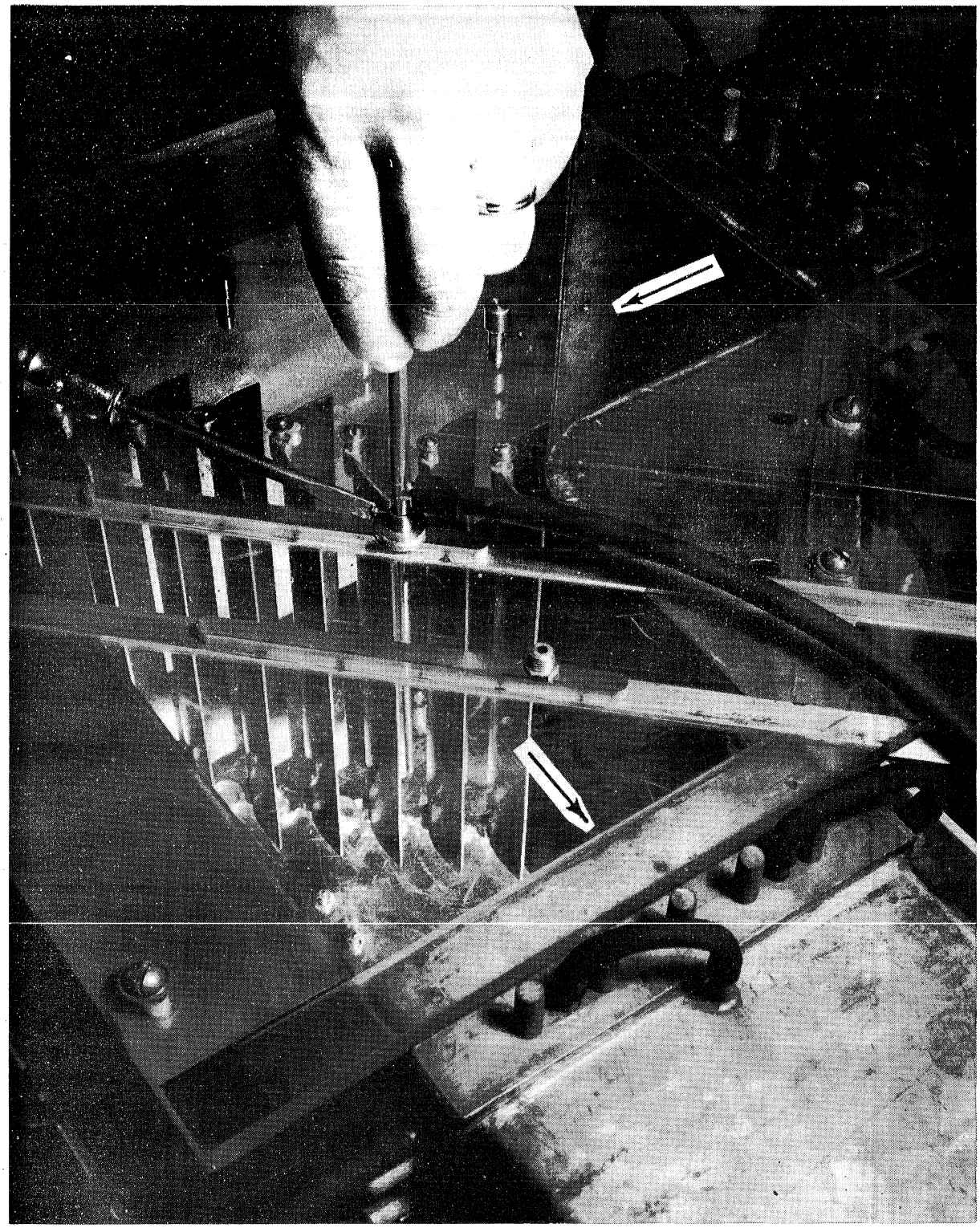

Fig. 10 – Guide Vanes Installed in the 9-in. High Bend

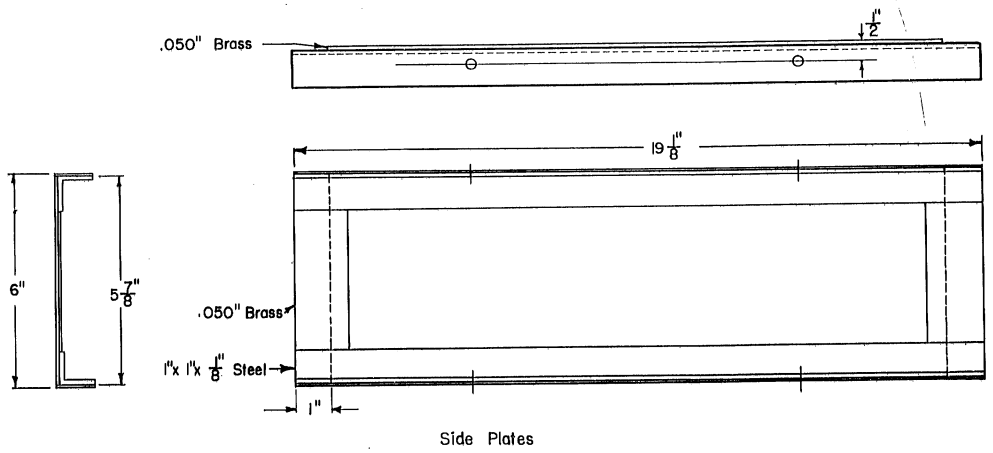

Side Plates

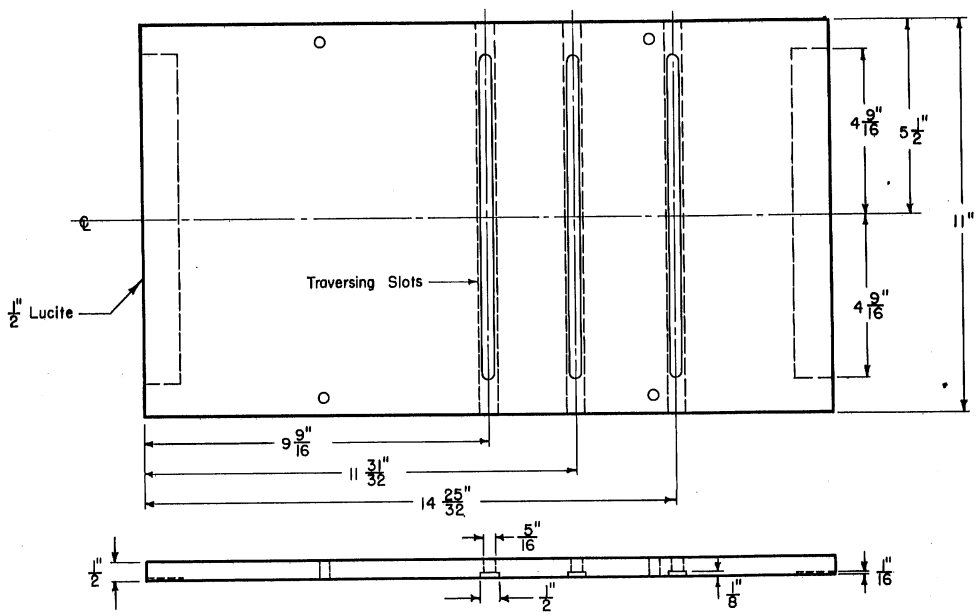

Top Plate

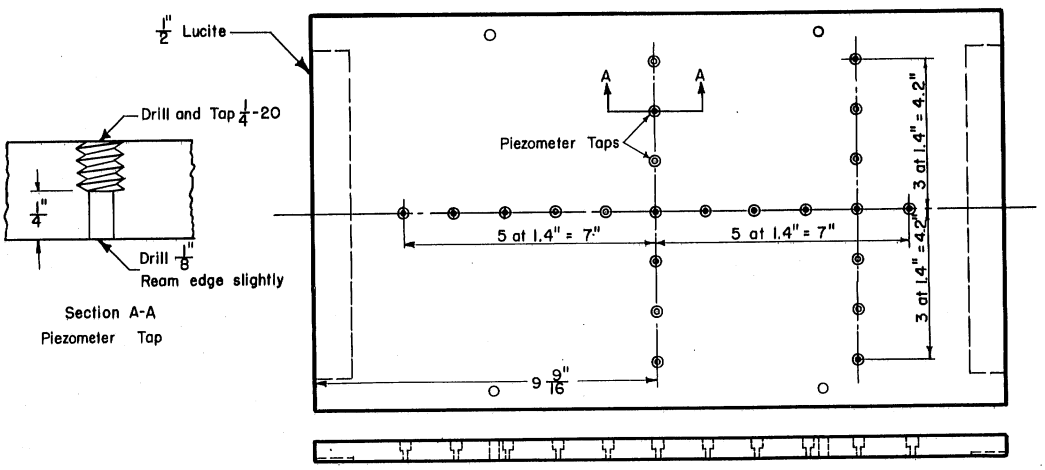

Bottom Plate

Fig. 11- Straight Test Section

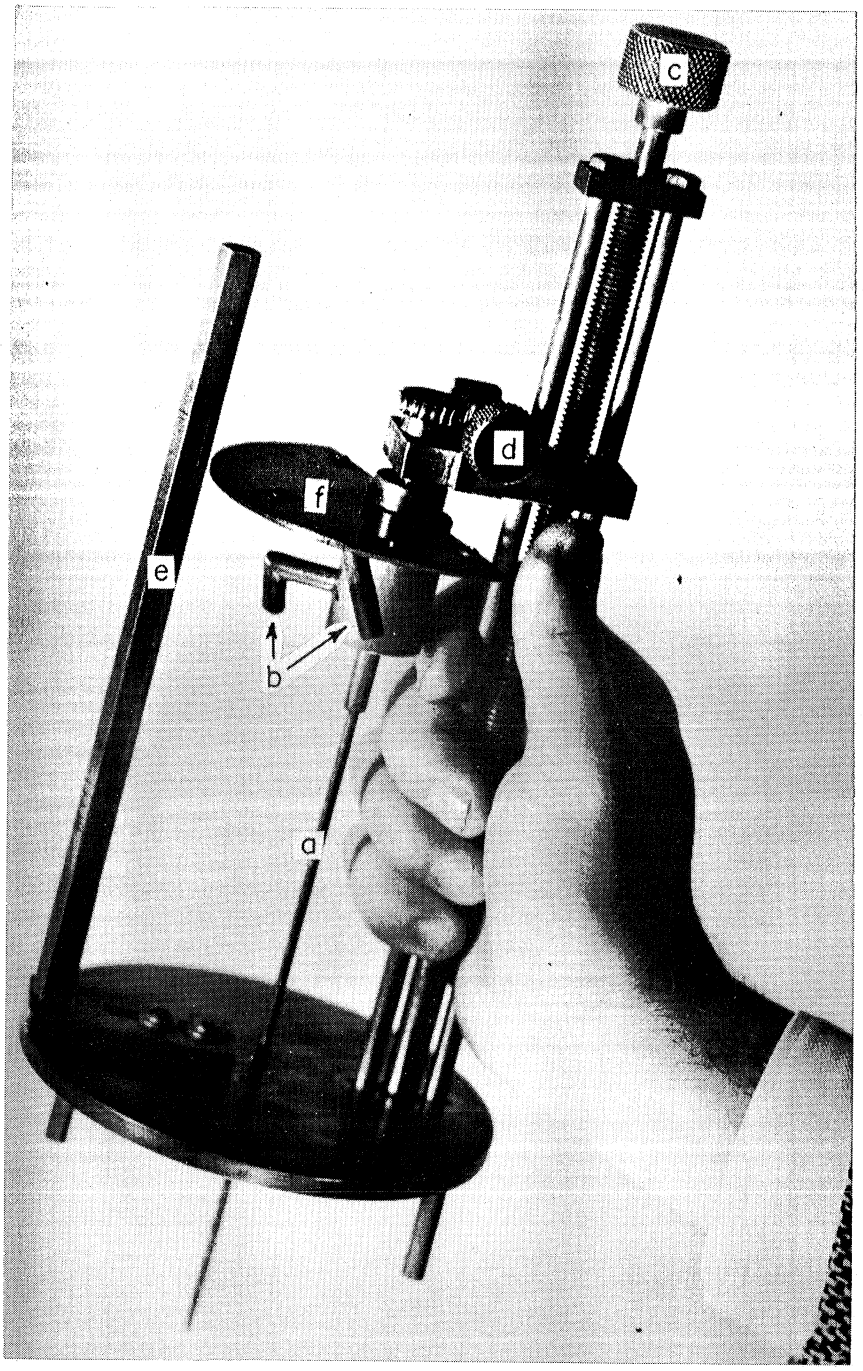

LEGEND

a - Pitot Cylinder
b - Pressure Take-offs
c - Vertical Traversing Knob
d - Direction Knob
e - Vertical Scale and Zero Direction Indicator
f - Protractor for Reading Flow Direction

Note: The carriage is traversed horizontally by the slider shown in Fig. 9b (2).

Fig. 12 - Pitot Cylinder and Traversing Carriage

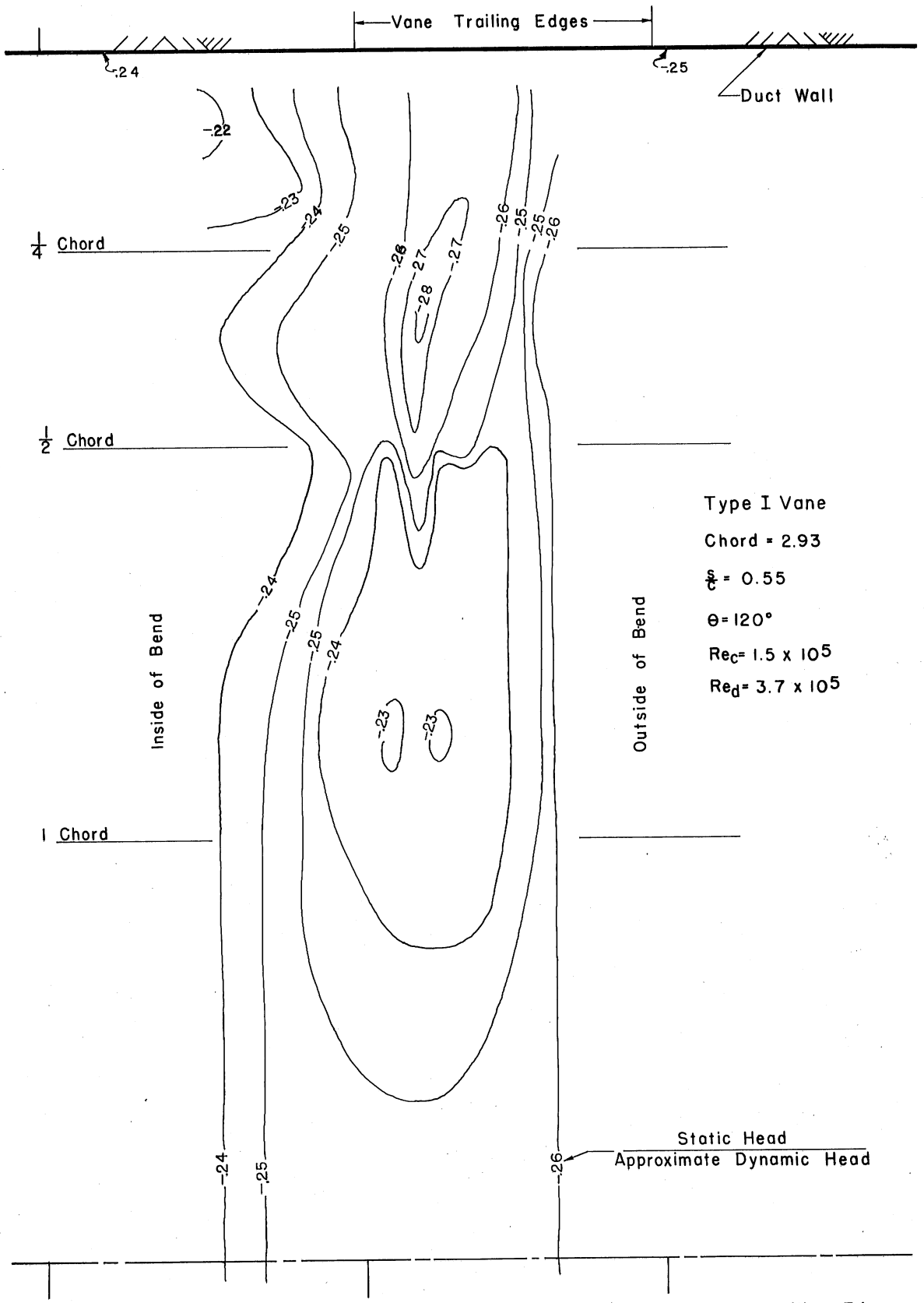

Fig. 13 – Dimensionless Static Head Distribution 0.5 Chord Downstream of Vane Trailing Edges

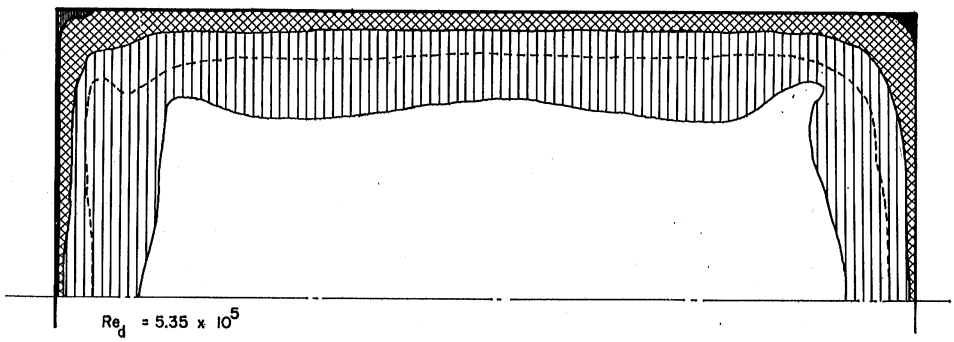

a. At the Station Corresponding to the Miter Line (26.5 in. from Bell Mouth)

Dimensionless Total Head	
	Less than 0.3
	0.3 to 0.7
	0.7 to 0.98
	0.9
	Over 0.98

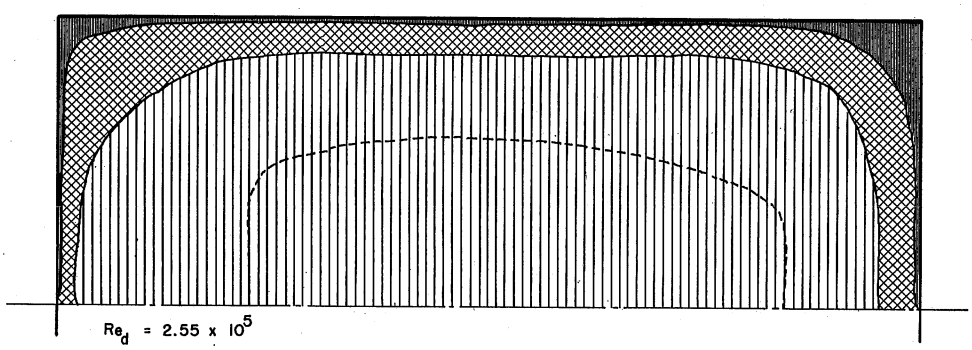

b. At Section M-M

Fig. 14- Total Head Distribution in the Wind Tunnel with Straight Test Section

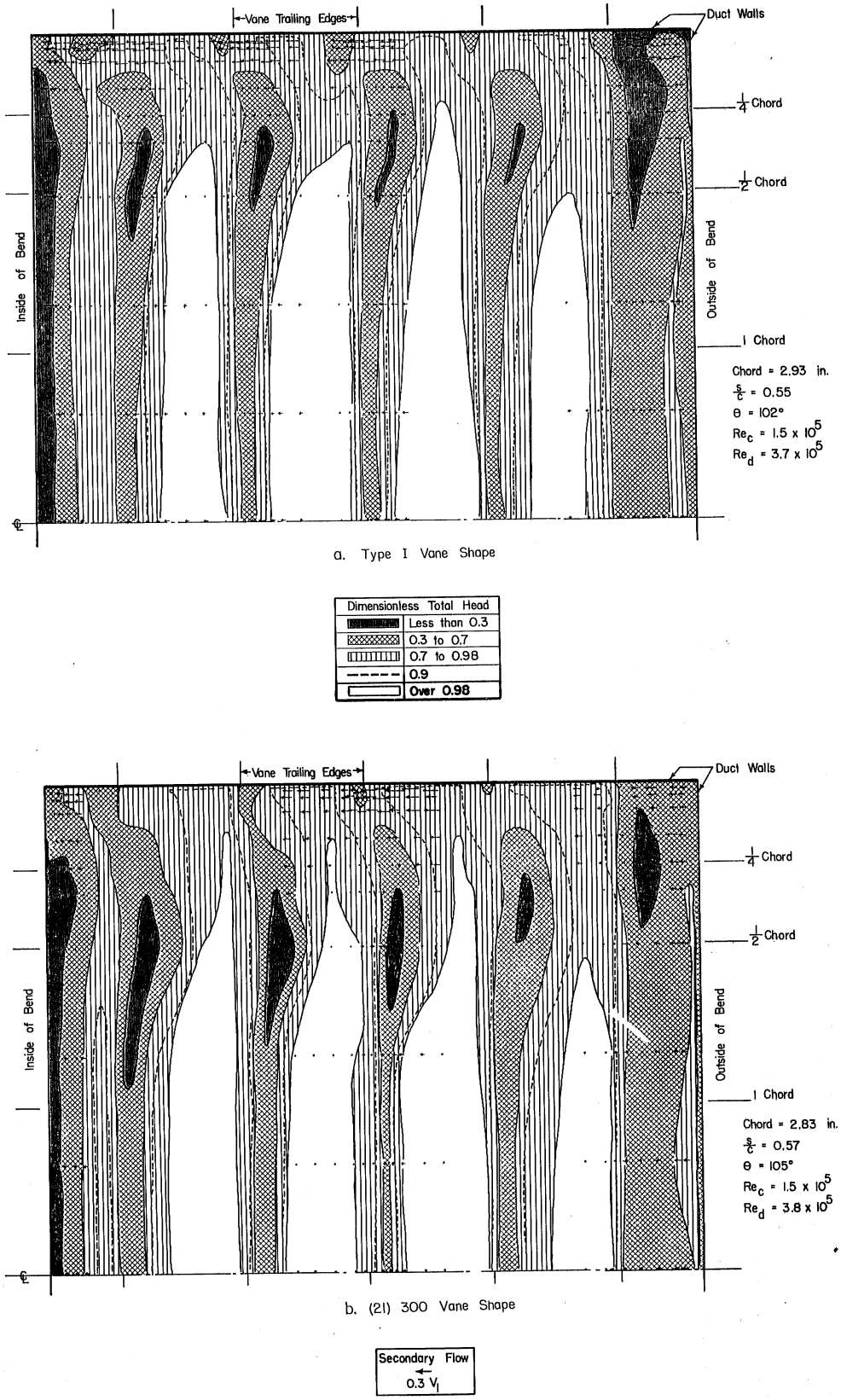

Fig. 15 – Total Head and Secondary Flow Measured 0.5 Chord Behind a Guide Vane Bend

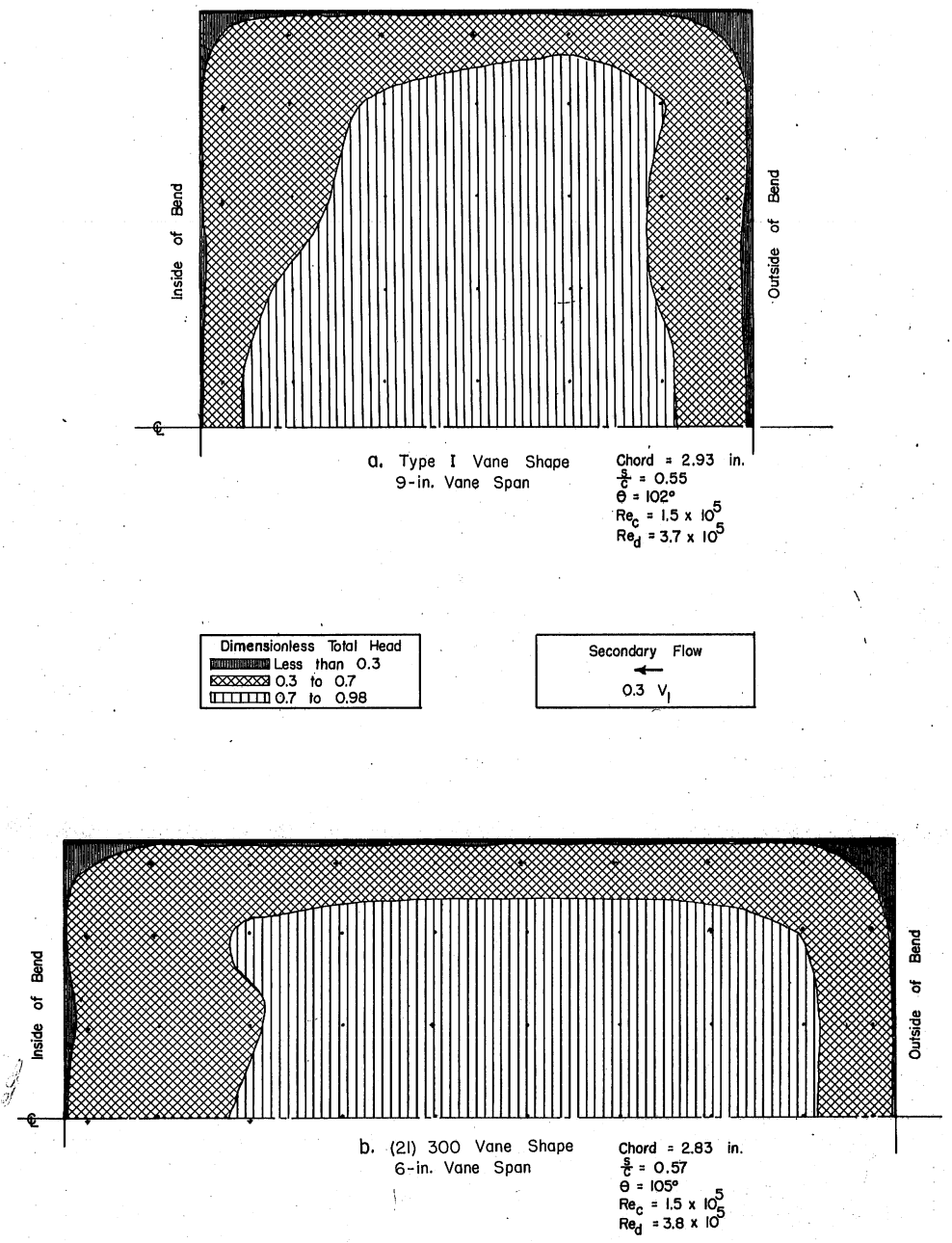

Fig. 16 - Total Head and Secondary Flow Behind a Guide Vane Bend Measured Far Downstream

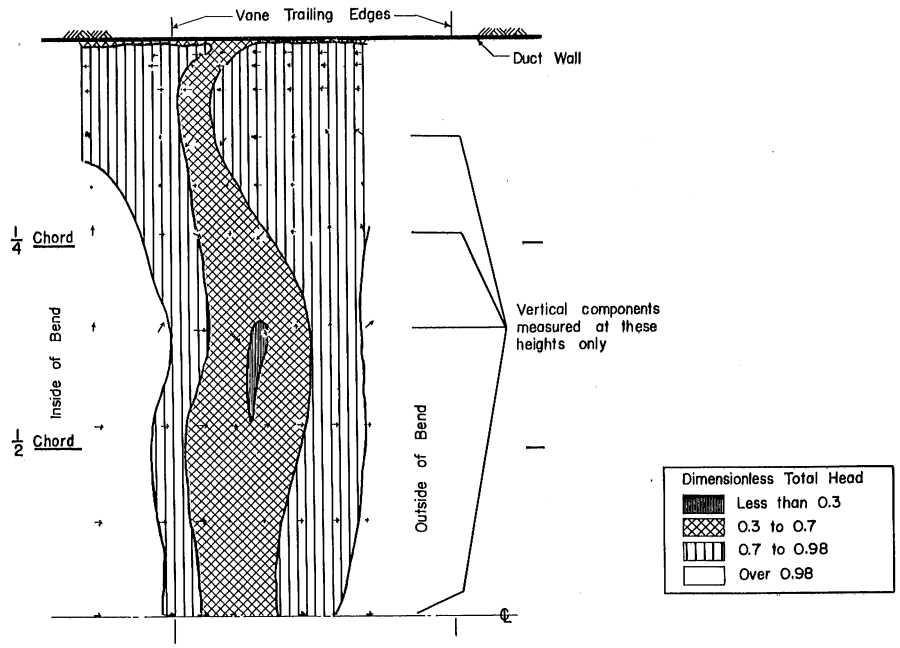

a. 0.5 Chord Length Behind Trailing Edges of Vanes

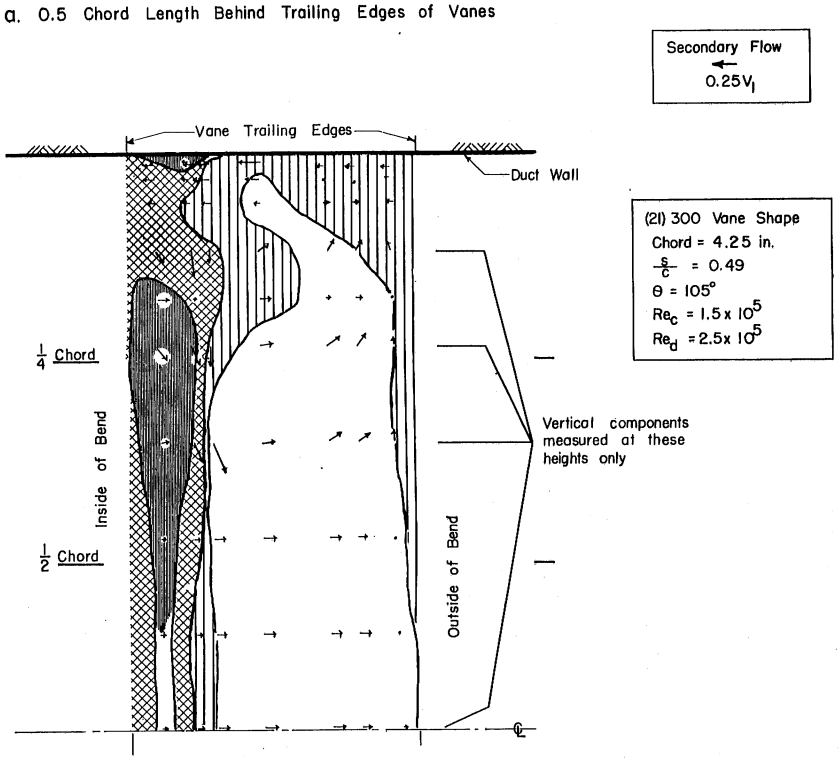

b. 0.1 Chord Length Behind Trailing Edges of Vanes

Fig. 17 – Variation of Total Head and Secondary Flow with Distance Behind a Guide Vane Bend

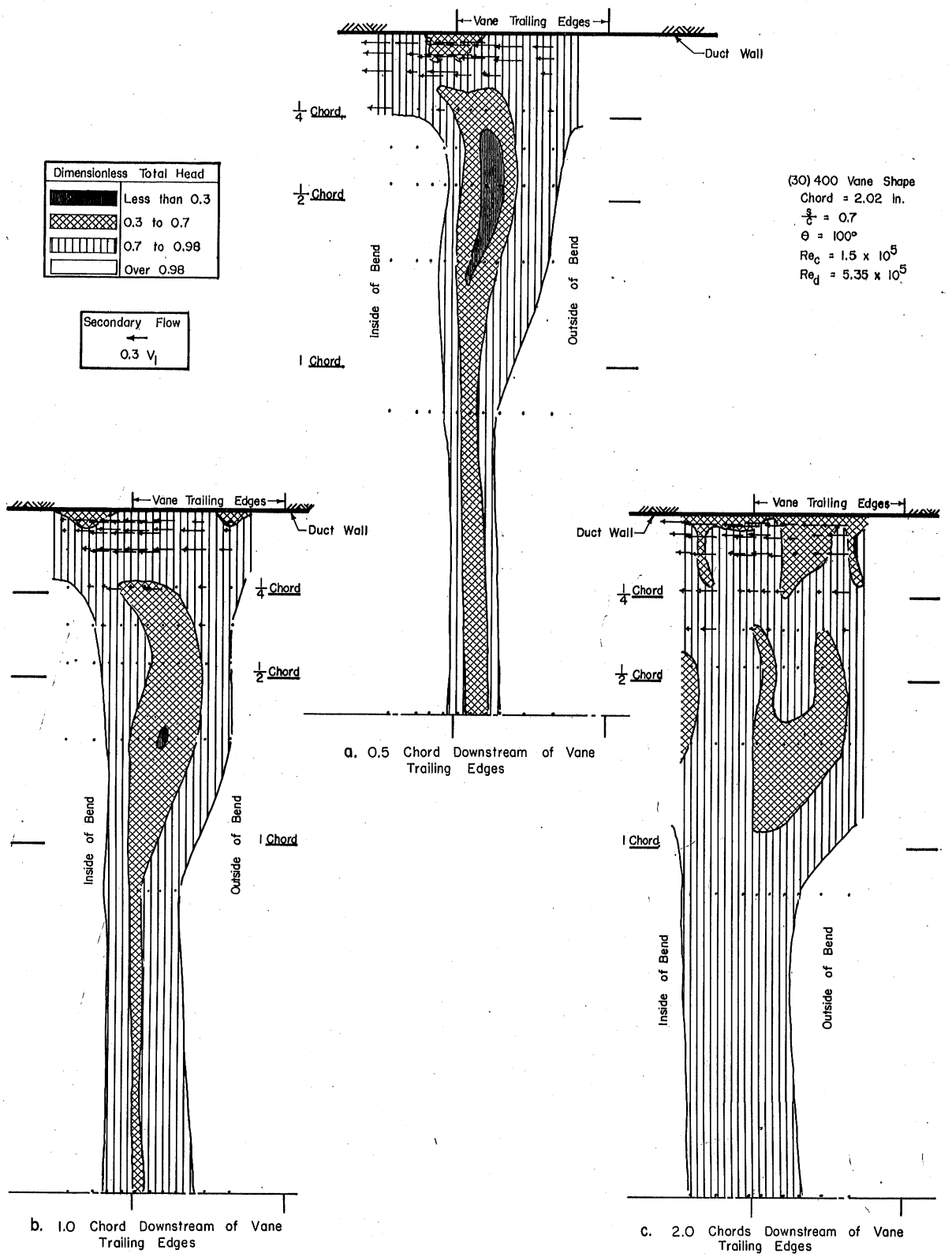

Fig. 18—Variation of Total Head and Secondary Flow with Distance Behind a Guide Vane Bend

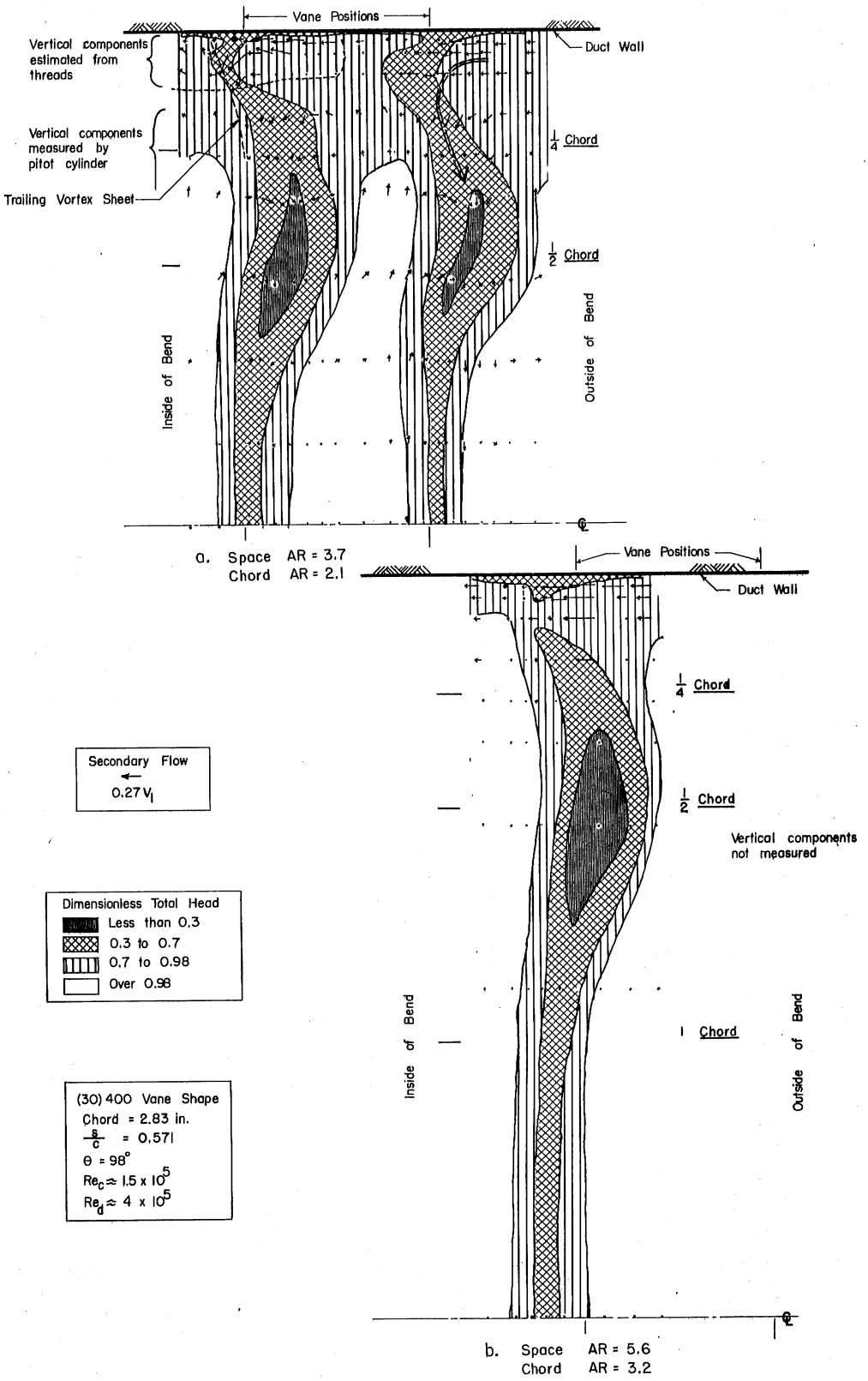

Fig. 19— Variation of Total Head and Secondary Flow with Aspect Ratio

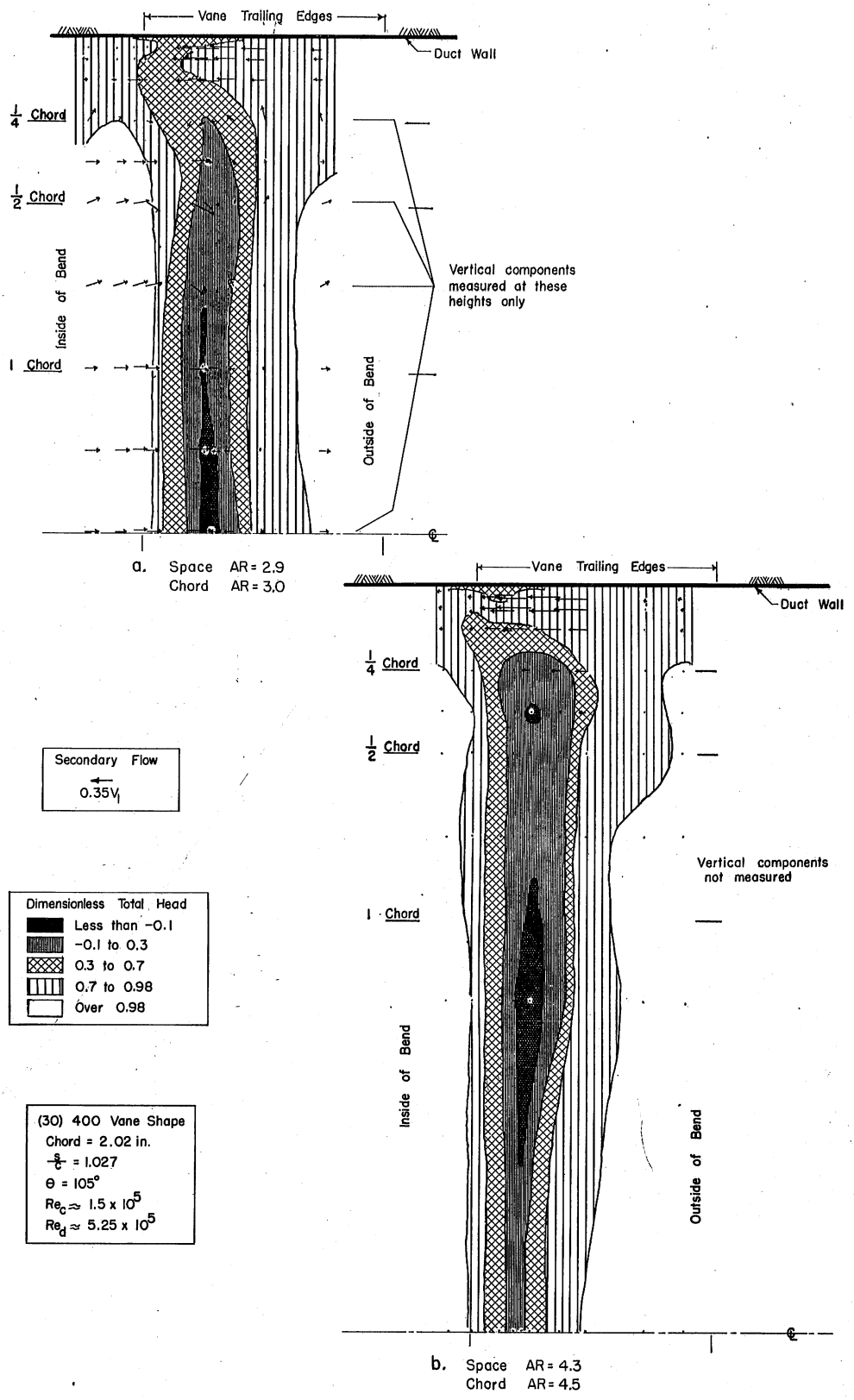

Fig. 20 – Variation of Total Head and Secondary Flow with Aspect Ratio

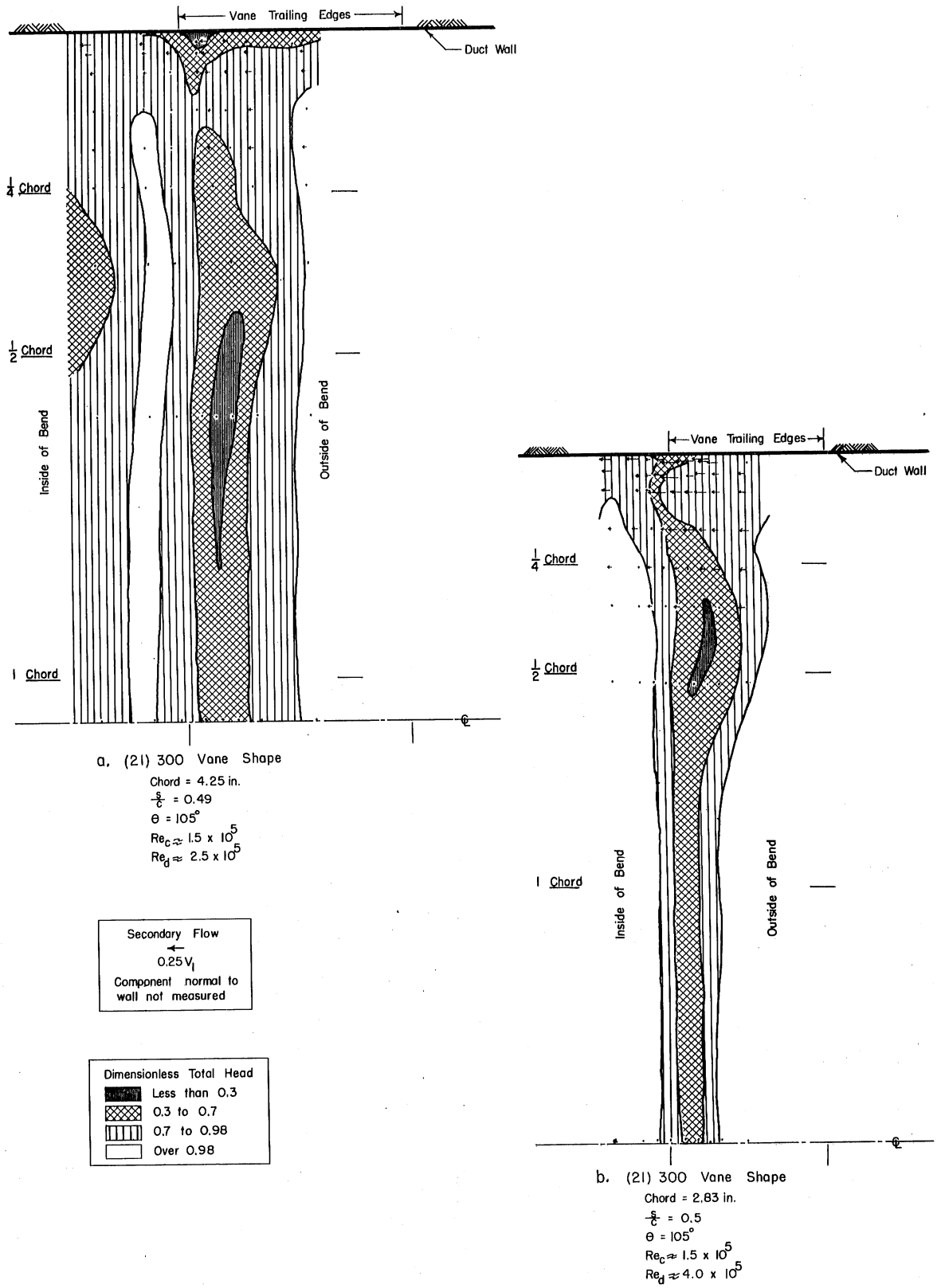

Fig. 21– Variation of Total Head and Secondary Flow with Chord Length

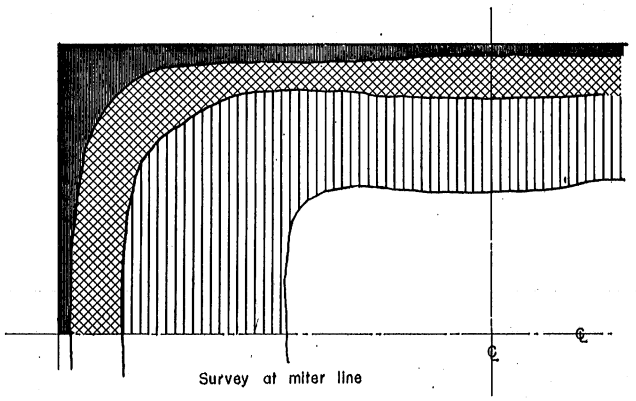

a. Straight Test Section

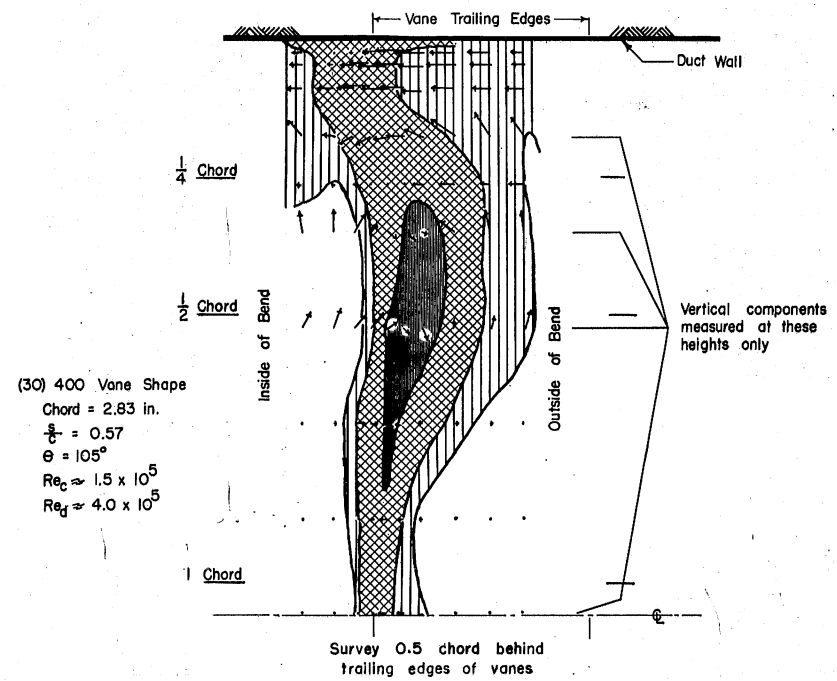

b. Miter Elbow

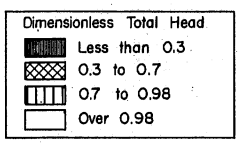

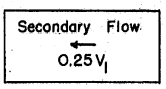

Fig. 22- Total Head Distribution and Secondary Flow as Influenced by Altered Entrance Conditions

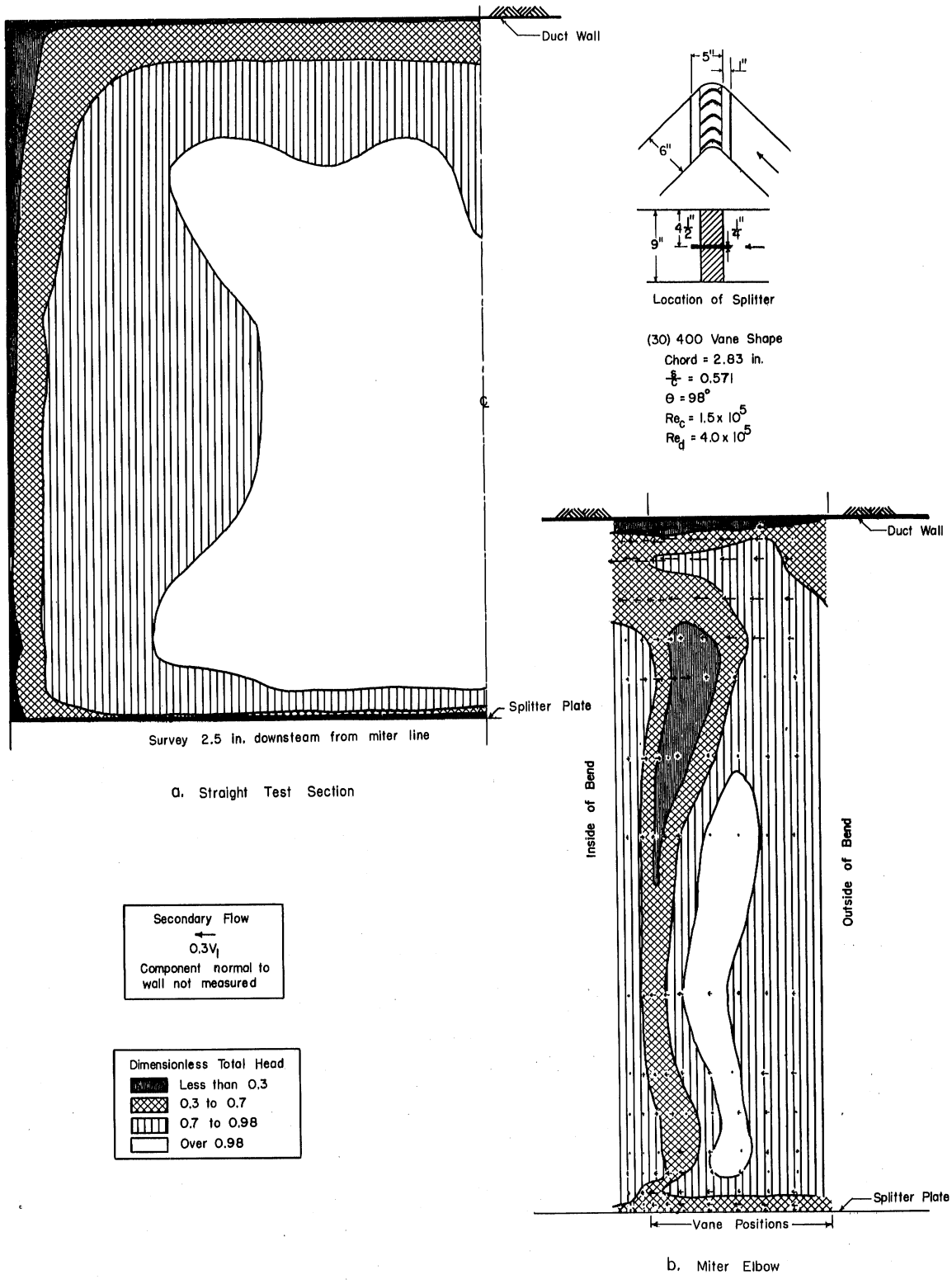

Fig. 23 – Total Head Distribution and Secondary Flow as Influenced by Altered Entrance Profile

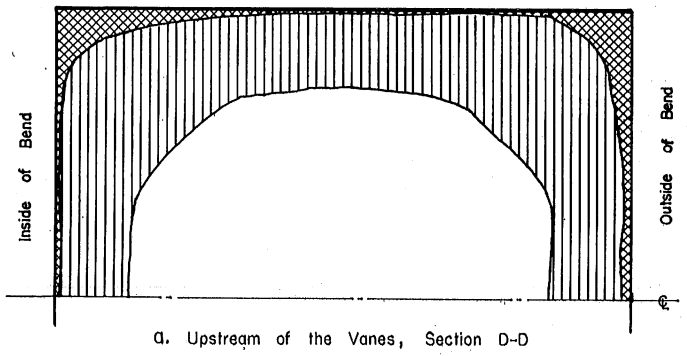

a. Upstream of the Vanes, Section D-D

Type I Vane Shape
Chord = 2.93 in.
$\frac{s}{c}$ = 0.55
θ = 102°
Re_c = 1.5 x 10^5
Re_d = 3.1 x 10^5

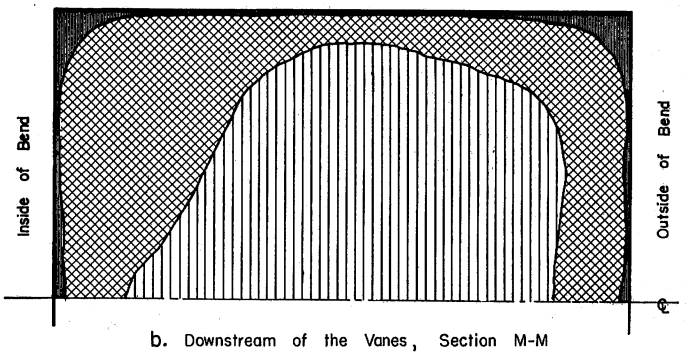

b. Downstream of the Vanes, Section M-M

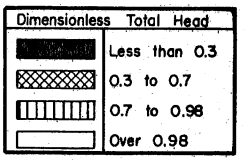

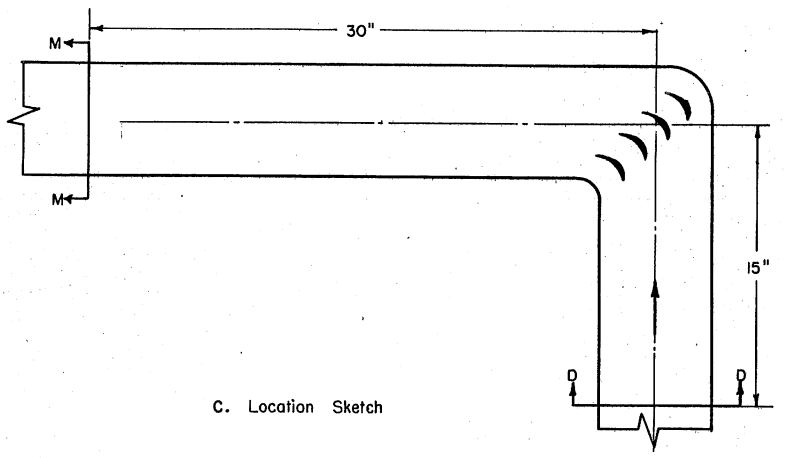

c. Location Sketch

Fig. 24 - Total Head Distribution in the 6-in. by 6-in. Tunnel

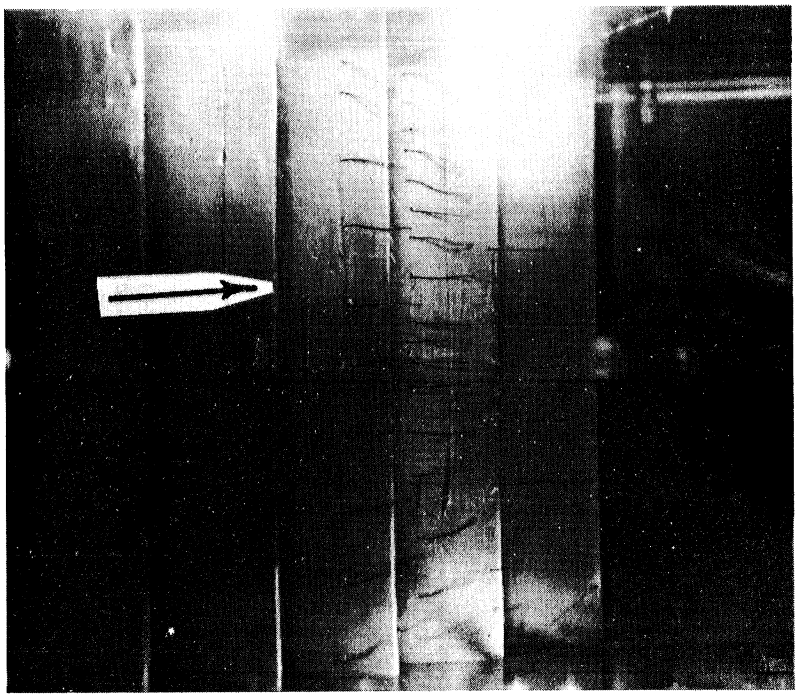

a. Flow Direction on Suction Surfaces of Vanes (Type I Vanes)

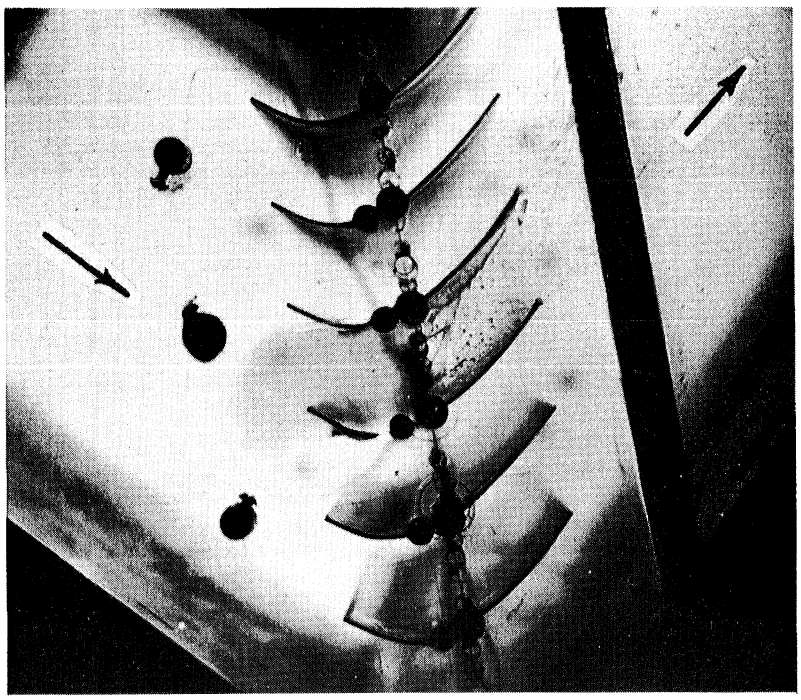

b. Flow Direction Near Duct Wall ((21) 300 Vanes)

Note two black threads about 1/4 in. from wall marking interior flow and water layer on wall marking boundary layer flow. Water was admitted from puddle on top of wall through spaces surrounding hypodermic needles holding threads.

Fig. 25 - Air Flow Direction Between the Vanes

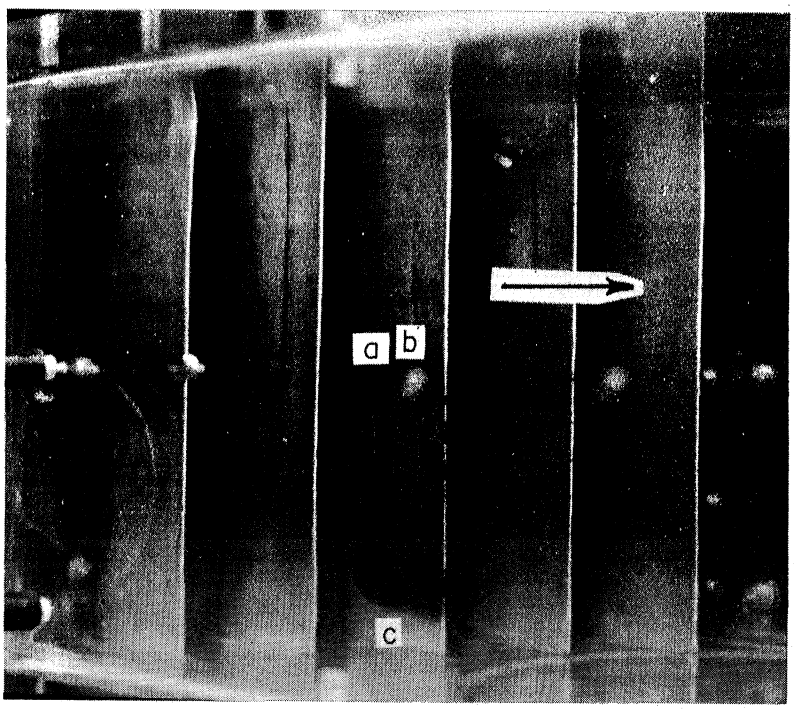

a. Air Flow on Suction Surface of Vane (Type I Vane)

Note: Dyed water was admitted through a piezometer tap at a. The water was carried by the air in the boundary layer until separation occured at b. It then dropped by gravity to c where the secondary flow prevented separation.

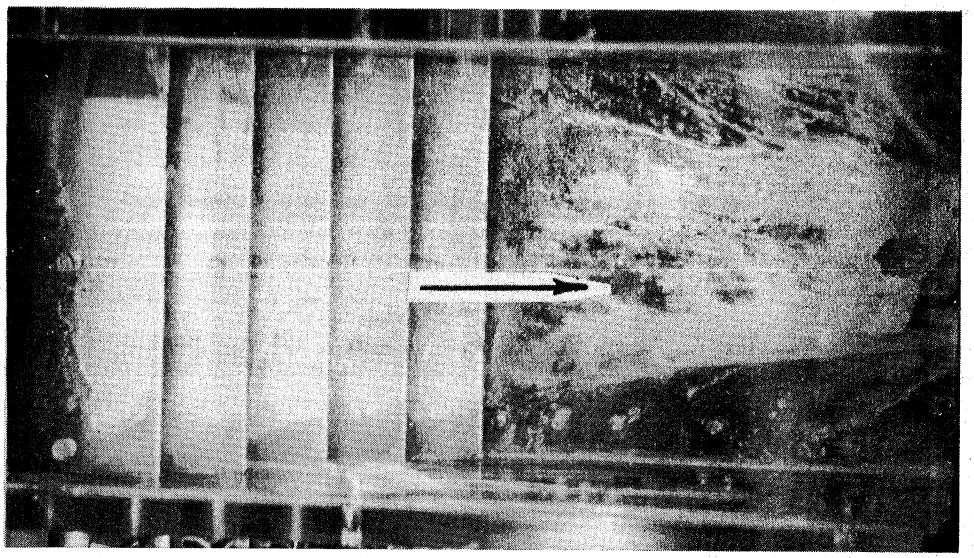

b. Water Flow on Suction Surface of Vanes and on Inside Bend Wall (Type I Vane)

Note: The walls were coated with aluminum powder in SAE 30 oil. Erosion after operation for 5 minutes with $V_1 \simeq 8$ fps is shown.

Fig. 26 - Flow Direction as Indicated by Wall Coatings

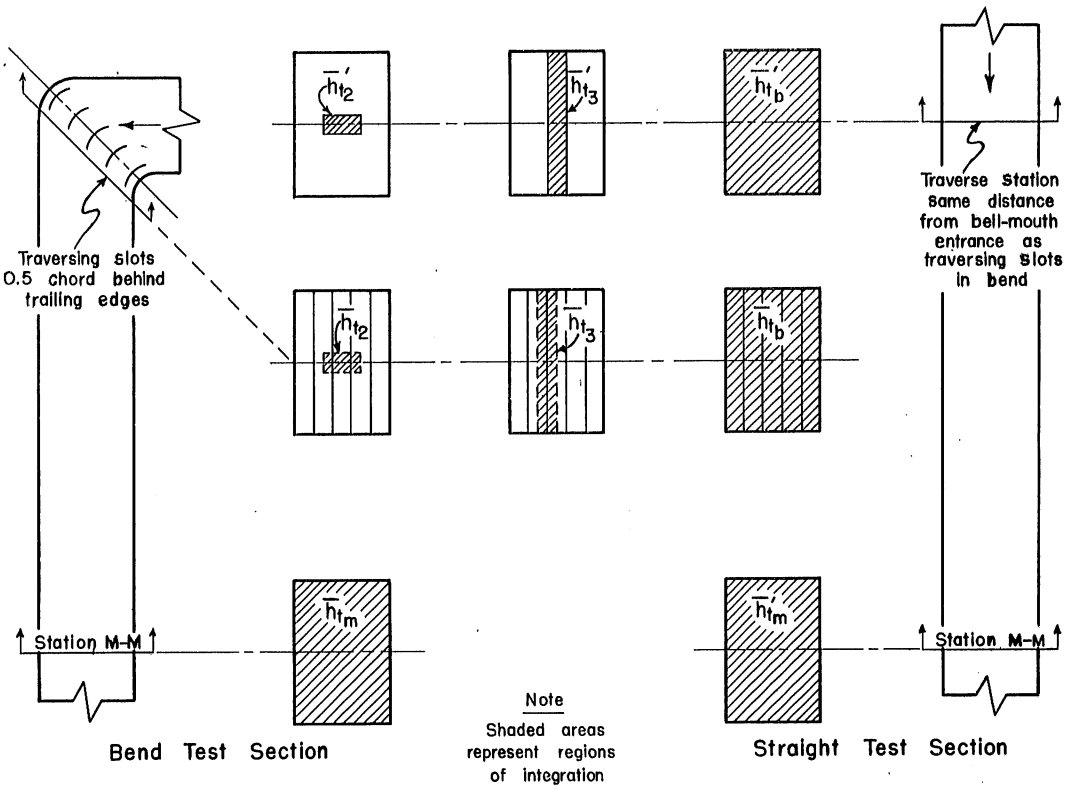

Fig. 27 – Definitions of Average Total Head Terms

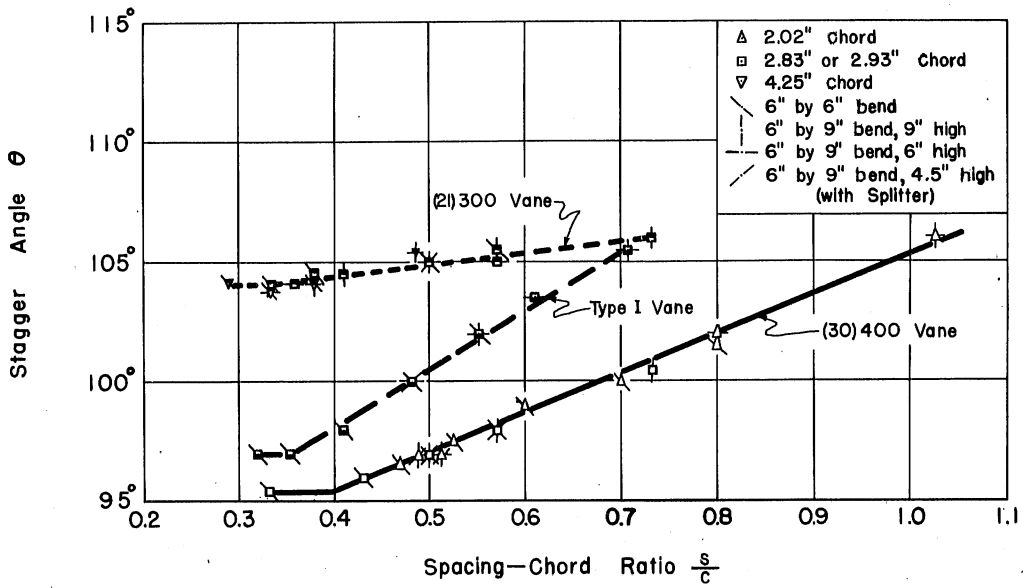

Fig. 28 – Stagger Angle Required to Produce 90° Flow Deflection

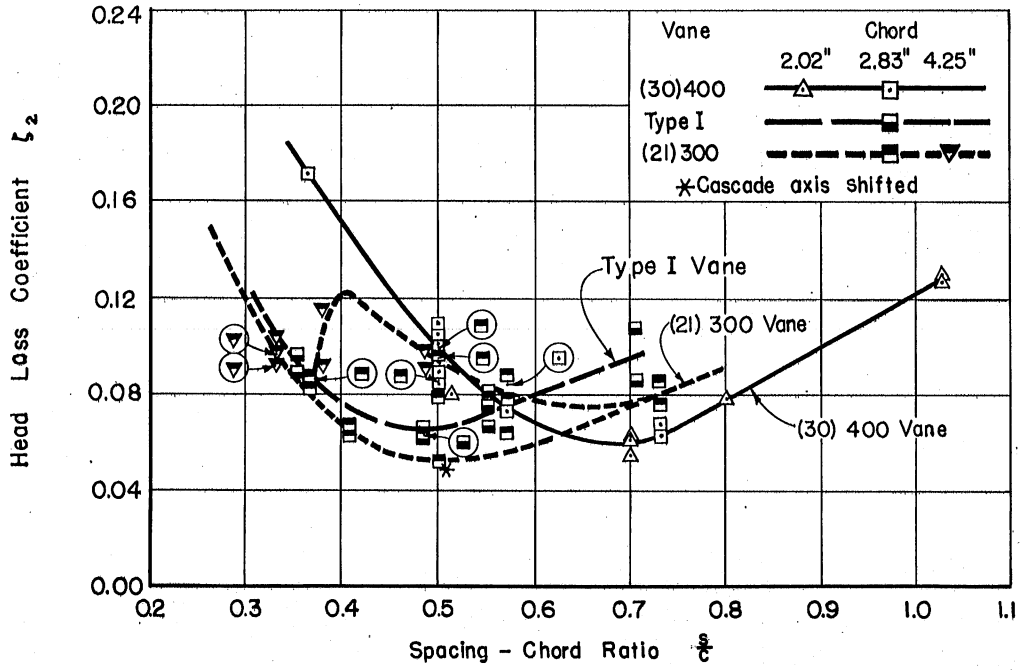

a. Head Loss Coefficient

$Re_c = 1.5 \times 10^5$

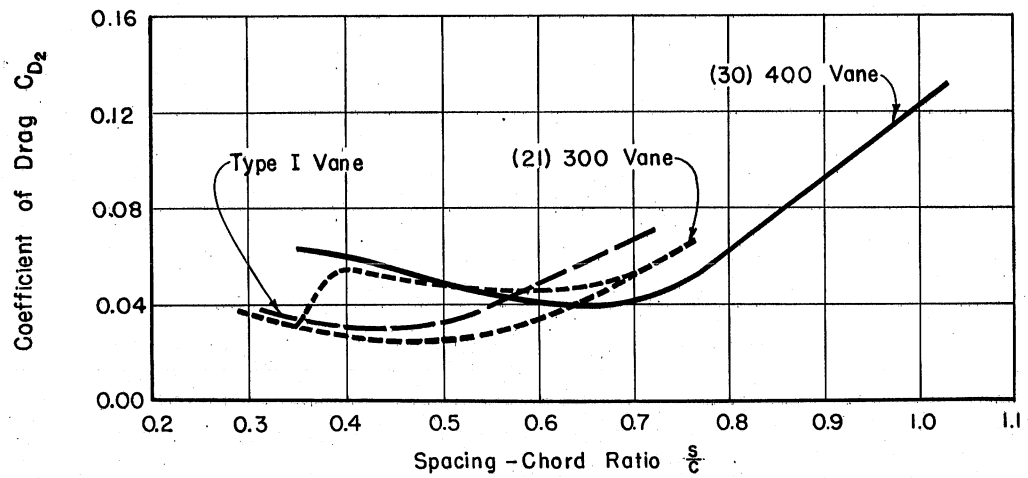

b. Coefficient of Drag

$Re_c = 1.5 \times 10^5$

Fig. 29 — Two-Dimensional Head Loss and Drag Coeffients

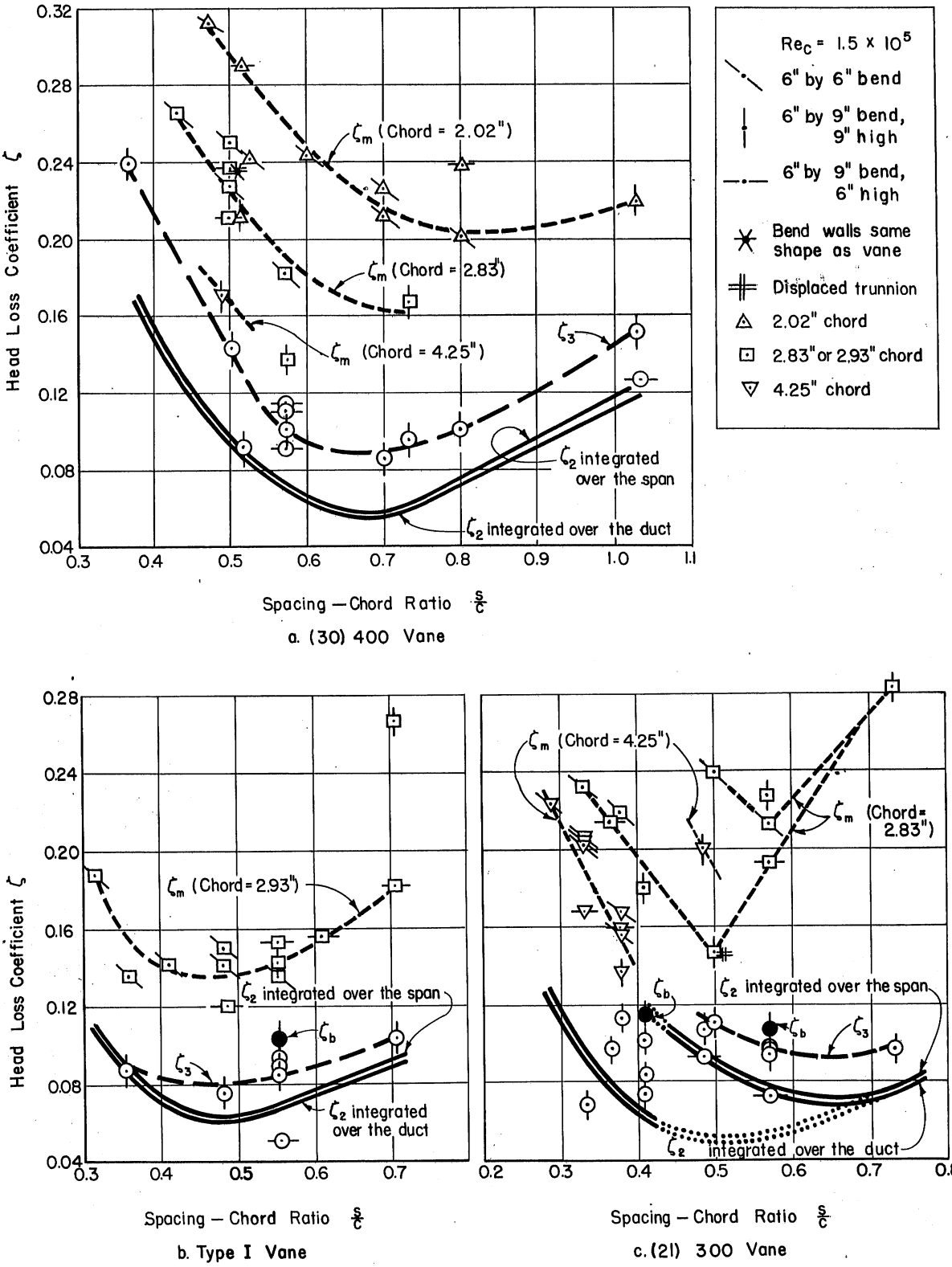

Fig. 30 — Comparison of Two-Dimensional and Three-Dimensional Head Loss Coefficients

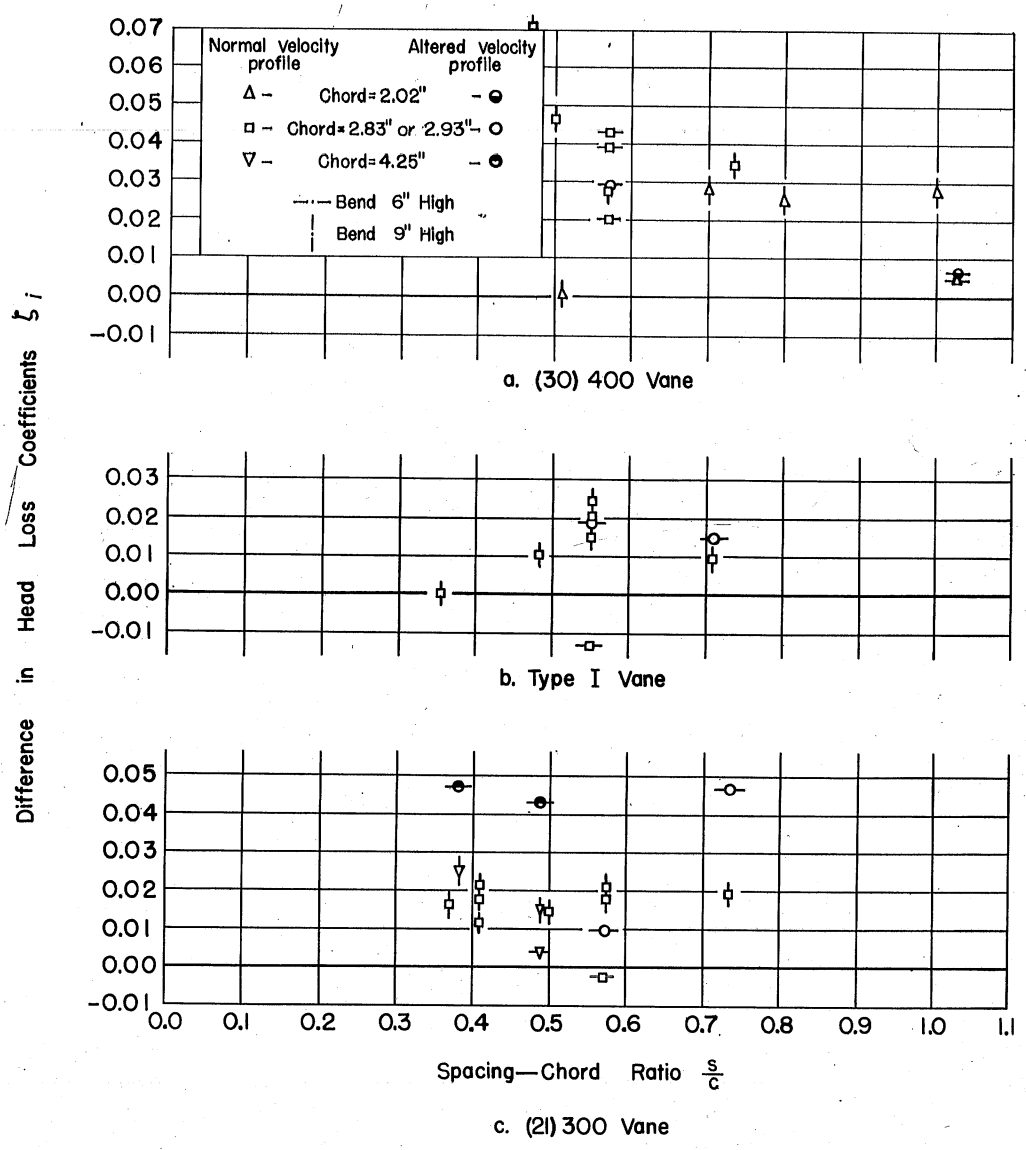

Fig. 31 – Difference Between Three-Dimensional and Two-Dimensional Head Loss Coefficients Measured 0.5 Chord Behind the Vanes

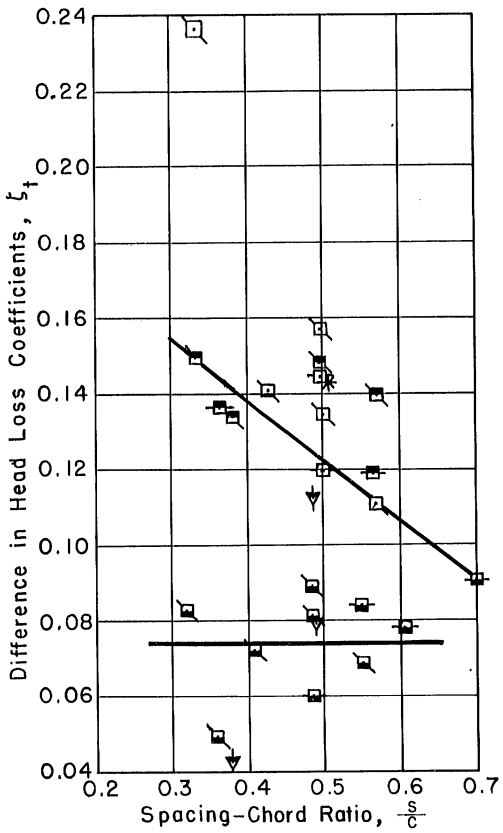

a. $AR_c = 2.1$

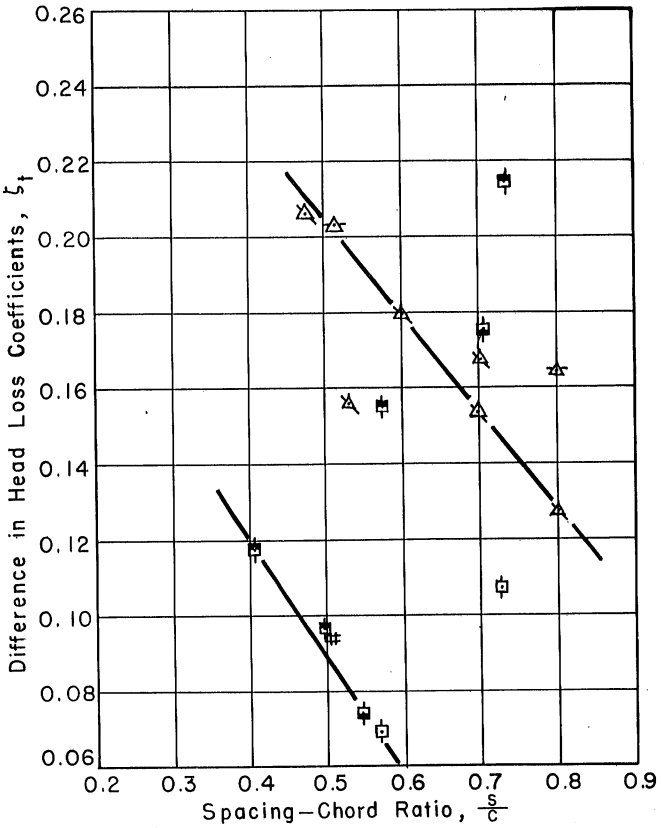

b. $AR_c = 3.1$

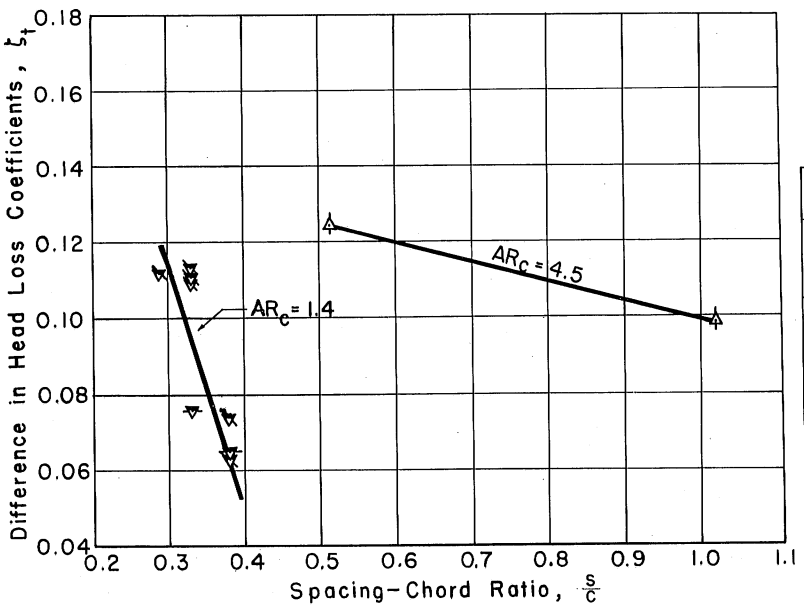

c. $AR_c = 1.4$ & 4.5

Chord Length	(30) 400 Vanes	(21) 300 Vanes	Type I Vanes
2.02 in.	△		
2.83 or 2.93 in.	⊡	▬	▬
4.25 in.	▽	▼	

6-in. x 6-in. bend
6-in. x 9-in. bend, 9 in. high
6-in. x 9-in. bend, 6 in. high
✳ Walls same shape as vanes
\# Trunnions shifted

Fig. 32– Difference Between Three-Dimensional and Two-Dimensional Head Loss Coefficients Measured Far Downstream as a Function of Spacing-Chord Ratio

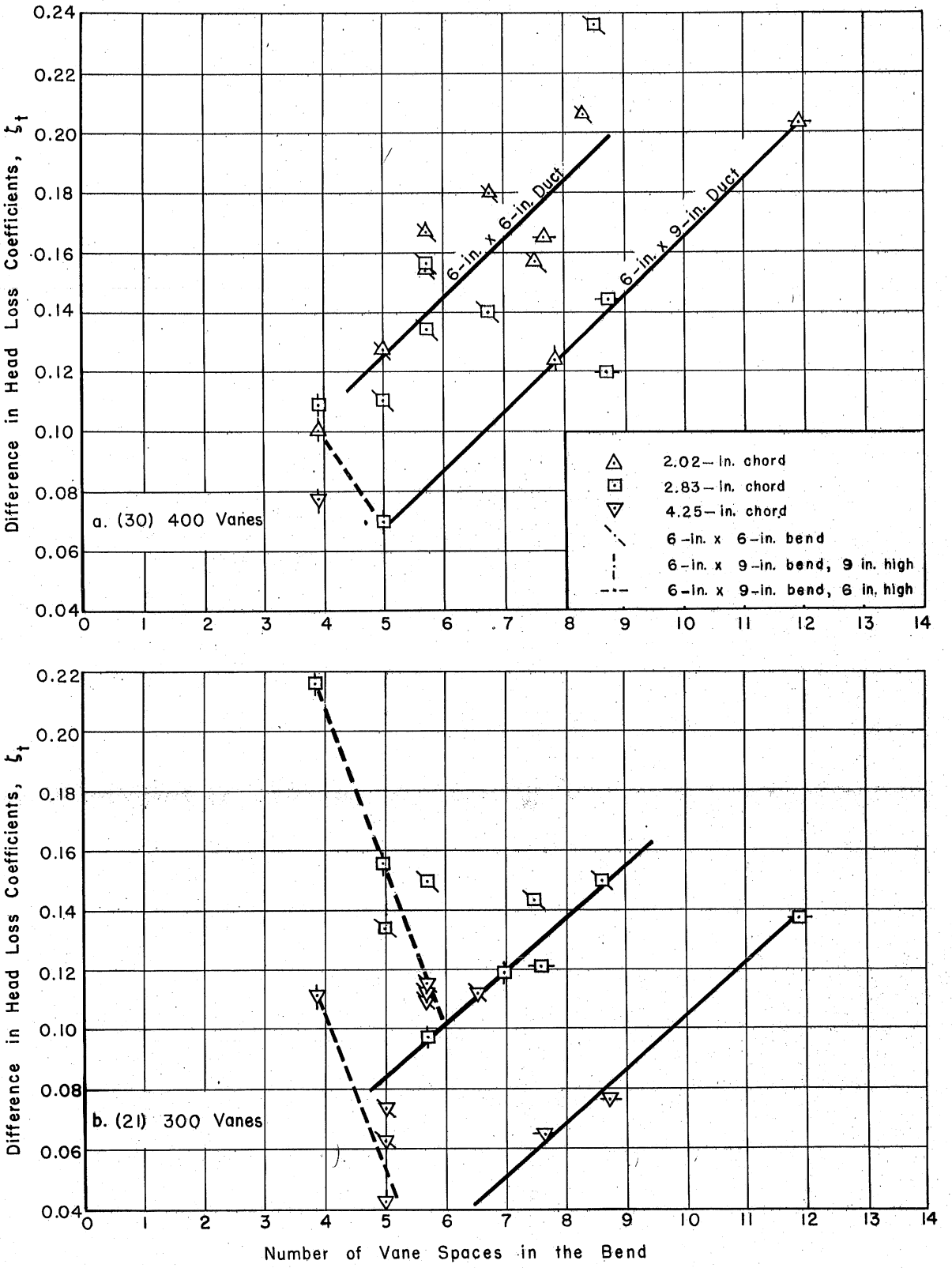

Fig. 33- Difference Between Three-Dimensional and Two-Dimensional Head Loss Coefficients Measured Far Downstream as a Function of Number of Vane Spaces

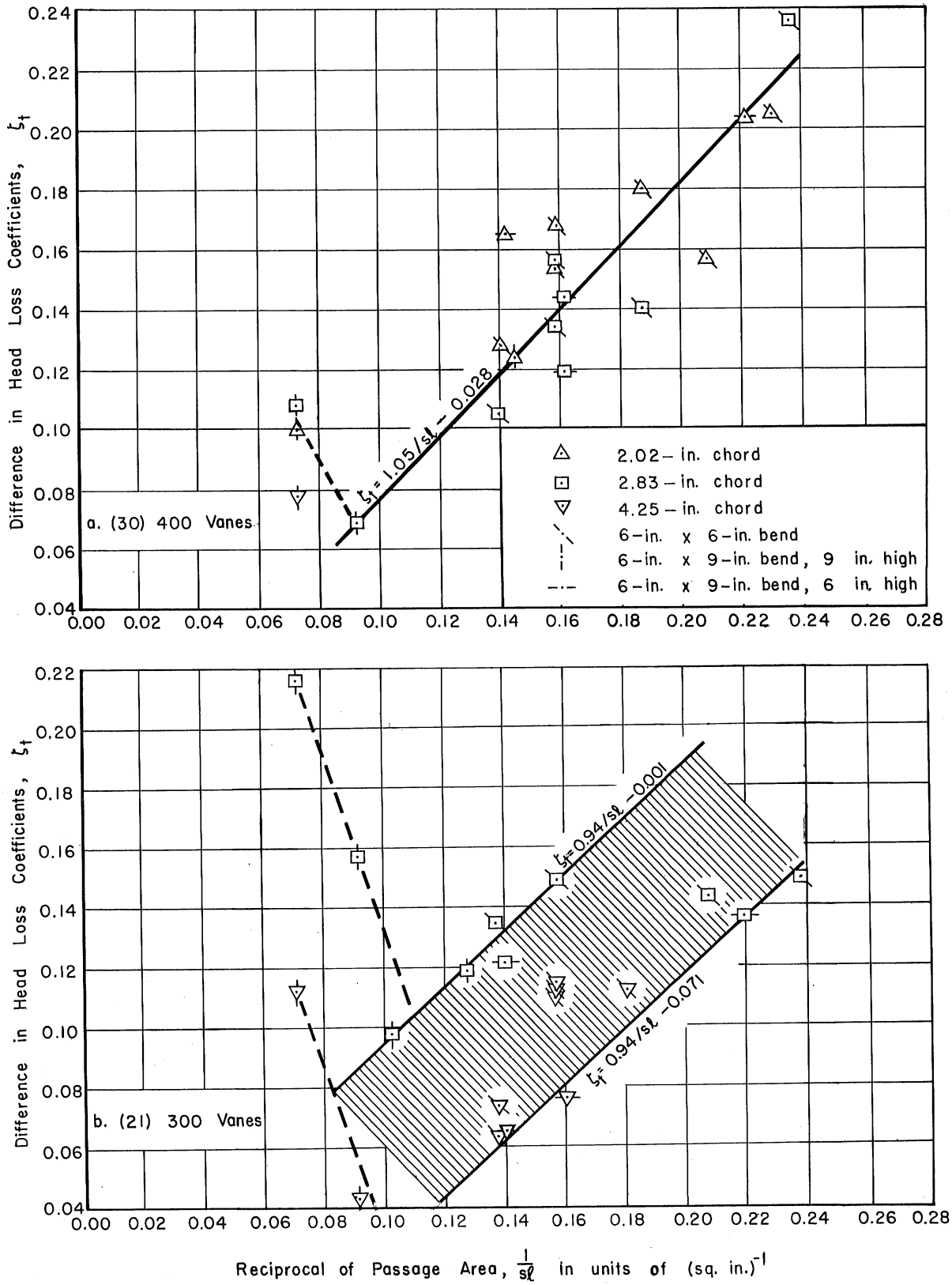

Fig. 34– Difference Between Three-Dimensional and Two-Dimensional Head Loss Coefficients Measured Far Downstream as a Function of Passage Area

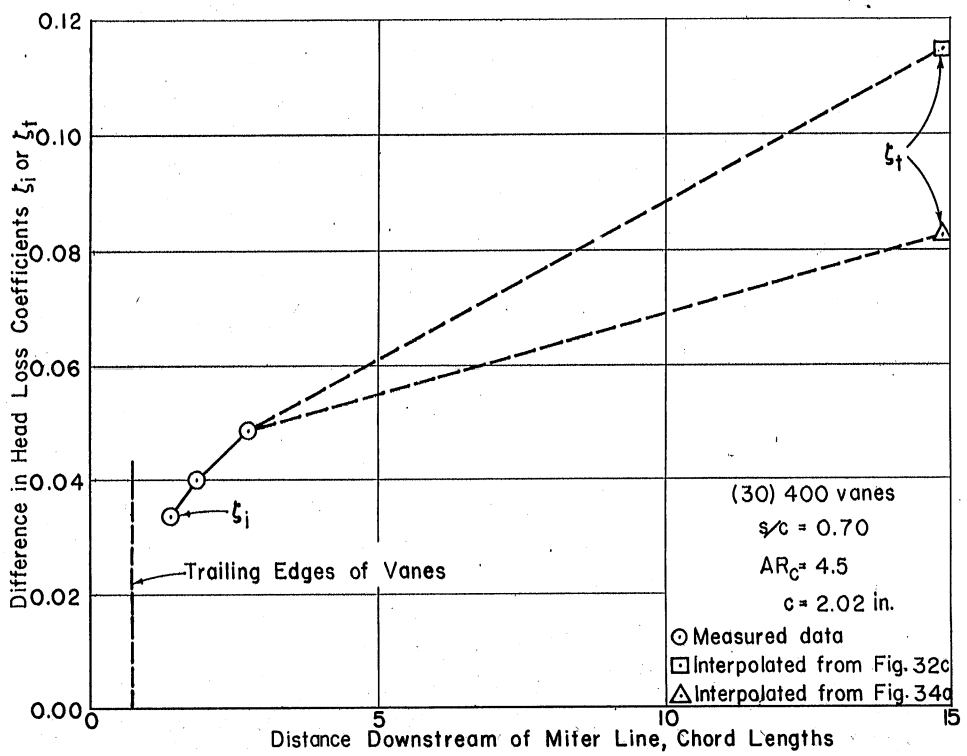

Fig. 35 — Effect of Distance to Measuring Station on Difference Between Three-Dimensional and Two-Dimensional Head Loss Coefficients

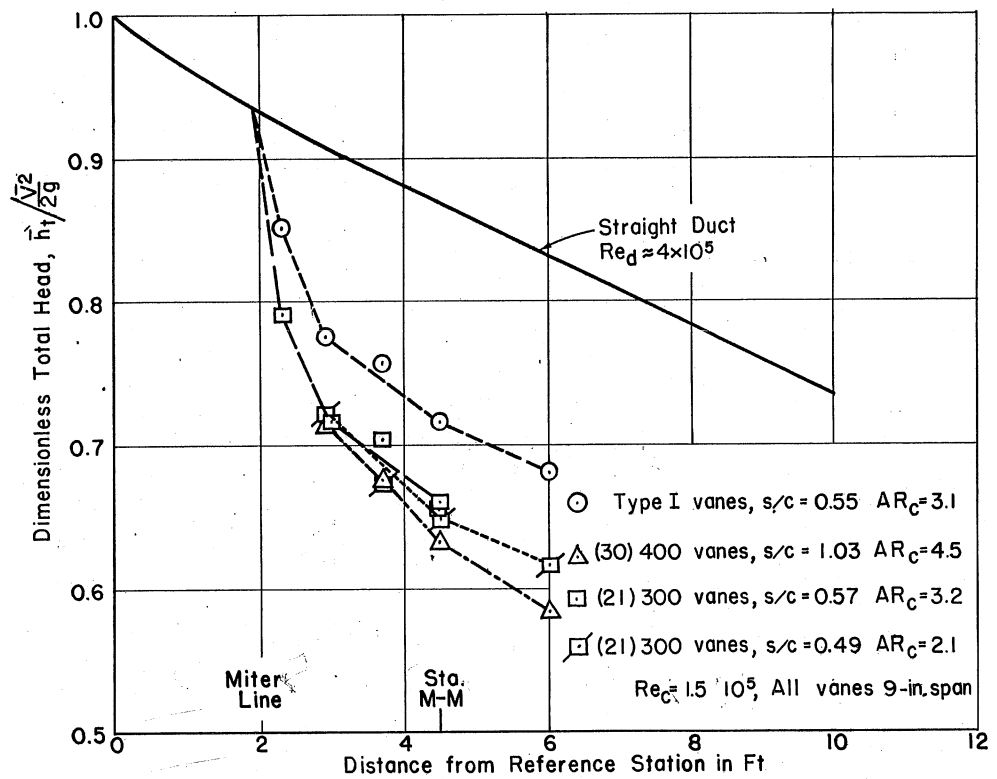

Fig. 36—Variation with Distance of Average Total Head Over the Duct Cross Section

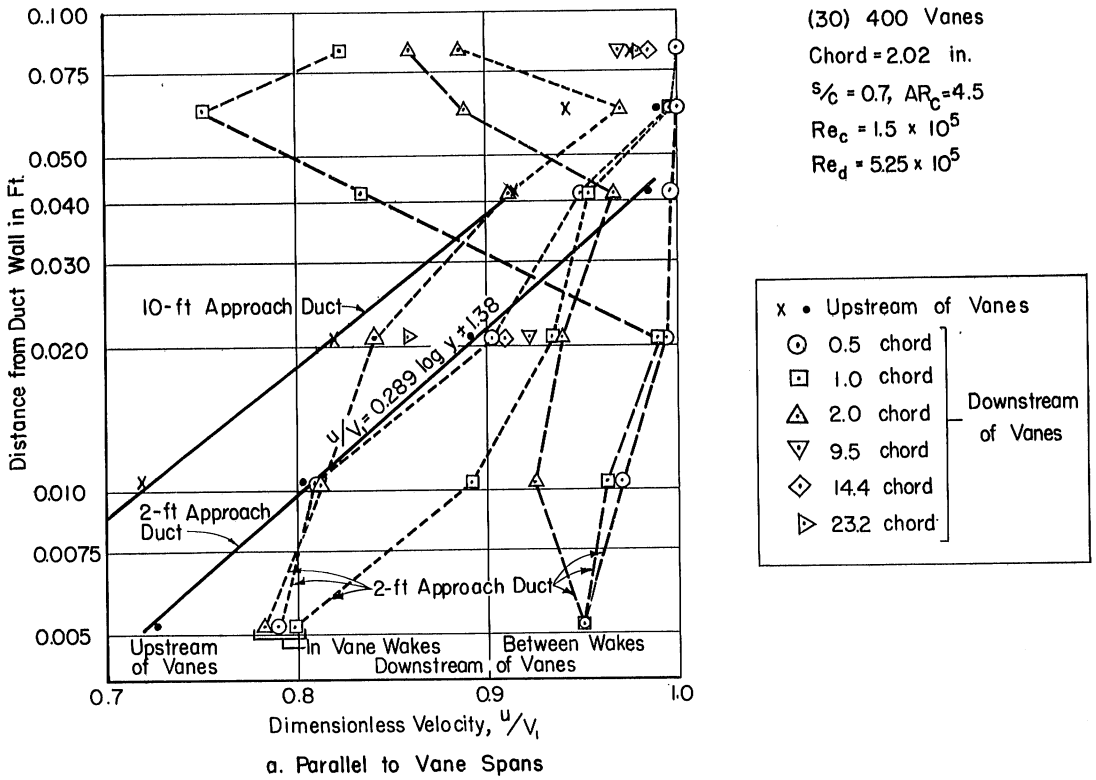

a. Parallel to Vane Spans

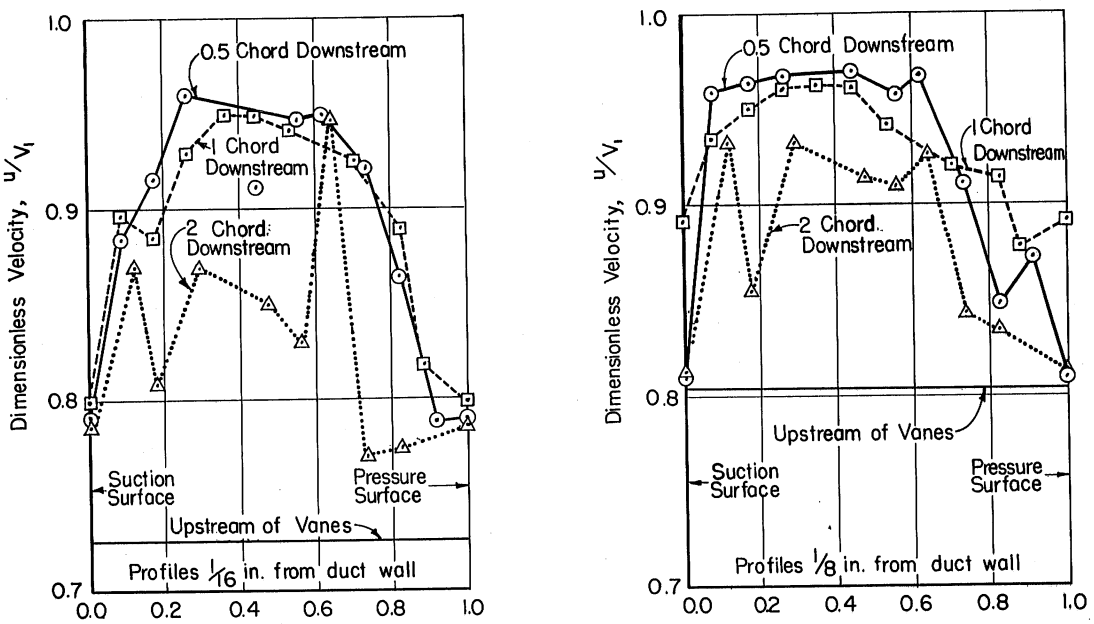

b. Normal to Vane Spans

Fig. 37— Typical Boundary Layer Velocity Distribution

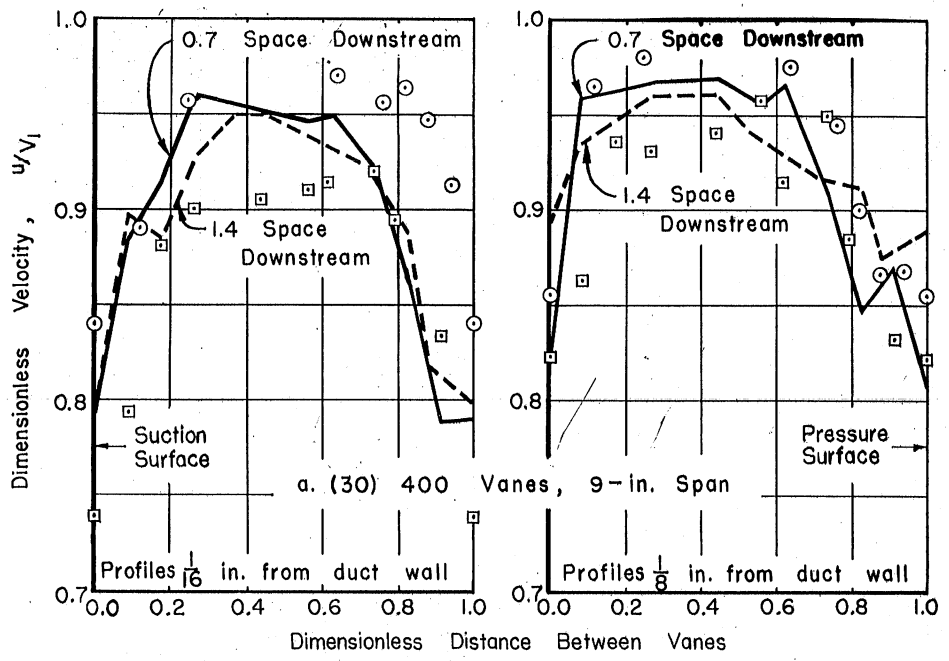

	Chord	Spacing	s/c	
═══	2.02 in.	1.414 in.	0.7	Fig. 37b
⊙	2.83 in.	2.075 in.	0.732	Profile 0.7 Space Downstream
⊡	2.83 in.	1.414 in.	0.5	Profile 1.0 Space Downstream

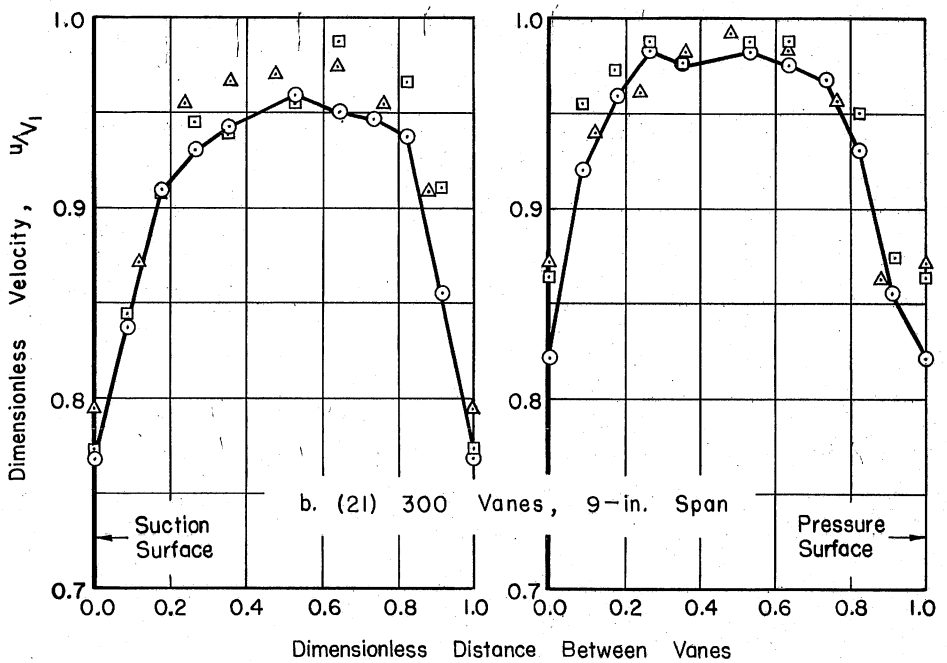

	Chord	Spacing	s/c	
⊡	2.83 in.	1.414 in.	0.5	Profile 1.0 Space Downstream
⊙	4.25 in.	1.414 in.	0.333	Profile 1.5 Space Downstream
△	2.83 in.	1.04 in.	0.366	Profile 1.4 Space Downstream

Fig. 38 – Comparison of Boundary Layer Velocity Distributions Behind the Vanes for Several Cascades

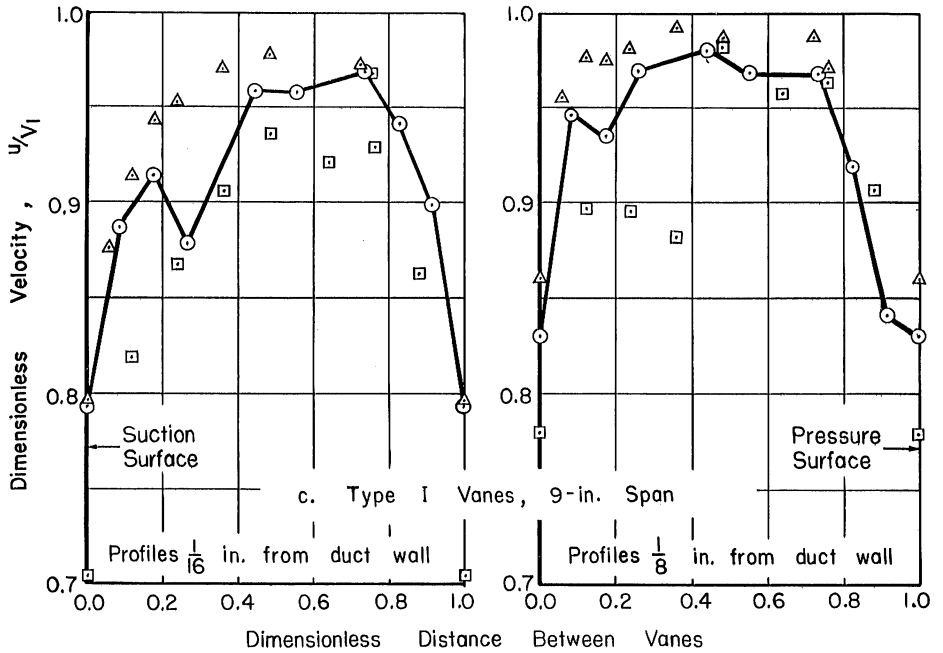

	Chord	Spacing	s/c				
⊙	2.93 in.	1.414 in.	0.48	Profile	1.03	Space	Downstream
⊡	2.93 in.	1.04 in.	0.36	Profile	1.414	Space	Downstream
△	2.93 in.	2.075 in.	0.71	Profile	0.7	Space	Downstream

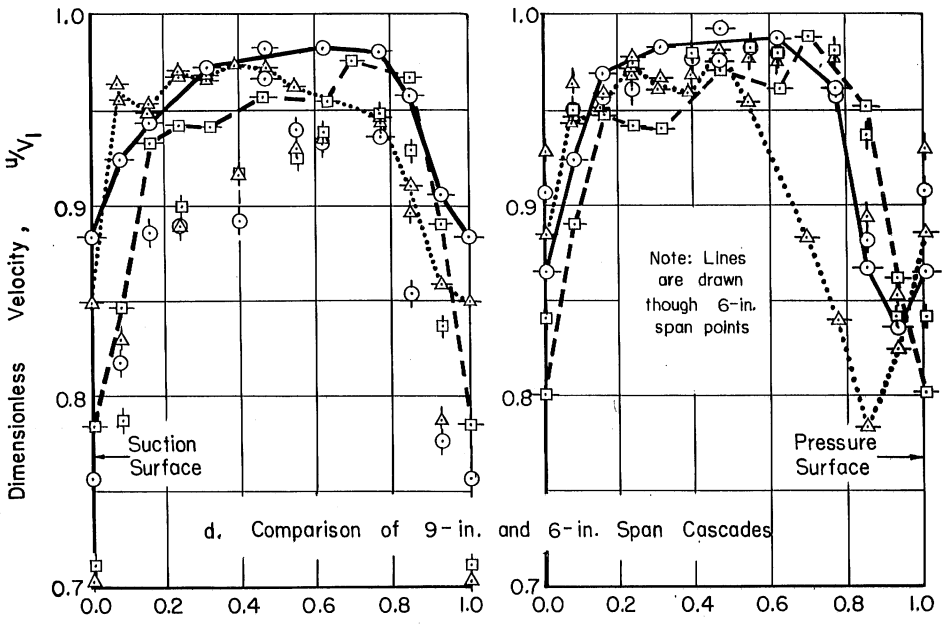

△ (30) 400 Vanes	Spacing = 1.616 in.
⊙ Type I Vanes	Chord = 2.83 or 2.93 in.
⊡ (21) 300 Vanes	Profiles 0.875 Space Downstream
—·— 6-in. Span	9-in. Span

Fig. 38 (Cont'd.)- Comparison of Boundary Layer Velocity Distributions Behind the Vanes for Several Cascades

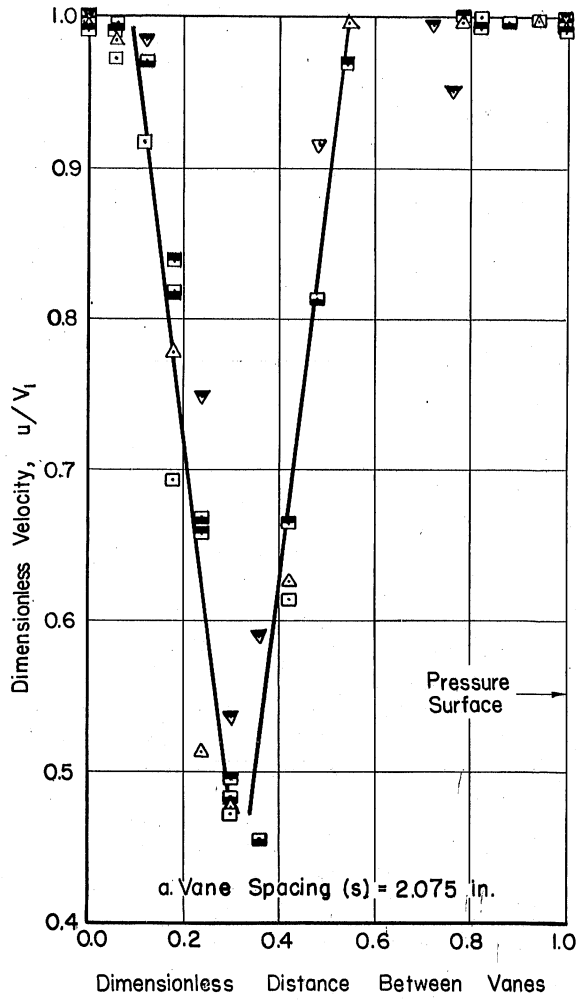

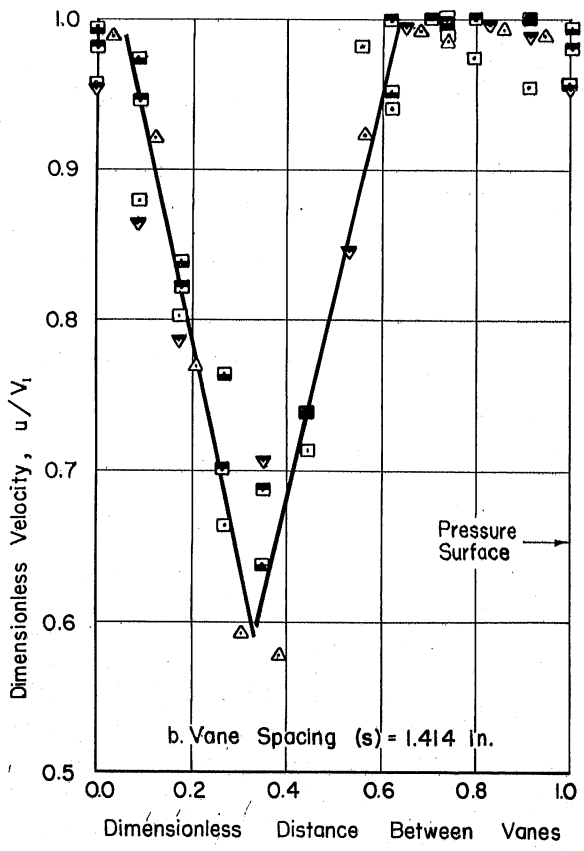

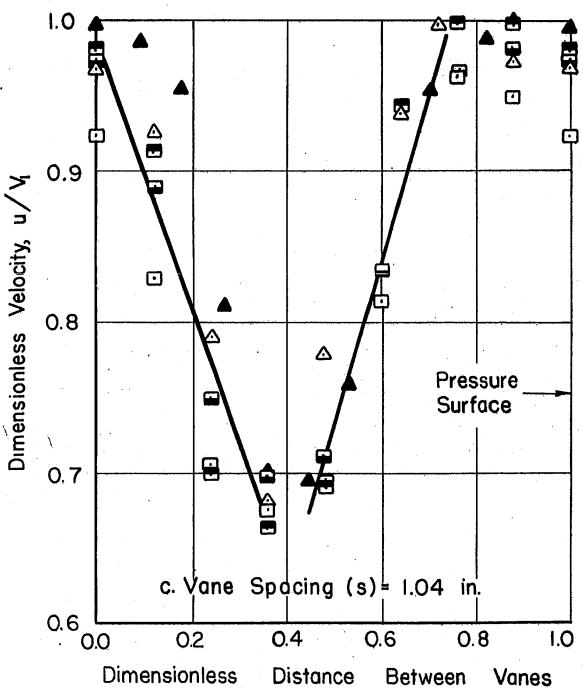

Chord Length	(30) 400 Vanes	(21) 300 Vanes	Type I Vanes
2.02 in.	△		
2.83 or 2.93 in.	⊡	▬	▬
4.25 in.		▽	

Note:

In (a.) only, ▬ = 0.5 space from duct wall.
▽ = 1.2 space from duct wall.

In (c.) only, ▲ spacing = 1.414 in. but profiles taken at 1 chord behind trailing edges and 1 space from duct wall.

Fig. 39–Typical Interior Velocity Distribution
(Profiles taken 0.5 chord behind the vane trailing edges and 0.7 space from the duct wall)

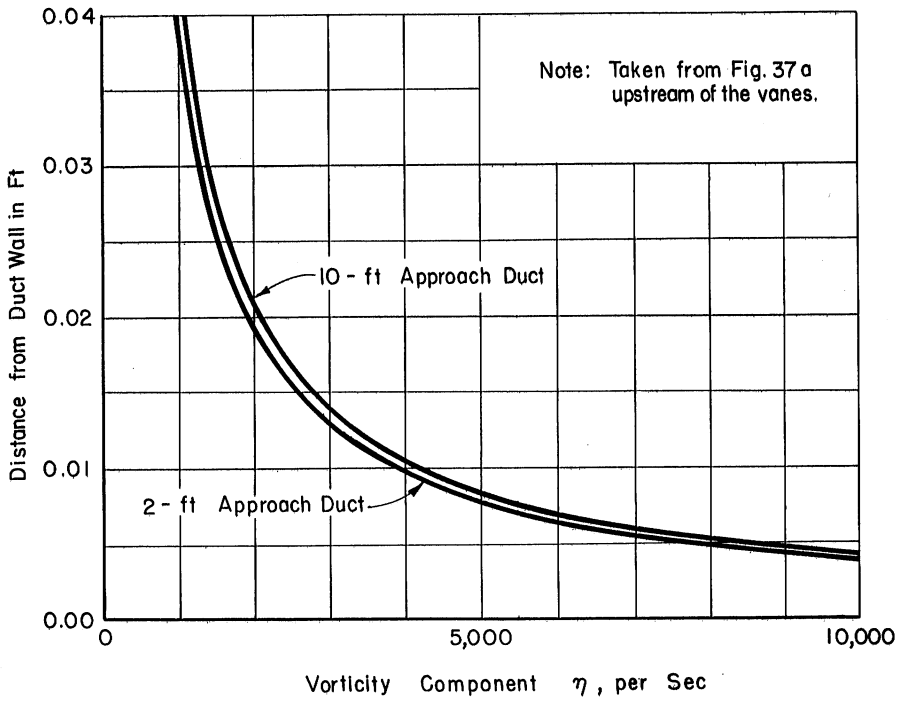

Fig. 40 — Typical Boundary Layer Vorticity Distribution

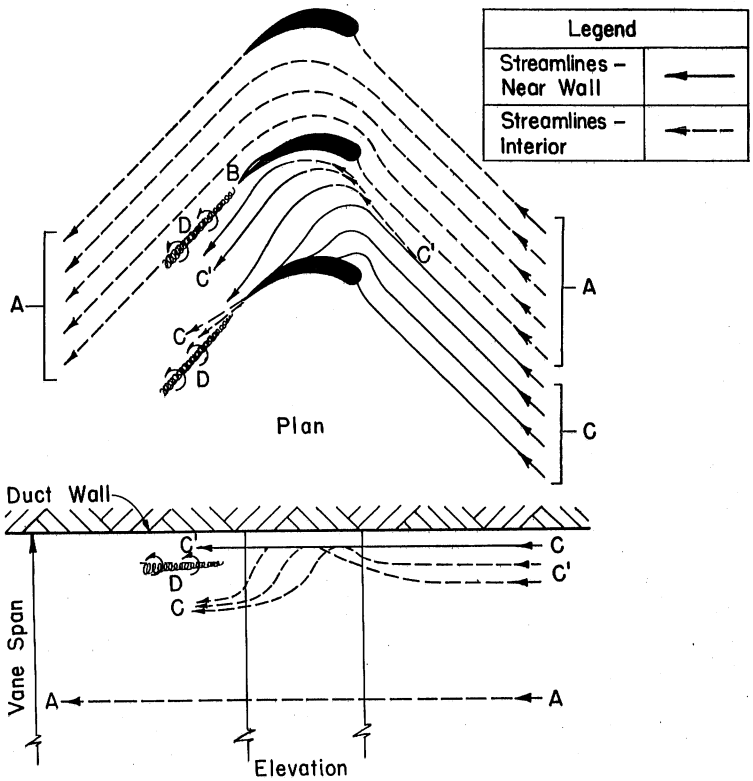

Fig. 41 - Schematic Streamlines in a Three-Dimensional Guide Vane Bend

DISTRIBUTION LIST FOR PROJECT REPORT NO. 36
of the St. Anthony Falls Hydraulic Laboratory

Copies	Organization
6	Office of Naval Research, Department of the Navy, Washington 25, D. C., Attn: Mechanics Branch (Code 438).
1	Commanding Officer, Branch Office, U. S. Navy Office of Naval Research, 346 Broadway, New York 13, New York.
2	Commanding Officer, Branch Office, U. S. Navy Office of Naval Research, The John Crerar Library Building, Tenth Floor, 86 East Randolph Street, Chicago 1, Illinois.
1	Commanding Officer, Branch Office, U. S. Navy Office of Naval Research, 801 Donahue Street, San Francisco 24, California.
1	Commanding Officer, Branch Office, U. S. Navy Office of Naval Research, 1030 East Green Street, Pasadena 1, California.
2	Officer in Charge, U. S. Navy Office of Naval Research, Branch Office, Navy 100, F.P.O. New York, New York.
9	Director, Naval Research Laboratory, Office of Naval Research, Washington 25, D. C., Attn: Technical Information Officer.
1	Executive Secretary, Research and Development Board, The Pentagon, Washington 25, D. C.
1	Chief of Naval Operations, Washington 25, D. C., Attn: DONO (Air).
1	Librarian, U. S. Naval Postgraduate School, Monterey, California.
1	Bureau of Aeronautics, Department of the Navy, Washington 25, D. C., Attn: Director, Airborne Equipment Division.
1	Bureau of Aeronautics, Department of the Navy, Washington 25, D. C., Attn: Design Elements Division.
1	Bureau of Ordnance, Department of the Navy, Washington 25, D. C., Attn: Code Ad3.
1	Naval Ordnance Laboratory, White Oak, Silver Spring 19, Maryland, Attn: Commander.
1	Underwater Ordnance Department, U. S. Naval Ordnance Test Station, Pasadena Annex, 3202 East Foothill Boulevard, Pasadena 8, California.
1	Naval Torpedo Station, Newport, Rhode Island.
1	Bureau of Ships, Department of the Navy, Washington 25, D. C., Attn: Research Division.

Copies	Organization
1	Bureau of Ships, Department of the Navy, Washington 25, D. C., Attn: Propeller and Shafting Branch.
6	David Taylor Model Basin, Washington 7, D. C., Attn: Hydromechanics Department.
1	Bureau of Yards and Docks, Department of the Navy, Washington 25, D. C., Attn: Research Division.
1	Underwater Sound Laboratory, Fort Trumbull, New London, Connecticut.
1	Waterways Experiment Station, Vicksburg, Mississippi.
1	Office Chief of Engineers, Building T-7, Gravelly Point, Washington 25, D. C., Attn: Research Division.
1	Air Materiel Command, Wright-Patterson Air Force Base, Dayton, Ohio, Attn: Air Documents Division.
1	Director of Research, National Advisory Committee for Aeronautics, 1724 F Street, N.W., Washington 25, D. C.
1	Geological Survey, Department of the Interior, Washington 25, D. C., Attn: C. G. Paulsen, Chief Hydraulic Engineer.
1	Bureau of Reclamation, Denver, Colorado, Attn: I. A. Winter.
1	National Bureau of Standards, National Hydraulic Laboratory, Washington 25, D. C., Attn: H. N. Eaton.
1	Captain H. E. Saunders, 206 Maple Avenue, Takoma Park, Washington 12, D. C.
1	Columbia University, Department of Civil Engineering, New York 27, New York.
1	Illinois Institute of Technology, Department of Fundamental Mechanics Research, Chicago 16, Illinois, Attn: Dr. V. L. Streeter.
1	The Johns Hopkins University, Mechanical Engineering Department, Baltimore, Maryland, Attn: Dr. G. F. Wislicenus.
1	Massachusetts Institute of Technology, Department of Civil and Sanitary Engineering, Cambridge 39, Massachusetts, Attn: Dr. A. T. Ippen.
1	Massachusetts Institute of Technology, Department of Naval Architecture and Marine Engineering, Cambridge 39, Massachusetts, Attn: Admiral E. L. Cochrane.
1	University of Michigan, Engineering Mechanics Department, Ann Arbor, Michigan, Attn: Prof. R. A. Dodge.

Copies	Organization
1	University of Minnesota, St. Anthony Falls Hydraulic Laboratory, Minneapolis 14, Minnesota, Attn: Dr. L. G. Straub.
1	Northwestern University, Department of Civil Engineering, Evanston, Illinois, Attn: Prof. W. S. Hamilton.
1	University of Notre Dame, College of Engineering, Notre Dame, Indiana, Attn: Dean K. E. Schoenherr.
1	The Pennsylvania State College, School of Engineering, Ordnance Research Laboratory, State College, Pennsylvania.
1	University of Southern California, Department of Physics, Los Angeles, California, Attn: Dr. R. E. Vollrath.
1	Stanford University, Department of Civil Engineering, Stanford, California, Attn: Prof. J. K. Vennard.
1	University of Tennessee, Engineering Experiment Station, Knoxville, Tennessee, Attn: Dr. G. H. Hickox.
1	Woods Hole Oceanographic Institute, Woods Hole, Massachusetts, Attn: Dr. Columbus Iselin.
1	Worcester Polytechnic Institute, Alden Hydraulic Laboratory, Worcester, Massachusetts, Attn: Prof. L. J. Hooper.
1	Kimberly Clark Corporation, Research and Development Laboratories, Neenah, Wisconsin, Attn: C. A. Lee.
1	Library, California Institute of Technology, Pasadena 4, California.
1	Engineering Societies Library, 29 West 39th Street, New York, New York.
1	John Crerar Library, Chicago 1, Illinois.
1	Library, Massachusetts Institute of Technology, Cambridge 39, Massachusetts.
1	Polytechnic Institute of Brooklyn, 99 Livingston Street, Brooklyn 2, New York, Attn: Dr. L. Meyerhoff.
1	Library, University of Texas, Austin, Texas.
1	Dean M. P. O'Brien, School of Engineering, University of California, Berkeley 4, California.
1	Prof. G. Birkhoff, Department of Mathematics, Harvard University, 21 Vanserg Building, Cambridge 38, Massachusetts.
1	Dr. F. H. Clauser, Department of Aeronautics, The Johns Hopkins University, Baltimore 18, Maryland.

Copies	Organization
1	Dr. J. W. Daily, Department of Civil and Sanitary Engineering, Massachusetts Institute of Technology, Cambridge 39, Massachusetts.
1	Dr. K. S. M. Davidson, Experimental Towing Tank, Stevens Institute of Technology, 711 Hudson Street, Hoboken, New Jersey.
1	P. Eisenberg, Hydromechanics Department, David Taylor Model Basin, Washington 7, D. C.
1	Dr. R. T. Knapp, Hydrodynamics Laboratories, California Institute of Technology, 1201 East California Street, Pasadena 4, California.
1	Dr. F. A. Maxfield, Bureau of Ordnance (Code Re6a), Department of the Navy, Washington 25, D. C.
1	Dr. J. H. McMillen, Naval Ordnance Laboratory, White Oak, Silver Spring 19, Maryland.
1	Dr. A. Miller, Bureau of Ordnance (Code Re3d), Department of the Navy, Washington 25, D. C.
1	Dr. J. M. Robertson, Ordnance Research Laboratory, The Pennsylvania State College, State College, Pennsylvania.
1	Dr. H. Rouse, Iowa Institute of Hydraulic Research, State University of Iowa, Iowa City, Iowa.
1	Dr. J. H. Wayland, Department of Applied Mechanics, California Institute of Technology, 1201 East California Street, Pasadena 4, California.
3	Serials Division, Library, University of Minnesota, Minneapolis 14, Minnesota.

Reference: ONR ltr. ONR:438:EH, NR-062-065 of October 31, 1950, to Director, St. Anthony Falls Hydraulic Laboratory.)